TESIS DE LA UNIVERSIDAD DE ZARAGOZA

2013

50

Daniel Casanova Ortega

Flower Constellations: Optimization and Applications

Departamento
Matemática Aplicada

Director/es
Elipe Sánchez, Antonio
Avendaño González, Martín Eugenio

ISSN 2254-7606

Prensas de la Universidad
Universidad Zaragoza

Universidad Zaragoza
1542

Tesis Doctoral

FLOWER CONSTELLATIONS: OPTIMIZATION AND APPLICATIONS

Autor

Daniel Casanova Ortega

Director/es

Elipe Sánchez, Antonio
Avendaño González, Martín Eugenio

UNIVERSIDAD DE ZARAGOZA

Matemática Aplicada

2013

Flower Constellations: Optimization and Applications

Daniel Casanova Ortega

IUMA - Universidad de Zaragoza

Flower Constellations: Optimization and Applications

Daniel Casanova Ortega

Memoria presentada para optar al grado de
Doctor en Ciencias Matemáticas.
Dirigida por D. Antonio Elipe Sánchez y
D. Martín Eugenio Avendaño González.

IUMA - Universidad de Zaragoza

Acknowledgements

First of all thanks to Dr. Antonio Elipe for the direction of this thesis. His advice, always successful, have been vital for the development of this work. Thanks to Dr. Martín Avendaño for the co-direction of this thesis, his devotion, his scientific contributions and his help with English has been essential to move forward this thesis.

Thanks to Dr. Daniele Mortari, for letting me know the main topic of this thesis, the *Flower Constellations*, but also his hospitality during my research visit in Texas A&M University. Thanks to Dra. Anne Lemaître for the research visit in *L'Université de Namur*, and finally to Dr. Gilles Métris for the pleasant research visit in *L'Observatoire de la Côte d'Azur*.

Thanks in particular to Professors Alberto Abad and Roberto Barrio, and also the other colleagues from the Space Mechanics Group, the Department of Applied Mathematics, and the IUMA. I can not forget to mention Conchi, Bea or Lourdes administrative and service staff that make daily work easier and enjoyable.

Thanks to the Ministry of Science and Innovation for the Predoctoral Research Scholarship with reference BES-2009-021968 associated to the research project AYA2008--05572, as well as the financial support received for the research visits.

Thanks to all the friends I have made during the development of my PhD, at the beginning it was a simple coffee but at the end it turned out to be the best time of the morning. Thanks to the strong support of my degree colleagues, their constant encouragement and trust in me have been fundamental. Thanks to the people that I have known these years in Zaragoza, especially the "equipo" that always have been there when I needed. And of course, my friends from my hometown Alcañiz, that in one way or another have contributed to this project.

Thank to Laura's family. They always have seen me capable of doing this work and they have been encouraging me to keep going.

Thanks to my mother and my father for their infinity support, for bringing me up and endeavoring as they have done for me to achieve this goal, as proud of them as they are of me. Thanks to my brother, aunt, uncle, cousins and all my family, not forgetting of course people no longer with us to enjoy this moment, especially my grandmother.

Last but not least, thanks to you, Laura, for accompanying me during this long journey in the good and the less good times, understanding me, always helping me, supporting me in all my decisions, and getting up the courage when I needed. Without you, this work would not have gone ahead. Thank you.

Agradecimientos

En primer lugar agradecer al Dr. D. Antonio Elipe la dirección de esta tesis. Sus consejos, siempre acertados, han sido de vital importancia para el desarrollo de este trabajo. También agradecer al Dr. D. Martín Avendaño la co-dirección de esta tesis, su dedicación, sus aportaciones científicas y su ayuda con el inglés han sido imprescindibles para sacar adelante esta tesis.

Gracias al Dr. D. Daniele Mortari, por su entusiasmo dándome a conocer el tema principal de esta tesis, las *Flower Constellations*, así como su hospitalidad en la estancia en Texas A&M University. Gracias a la Dra. Dña. Anne Lemaître por la estancia en *L'Université de Namur*, y finalmente al Dr. D. Gilles Métris por su acogedora estancia en *L'Observatoire de la Côte d'Azur*.

Gracias en especial a los profesores Alberto Abad y Roberto Barrio, así como al resto de compañeros del Grupo de Mecánica Espacial, del departamento de Matemática aplicada y del IUMA. No puedo olvidarme de mencionar a Conchi, Bea o Lourdes PAS que hacen el trabajo diario más sencillo y agradable.

Agradecer al Ministerio de Ciencia e Innovación la adjudicación de la ayuda Predoctoral de Formación de Personal Investigador de referencia BES-2009-021968 asociada al proyecto de investigación AYA2008-05572, así como la financiación de las estancias realizadas.

Gracias a todos los amigos y amigas que he hecho durante el desarrollo de mi doctorado, al comienzo era un simple café y al final resulto siendo el mejor rato de la mañana. Gracias al gran apoyo de mis compañeras de la carrera, sus constantes ánimos y su confianza en mí han sido fundamentales. Gracias a la gente que he conocido estos años en Zaragoza, en especial al "equipo" que siempre ha estado ahí cuando lo he necesitado. Y por supuesto, a los amigos y amigas de Alcañiz, que de una manera u otra han aportado su granito de arena a este proyecto.

Agradecer a la familia de Laura el haberme visto desde el primer momento capaz de realizar este trabajo y animarme a seguir adelante.

Gracias a mi madre y a mi padre por su infinito apoyo, por educarme y esforzarse como lo han hecho para que yo pueda alcanzar este objetivo. Tan orgulloso de ellos como ellos lo están de mí. Gracias a mi hermano, mis tíos, mis primos y toda mi familia, sin olvidarme por supuesto de los que ya no están para disfrutar de este momento, en especial mi abuela.

Por último y no por ello menos importante, gracias a ti, Laura, por acompañarme durante este largo camino en los buenos y en los menos buenos momentos, entendiéndome, siempre ayudándome, apoyándome en todas mis decisiones, y levantándome el ánimo cuando lo he necesitado. Sin ti, este trabajo no hubiera salido adelante. Gracias.

I know that I know nothing.
Sócrates

Contents

Introduction

An artificial satellite is an object that orbits around a celestial body due to natural gravitational forces. Satellites are launched to the space by humans to overcome different spacial missions. The first artificial satellite, orbiting around the Earth, was launched in 1957 by the Soviet Union, and its name was Sputnik I. After that event, thousands of satellites have been launched into different orbits around the Earth. There are different ways to classify the satellites, depending on their weight, their altitude, sort of mission, etc. [1]

In many occasions one satellite is not enough to succeed in a spacial mission, and a group of satellites is required. In this case we have a group of artificial satellites, in the same or different inertial orbit, working together and following the same goal. This is called a satellite constellation. In the last decades, humans have designed satellite constellations for different purposes [32, 42]; Global Positioning System (GPS), Galileo or GLONASS are examples of satellite constellations whose purpose is navigation and geodesy. Orbcomm constellation, operated by the American satellite communications company Orbcomm, Inc. has a total of 29 operational satellites today, in Low Earth Orbits. The main goal of this constellation is to provide communication between different data centers. Iridium and Globalstar are the direct competitors of Orbcomm. Molniya and Tundra are communication satellite constellations using highly elliptic orbits. The purpose of other satellite constellations are human protection such as Disaster Monitoring Constellation, Earth observation, etc. These are, among others, examples of satellite constellations.

The existing constellations use, in general, circular orbits. However, as Draim indicates in his work [21], eccentric orbits could be better than circular ones. Thus, another way to design satellite constellations without the requirement of circular orbits was necessary. Thus, Dr. Daniele Mortari developed around the year 2004, the *Flower Constellations* [34, 35, 50] that solve this problem by leaving the eccentricity as other design variable. These constellations were expanded in the *Harmonic Flower Constellations (HFC)* [8], the *2D Lattice Flower Constellations (2D-LFC)* [7, 12], which are the main tool in this work and, finally, the *3D Lattice Flower Constellations (3D-LFC)* [18].

Global and regional coverage problems are the main topic of research in satellite constellations. In particular, the global positioning problem consists of determining the position of a user with a few centimeters of accuracy. This problem requires a minimum of four visible satellites from any point on the Earth surface at any instant

of time [31, 52]. For that purpose a constellation with a rather complex geometry is required.

The first goal of this work consist of searching 2D-LFCs whose geometry will be optimal for solving the problem of global positioning. The Geometric Dilution of Precision (GDOP) [28] is the metric that quantifies how good the geometry of a constellation is for finding the exact position of a user and the time offset that exists between system and user clock. Therefore, the metric which defines the optimality of the 2D-LFCs in our problem is the maximum value of the GDOP experienced from any point on the Earth surface during the propagation time. For practical purposes, we discretize the time in steps of $60.0\,sec$ and we consider $30,000$ ground stations randomly distributed over the Earth surface with uniform probability density. Evolutive algorithms [49] are the main tool used to solve this optimization problem. In particular, in this thesis we use Genetic Algorithms and the Particle Swarm Optimization. We found 2D-LFCs whose maximum GDOP value is better than the existing Galileo or GLONASS constellations during the entire propagation time. Due to the high computational cost required to propagate a constellation and the huge size of the search space, we have developed several techniques to reduce the search space and the propagation time being mathematically correct. Furthermore, we use certain parallelization techniques when implementing the evolutive algorithms.

Through the analysis of this problem we have compared different optimization techniques, concluding that the *Particle Swarm Optimization Algorithm* is the method that gives better results in our search. In this work we searched among all possible 2D-LFCs varying the number of satellites between 18 and 40. We have obtained surprising results, such as our 27-satellite constellation has a better GDOP than the best configuration found with 28 satellites. Since the GDOP of our 27-satellite 2D-LFC can only be improved by adding at least two satellites, we conclude that it is one of the best constellations. Thanks to the 2D-LFCs, we have been able to include eccentric orbits in our search, finding some optimal configurations whose orbits have an eccentricity around 0.3. In this study we compared the evolution of the GDOP of our best 2D-LFCs with respect to the existing GLONASS and Galileo, noting that our constellations are slightly better because the maximum GDOP value experienced at any time is always lower. In our optimization approach the collision problem is automatically excluded because alignment of satellites will imply a large GDOP and the constellation will be excluded automatically of the search.

The previous study was made in a purely Keplerian model. The next step is to bring our constellations to a more realistic situation consists of introducing the perturbed two-body problem [45]. In the Keplerian model the Earth is considered as a perfect sphere. However, as a first approximation to a more realistic model, we consider the Earth as a solid of revolution flattened at the center (ellipsoid). This leads us to include the zonal harmonic J_2 in the potential function. The introduction of higher zonal harmonics is disregard since they are at least 3 orders of magnitude smaller than J_2 [1].

The introduction of the J_2 term in the potential function leads to the second problem

considered in this thesis. The problem consists of finding parameters to have a stable 2D-LFC, meaning that the satellites of the constellation are affected by the J_2 effect but all in the same way. Thus, the relative position between the satellites in the osculating elements space will remain almost constant, thus we obtain Rigid Constellations.

Most of the literature deals with the perturbed two body problem average the non-secular perturbations in one orbital period [10]. Thus, they only consider long periodic and secular perturbations. In this thesis, we consider the secular and non-secular perturbations that affect the acceleration of the satellite. Thus, instead of averaging the expression of the potential in an orbital period, we consider the full expression of the potential function [1]. By using the full expression of the potential and Lagrange Planetary Equations [45] we can study the evolution of the orbital elements over time.

The main goals consist of; controlling the secular perturbation in order to be identical in all the satellites of the constellation, and minimizing the non-secular perturbation that affects the satellites. If we succeed in these two goals, the satellites in the constellation will be disturbed by J_2, but all of them in the same way. Thus, the relative positions of the satellites will be almost constant (in the osculating elements space) so the structure of *Flower Constellation* will be preserved over time, what we call *Rigid Constellation*.

To control the secular part of the satellites in a constellation, we consider a reference satellite. We study first the dependency of the secular components of the osculating elements as a function of the initial Ω and M. We observe that none of the secular components depend on Ω, but there is a strong dependency on M. In the particular case of a 2D-LFC, all satellites have the same values of a, e, i, ω, but have different values of Ω and M. Therefore, a priori, the secular component of the osculating elements will be different for each satellite. To ensure that they are identical, we apply a correction method. The method consists of modifying the semi-major axis of all satellites a few kilometers. Thus, the period (T_p) will be changed and in particular the slope of the mean anomaly since $\dot{M}_{sec} = 2\pi/T_p$. With this correction, we get that the secular component of the osculating elements of all the satellites in the constellation match up to an order of 10^{-11}. With this technique, we can control the secular perturbation of our satellites. Trying to control the non secular perturbation is somewhat more complicated. First, we apply to each osculating element $q \in \{a, e, i, \omega, \Omega, M\}$ linear interpolation on the data set $(t, q(t))$ which have been previously obtained to calculate the exact position of the satellites. Through these linear functions of the osculating elements we can calculate at each instant of time what we called linear or approximate position of the satellite. So that, the distance between the two positions (real and linear) will be due to the non-secular perturbations that affect our reference satellite. The last goal consist of searching among the possible values of the eccentricity and inclination those that reduce this deviation as much as possible. In this way, we minimize the non-secular perturbation that affects our reference satellite. These values extrapolate to the remaining satellites of our constellation.

This work shows that it is possible to obtain 2D-LFCs whose configuration remain constant under the J_2 effect, i.e. *Rigid Constellations*. The theory we developed has two direct applications. First, it validates the theory of the 3D Lattice Flower

Constellation [19] (3D-LFC) under the full expression of the potential function with the J_2 term, assuming that the semi-major axes are corrected and the value of the deviation is small. Second, it shows that in the Global Coverage Problem (with J_2) it will be enough to find a Rigid Constellation that minimizes a slightly modified fitness function (computable using Keplerian propagation).

Our last goal consist of reducing the unpractical high number of satellites that most 2D-LFCs need to obtain full symmetry. We provide a methodology to compute all the subsets of the 2D-LFC that still have symmetric phasing distributions [14].

To achieve this goal we have identified the first orbit of our constellation, which has N_{so} admissible positions with a necklace of N_{so} pearls [15]. We took a number N_{rso} ($N_{rso} < N_{so}$) representing the actual satellites per orbit. Thus, we consider the first orbit of the constellation as a *necklace* of N_{so} pearls, of which N_{rso} are black and the remaining ones are white. That is, an orbit with N_{so} admissible positions, of which N_{rso} are occupied by a satellite and the others are not. The distribution of satellites in the remaining orbits is identical to the first, but shifted k pearls.

In this way a Necklace Flower Constellation (NFC) is characterized by a pair $(\mathcal{G}, k)$. However, not all such pairs produce a valid NFC, nor two distinct pairs produce distinct NFC. These two problems are called consistency and minimality problem, respectively. They are completely solved by using number theory [3]. Finally, we introduce several counting theorems for determining the possible pairs $(\mathcal{G}, k)$ from the phasing parameters of a 2D-LFC.

Satellite constellations are a current topic for the possibilities that they can provide, for commercial and institutional applications, such as telecommunications, positioning determination or Earth observation, with reasonable costs. The results obtained in this thesis encourage the future study of satellite constellations, which may result more efficient than the current ones.

Introducción

Un satélite artificial es un objeto diseñado por el ser humano y lanzado al espacio mediante un vehículo espacial con el objetivo de sobrellevar una misión específica. El primer satélite artificial, orbitando en torno a la Tierra, fue lanzado in 1957 por la Unión Soviética, y su nombre es Sputnik I. Después de dicho evento, miles de satélites artificiales han sido lanzado en diferentes orbitas en torno a la Tierra. Hay diferentes formas de clasificar estos satélites, dependiendo de su peso, su altura, el tipo de misión, etc. [1]

En muchas ocasiones, un satélite no es suficiente para tener éxito en una misión espacial, por lo que un grupo de satélites es necesario. Definiremos una constelación de satélites como un conjunto de satélites persiguiendo un objetivo común y operando de manera conjunta. En las últimas décadas el ser humano ha diseñado constelaciones de satélites con diferentes objetivos [32, 42]; Global Positioning System (GPS), Galileo o GLONASS son ejemplos de constelaciones de satélites cuya finalidad es la navegación y la geodesia. La constelación estadounidense Orbcomm formada actualmente por 29 satélites operativos situados en órbitas bajas es un sistema de telecomunicación. Iridium y Globalstar son las competidoras directas de Orbcomm. Las constelaciones rusas Molniya y Tundra son sistemas de telecomunicación famosas por su gran excentricidad. Otros objetivos de las constelaciones pueden ser la observación de la Tierra, aplicaciones militares, la protección del ser humano (Disaster Monitoring Constellation), etc. Estos, entre muchos otros, son ejemplos concretos de constelaciones de satélites.

Las constelaciones existentes utilizan, en general, orbitas circulares. Sin embargo, como Draim indica en su trabajo [21], las orbitas excéntricas podrían ser mejores que las circulares. Así, otra forma de diseñar constelaciones de satélites, sin la necesidad de tener órbitas circulares, era necesaria. Por ello, el Dr. D. Daniele Mortari desarrollo en torno al año 2004 las *Flower Constellations* [34, 35, 50] que solucionan este problema dejando la excentricidad como otra variable libre. Estas constelaciones fueron extendidas en los años posteriores a las *Harmonic Flower Constellations (HFC)* [8], las *2D Lattice Flower Constellations (2D-LFC)* [7, 12], que serán la principal herramienta en este trabajo, y finalmente las *3D Lattice Flower Constellations (3D-LFC)* [18].

Los problemas de cobertura regional y global constituyen el principal tema de investigación en torno a las constelaciones de satélites. En particular, el problema de posicionamiento global consiste en la determinación de la posición de un usuario con unos pocos centímetros de error en la precisión. Este problema requiere de al menos

cuatro satélites visibles desde cualquier punto de la esfera terrestre en cualquier instante de tiempo, para lo que se requiere una geometría de la constelación bastante compleja [31, 52].

El primer objetivo de este trabajo consiste en la búsqueda de 2D-LFCs cuya geometría sea óptima para la resolución del problema de posicionamiento global. El GDOP, del inglés Geometric Dilution of Precision [28], es la métrica que determina cómo de buena es la geometría de una constelación para encontrar la posición exacta de un usuario y el desfase horario entre el reloj del satélite y el del usuario. Por lo tanto, la métrica que define la optimalidad de las 2D-LFCs en nuestro problema es el máximo valor del GDOP experimentado desde cualquier punto de la superficie terrestre durante el tiempo de propagación. Por motivos prácticos, discretizamos el tiempo de propagación en pasos de 60.0 *sec* y consideramos 30000 estaciones terrestres aleatoriamente distribuidas sobre la superficie terrestre con probabilidad uniforme. Los algoritmos evolutivos [49] son la principal herramienta para tratar este problema de optimización. En particular, en este trabajo utilizamos Algoritmos Genéticos y los *Particle Swarm Optimization Algorithms*. Mediante este análisis, encontramos 2D-LFCs cuyos satélites presentan configuraciones que mejoran ligeramente el máximo valor del GDOP experimentado con respecto a las constelaciones existentes de Galileo y GLONASS. El gran costo computacional requerido para propagar las constelaciones y el enorme tamaño de nuestro espacio de búsqueda nos ha llevado a desarrollar diferentes técnicas que reducen el tiempo necesario para encontrar las soluciones óptimas. Dichas técnicas consisten en la reducción del espacio de búsqueda, así como la reducción del tiempo de propagación de manera que todo siga siendo matemáticamente correcto. Además, hemos utilizado técnicas de paralelización en la implementación de los algoritmos evolutivos.

El análisis de este problema ha permitido comparar las diferentes técnicas de optimización empleadas, concluyendo que el *Particle Swarm Optimization Algorithm* es el método que mejores resultados proporciona en nuestra búsqueda. En este trabajo hemos realizado una búsqueda entre todas las 2D-LFCs posibles variando el número de satélites entre 18 y 40. Hemos obtenido resultados sorprendentes como sería el hecho de que con 27 satélites encontramos mejores configuraciones que con 28 satélites para resolver el problema de posicionamiento global. Puesto que nuestra 2D-LFC de 27 satélites sólo puede mejorarse añadiendo al menos dos satélites, concluimos que es una de las mejores constelaciones. Además, gracias a las 2D-LFCs hemos podido incluir órbitas excéntricas en nuestra búsqueda, encontrando algunas configuraciones óptimas cuyas órbitas presentan una excentricidad en torno a 0.3, muy distinta de la excentricidad nula que presentan las órbitas más usuales. En este trabajo hemos comparado la evolución del GDOP de nuestras 2D-LFCs óptimas con respecto a las existentes GLONASS Y Galileo, observando que nuestras constelaciones son ligeramente mejores debido a que el máximo valor del GDOP que obtenemos en cada instante es siempre menor. El estudio de las colisiones entre satélites en la constelación, es un problema intrínseco en nuestro problema de optimización puesto que si hay próxima una alineación de satélites, el GDOP en ese instante es elevado y automáticamente dicha constelación queda excluida en nuestra búsqueda.

El estudio previo ha sido realizado en un modelo puramente kepleriano. El siguiente

paso para acercar nuestras constelaciones a una visión más realista consiste en introducir el problema de los dos cuerpos perturbado [45]. La Tierra es considerada como una esfera perfecta en el modelo kepleriano. Sin embargo, como una primera aproximación a un modelo más realista, consideramos la Tierra como un sólido de revolución achatado por el centro (elipsoide). Esto nos lleva a incluir el zonal harmónico J_2 en la función potencial. La introducción de zonales harmónicos de ordenes superiores no se considera en este trabajo ya que estos harmónicos son al menos tres ordenes de magnitud menores que el J_2 [1].

La introducción del zonal harmónico J_2 nos conduce a plantearnos el segundo problema tratado en esta tesis. Este problema consiste en la búsqueda de parámetros de una 2D-LFC para conseguir que sea estable, esto es, que los satélites de la constelación se vean afectados por las perturbaciones pero todos de la misma manera. De esta forma la posición relativa entre los satélites de la constelación (en el espacio de los elementos osculadores) quedará inalterada, obteniendo así las constelaciones que tienen por nombre *Rigid Constellations*.

La mayoría de autores que trabajan el problema principal del satélite promedian las perturbaciones no seculares en un periodo orbital, considerando únicamente las perturbaciones de largo periodo y las perturbaciones seculares [10]. En este trabajo, consideramos las perturbaciones seculares y no seculares (de largo y corto periodo) que afectan a la aceleración del satélite. Por ello, en lugar de promediar la expresión del potencial en un periodo orbital, consideramos la expresión completa de la función potencial [1]. Con la expresión completa del potencial y haciendo uso de las Ecuaciones de Lagrange [45] podemos estudiar la evolución de los elementos orbitales en el tiempo.

Los objetivos principales son; controlar la perturbación secular para que sea idéntica en todos los satélites de la constelación y minimizar las perturbaciones no seculares que afectan a nuestros satélites. Si logramos estos objetivos los satélites de la constelación se verán perturbados por el efecto del J_2 de la misma manera. De esta forma las posiciones relativas de los satélites serán prácticamente constantes (en el espacio de los elementos osculadores) y la estructura de *Flower Constellation* se mantendrá con el paso del tiempo, lo que denominamos como *Rigid Constellation*.

Para controlar la parte secular de los satélites de la constelación consideramos un satélite de referencia. Primero estudiamos la dependencia de la parte secular de los elementos osculadores con respecto a los valores iniciales de Ω y M. Observamos que ninguna de las componentes seculares depende del valor de Ω, pero observamos una fuerte dependencia con respecto al valor de M. En el caso particular de una 2D-LFC, todos los satélites tienen los mismos valores de a, e, i, ω, pero tienen distintos los valores de Ω y M. Por lo que, a priori, la componente secular de los elementos osculadores de cada satélite será distinta. Para conseguir que sea idéntica, aplicamos un método de corrección. Dicho método consiste en modificar el semieje mayor de todos los satélites unos pocos kilómetros. De esta forma el periodo (T_p) se verá modificado y en particular la componente secular de la variación de la anomalía media en el tiempo $\dot{M}_{sec} = 2\pi/T_p$. A través de esta corrección, conseguimos que la componente secular de los elementos osculadores de cada uno de los satélites de la constelación coincida hasta

un orden de 10^{-11}. Con esta técnica, conseguimos controlar la perturbación secular de nuestros satélites. Tratar de controlar la parte no secular resulta algo más complicado. En primer lugar, aplicamos para cada elemento osculador $q \in \{a, e, i, \omega, \Omega, M\}$ interpolación lineal sobre los pares de datos $(t, q(t))$ que han sido obtenidos previamente para calcular la posición exacta de los satélites. A través de estas funciones lineales de los elementos osculadores somos capaces de calcular en cada instante de tiempo una posición aproximada o lineal. De tal manera que la distancia entre ambas posiciones (real y lineal) será debida a las perturbaciones no seculares que afectan a nuestro satélite de referencia. El objetivo final consiste en analizar entre los posibles valores de la excentricidad y la inclinación aquellos que minimicen esta distancia (desviación). De esta forma, minimizamos la perturbación no secular que afecta a nuestro satélite de referencia. Estos valores serán extrapolables al resto de satélites de nuestra constelación. Consecuentemente, la perturbación no secular que afecta a los satélites de la constelación queda minimizada.

Mediante este trabajo somos capaces de diseñar 2D-LFCs cuya configuración se mantiene bajo los efectos del J_2, obteniendo las denominadas *Rigid Constellations*. La teoría que hemos desarrollado tiene dos aplicaciones directas. La primera consiste en validar la teoría de las 3D-LFCs, en el caso en que la función potencial no sea promediada en un periodo orbital, asumiendo que los semiejes son corregidos y el valor de la desviación es lo más pequeño posible. La segunda aplicación sirve para resolver problemas de cobertura global en los que se incluye el efecto del zonal J_2 en el potencial. Será suficiente con encontrar una *Rigid Constellation* que minimice una función fitness ligeramente modificada y podremos propagar los satélites en un modelo kepleriano.

Nuestro último objetivo consiste en reducir el elevado número de satélites que por lo general componen una constelación simétrica. Proporcionamos un método para determinar todos los subconjuntos de satélites de las 2D-LFCs de tal forma que sigan manteniendo las simetrías que las caracterizan [14].

Para conseguir este objetivo hemos identificado la primera órbita de nuestra constelación, que posee N_{so} posiciones admisibles con un collar ($\mathcal{G}$ (en inglés, *necklace*) de N_{so} perlas [15]. Tomamos un número N_{rso} ($N_{rso} < N_{so}$) representando los satélites reales por órbita. De esta forma consideramos la primer órbita de la constelación como un *necklace* de N_{so} perlas, de las cuales N_{rso} son negras y el resto blancas. Esto es, una órbita con N_{so} posiciones admisibles, de las cuales N_{rso} están ocupadas por un satélite y el resto no. La distribución de los satélites en las restantes órbitas es idéntica a la primera, pero desplazados k perlas.

De este modo una *Necklace Flower Constellation* (NFC) se caracteriza mediante un par $(\mathcal{G}, k)$. Notar que, no todos los pares producen NFC validas, ni dos pares distintos producen distintas NFC. Estos dos problemas se denominan problema de consistencia y de minimalidad, respectivamente. Utilizando teoría de numeros [3] somos capaces de resolverlos completamente. Finalmente, desarrollamos diversos teoremas de conteo para determinar la cantidad de pares posibles $(\mathcal{G}, k)$ que existen a partir de los parámetros de distribución de una 2D-LFC.

Las constelaciones de satélites son un tema de candente actualidad por las posibilidades que pueden proporcionar para los servicios comerciales e institucionales en aplicaciones como las telecomunicaciones, el posicionamiento dinámico o la observación de la Tierra, con costos razonables. Los resultados obtenidos en este trabajo estimulan el estudio de las mismas, que pueden resultar, en un futuro próximo, en constelaciones más eficientes que las actuales para diversas misiones espaciales.

Chapter 1

Preliminaries

This chapter introduces the background needed to understand all the remaining chapters of the thesis. A brief introduction to orbital mechanics is presented, not very extensive due to the wide and excellent bibliography that authors such as Vallado [45], Battin [10], Junkins [43], Chobotov [16], Arnold [6] or Abad [1], just to name a few, have written. One of the main subjects of this thesis is summarized, the theory of Flower Constellations developed by Mortari, Wilkins and Bruccoleri in [34], expanded by Mortari and Avendaño in [7], and also by Davis in [18]. Finally, two main tools are presented; the Dilution of Precision (DOP) which is a powerful accuracy metric of the observer-satellite geometry used by the Global Positioning System (GPS), and Evolutive algorithms, which are a novel way to solve certain optimization problems.

1.1 Orbital mechanics

1.1.1 Keplerian motion

In this work we are concerned in satellites orbiting around the Earth, hence the reference frames used to locate the position of the satellites have the Earth center as origin. The most commonly used reference frames with the previous property are:

- Earth Centered Inertial [45] (ECI): It has the origin at the center of the Earth, as the name implies, and it is designated with the letters IJK. The I and J axes are contained in Earth's equatorial plane. The I axis points towards the vernal equinox; the J axis is 90° to the East in the equatorial plane; the K axis extends through the North Pole.

- Earth Centered Earth Fixed [45] (ECEF): It is fixed to the rotating Earth and is designated with the letters XYZ. It has the origin at the center of the Earth. The X and Y axes are contained in Earth's equatorial plane. The X axis points to the Greenwich meridian; the Y axis is 90° to the East in the equatorial plane; the Z axis points to the North Pole.

Newton's laws of motion describe the relationship between the satellite motion and the forces acting on it. The three laws of motion were first compiled by Sir Isaac Newton

in his work Philosophiae Naturalis Mathematica [37], first published in 1687. These laws are [17, p.44]:

Newton's First Law: Every particle continues in a state of rest or uniform motion in a straight line unless it is compelled by some external force to change that state.

Newton's Second Law: The rate of change of the linear momentum of a particle is proportional to the force applied to the particle and takes place in the same direction as the force.

Newton's Third Law: The mutual actions of any two bodies are always equal and oppositely directed.

In *The Principia* of Newton [37] was also published in the Proposition 75, Theorem 35, the Newton's Gravitational law which states [17, p.135]:

Newton's Gravitational Law: Any two point masses attract one another with a force proportional to the product of their masses and inversely proportional to the square of the distance between them.

The starting points for studying the orbital motion are Newton's Laws. We examine the force that the Earth exerts on a satellite. If the satellite mass is m_{sat}, the Earth mass is $M_\oplus$, and the distance to the satellite from the center of the Earth is r, then the force that the Earth exerts on a satellite following the Gravitational Law is:

$$\mathbf{F} = -\frac{GM_\oplus m_{sat}}{r^2}\hat{r} = -\frac{GM_\oplus m_{sat}}{r^3}\mathbf{r}, \tag{1.1}$$

where G is the gravitational constant [45, p.136]

$$G = (6.67259 \pm 0.00085)\cdot 10^{-20} \quad km^3\ kg^{-1}\ sec^{-2},$$

$\hat{r}$ is the unit vector pointing from the Earth center to the satellite, and r represents the modulus of vector $\mathbf{r}$.

By using the Newton's Second Law, the acceleration that the Earth exerts to the satellite is given by:

$$\ddot{\mathbf{r}} = \frac{\mathbf{F}}{m_{sat}}. \tag{1.2}$$

All together this translates into the keplerian two-body equation of motion:

$$\ddot{\mathbf{r}} = -\frac{\mu}{r^3}\mathbf{r}, \tag{1.3}$$

where

$$\mu = GM_\oplus = 398,600.4405 \pm 0.001 \quad km^3\ sec^{-2}.$$

The discovery of the law of universal gravitation by Newton was motivated by the previous work done by Kepler. Newton was fascinated by the beauty and precision of Kepler's laws and set about the task of discovering what force law must be existing between bodies in the Solar system to be consistent with kepler's experimentally verified laws of planetary motion. The Kepler's laws are [45, p.10]:

First Law: The orbit of each planet is an ellipse with the Sun at one focus.

Second Law: The line joining the planet to the Sun sweeps out equal areas in equal times.

Third Law: The square of the period of a planet is proportional to the cube of its mean distance to the Sun.

These laws were published by Johannes Kepler, derived using Tycho Brahe's observations of Mars. We will show below that Kepler's Laws can be derived from Newton's Laws.

The *angular momentum* of the satellite is defined by:

$$\mathbf{h} = \mathbf{r} \times \mathbf{v},$$

where $\mathbf{r}$ and $\mathbf{v}$ are its position and velocity vector, respectively. We denote h the norm of the vector $\mathbf{h}$. The angular momentum in the keplerian motion is constant [41, p.2]:

$$\frac{d\mathbf{h}}{dt} = \frac{d(\mathbf{r} \times \mathbf{v})}{dt} = \mathbf{r} \times \ddot{\mathbf{r}} + \underbrace{\dot{\mathbf{r}} \times \mathbf{v}}_{=0} = \mathbf{r} \times -\frac{\mu}{r^3}\mathbf{r} = 0. \tag{1.4}$$

The sweep velocity of the satellite is given by [4, p.594]:

$$V_{sweep} = \frac{1}{2}|\mathbf{r} \times \mathbf{v}|, \tag{1.5}$$

and it represents half of the modulus of the angular momentum. The property of having a constant angular momentum implies that the sweep velocity is constant, which proves Kepler's second law. Note that, we always have $\mathbf{r} \perp \mathbf{h}$ by definition of $\mathbf{h}$. Then, if the angular momentum $\mathbf{h} \neq 0$ the motion is not rectilinear and it takes places on a plane.

The *eccentricity vector* $\mathbf{e}$ is defined as [45, p.106]:

$$\mu\mathbf{e} = \mathbf{v} \times \mathbf{h} - \frac{\mu}{r}\mathbf{r}.$$

We denote e the norm of the vector $\mathbf{e}$. In the keplerian motion the eccentricity vector is constant:

$$\begin{aligned}
\frac{d(\mu\mathbf{e})}{dt} &= \frac{d\mathbf{v}}{dt} \times \mathbf{h} + \underbrace{\mathbf{v} \times \frac{d\mathbf{h}}{dt}}_{=0} - \mu\frac{d(r^{-1}\mathbf{r})}{dt} \\
&= -\frac{\mu}{r^3}\mathbf{r} \times \mathbf{h} - \mu\frac{d\left((\mathbf{r}\cdot\mathbf{r})^{-1/2} \cdot \mathbf{r}\right)}{dt} \\
&= -\mu\frac{\mathbf{r}\cdot\mathbf{v}}{r^3}\mathbf{r} + \mu\frac{\mathbf{r}\cdot\mathbf{r}}{r^3}\mathbf{v} - \mu\left(-\frac{\mathbf{r}\cdot\mathbf{v}}{r^3}\mathbf{r} + \frac{1}{r}\mathbf{v}\right) \\
&= 0.
\end{aligned} \tag{1.6}$$

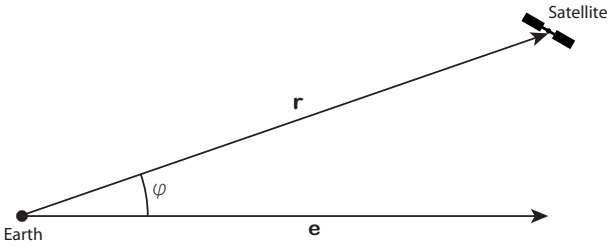

Figure 1.1: True anomaly.

The three components of $\mathbf{h}$ and the three of $\mathbf{e}$ are not independent since:

$$\begin{aligned} \mathbf{h}\cdot\mathbf{e} &= \mathbf{h}\cdot\frac{1}{\mu}\left(\mathbf{v}\times\mathbf{h}-\frac{\mu}{r}\mathbf{r}\right) \\ &= \frac{1}{\mu}\underbrace{\mathbf{h}\cdot(\mathbf{v}\times\mathbf{h})}_{=0}-\frac{1}{r}\underbrace{\mathbf{h}\cdot\mathbf{r}}_{=0} \\ &= 0. \end{aligned} \tag{1.7}$$

The *energy* of the satellite is defined as:

$$E=\frac{\mathbf{v}^2}{2}-\frac{\mu}{r}, \tag{1.8}$$

which is another constant:

$$\begin{aligned} \frac{dE}{dt} &= \frac{1}{2}\frac{d\mathbf{v}^2}{dt}-\mu\frac{d(r^{-1})}{dt} \\ &= \mathbf{v}\cdot\dot{\mathbf{v}}-\mu\frac{d\left((\mathbf{r}\cdot\mathbf{r})^{-1/2}\right)}{dt} \\ &= \mathbf{v}\cdot\left(-\frac{\mu}{r^3}\mathbf{r}\right)-\frac{\mu}{r^3}\mathbf{r}\cdot\mathbf{v} \\ &= 0. \end{aligned} \tag{1.9}$$

By taking the dot product of the eccentricity vector with the position, we get:

$$\begin{aligned} \mathbf{r}\cdot\mathbf{e} &= \frac{1}{\mu}\mathbf{r}\cdot\mathbf{v}\times\mathbf{h}-\frac{\mathbf{r}\cdot\mathbf{r}}{r} \\ &= \frac{(\mathbf{r}\cdot\mathbf{r})(\mathbf{v}\cdot\mathbf{v})-(\mathbf{r}\cdot\mathbf{v})(\mathbf{v}\cdot\mathbf{r})}{\mu}-r \\ &= \frac{h^2}{\mu}-r. \end{aligned} \tag{1.10}$$

If $\mathbf{e}\neq 0$ we define the *true anomaly* φ, illustrated in Figure 1.1, as the angle between vector $\mathbf{e}$ and the position vector $\mathbf{r}$,

$$\mathbf{r}\cdot\mathbf{e}=re\cos(\varphi). \tag{1.11}$$

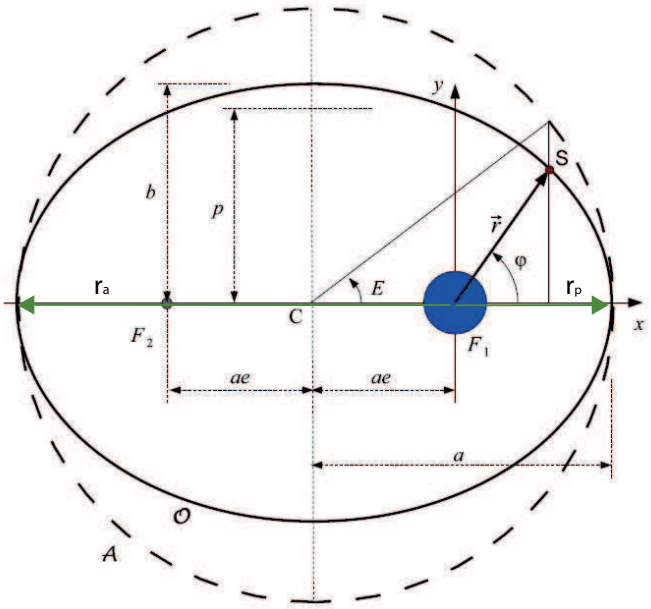

Figure 1.2: Elliptical orbit geometry.

By using Eq. (1.10) and Eq. (1.11) we obtain:

$$r = \frac{p}{1 + e\cos(\varphi)}, \tag{1.12}$$

where $p = h^2/\mu$. This is the polar equation of a conic section of eccentricity equal to e with focus at the origin. This together with the fact that the motion is planar proves Kepler's First Law. The eccentricity indicates whether the conic intersection is elliptic ($0 \leq e < 1$), parabolic ($e = 1$) or hyperbolic ($e > 1$).
In the case of an ellipse we have a maximum and a minimum value of r in two points named perigee ($\varphi = 0$) and apogee ($\varphi = \pi$), respectively. The distances to the focus from these two points are given by:

$$r_p = \frac{p}{1+e}, \qquad r_a = \frac{p}{1-e}. \tag{1.13}$$

Figure 1.2 [12] illustrates a satellite S orbiting the Earth on an elliptical orbit $\mathcal{O}$ of semi-major axis a and eccentricity e. It shows the perigee and apogee distances, the semilatus rectum p, the semi-minor axis b, and the constant $c = ae$:

$$p = a(1-e^2), \qquad b = a\sqrt{1-e^2}, \qquad c = ae = \frac{pe}{1-e^2}. \tag{1.14}$$

Finally, the Kepler's Third Law can be derived as follows:

$$\begin{aligned} T_p &= \frac{\text{Ellipse area}}{\text{Sweep velocity}} = \frac{\pi ab}{\frac{1}{2}h} \\ &= \frac{2\pi ab}{\sqrt{\mu p}} = \frac{2\pi a(a\sqrt{1-e^2})}{\sqrt{\mu a(1-e^2)}} \end{aligned}$$

$$= \frac{2\pi a^{3/2}}{\sqrt{\mu}}. \tag{1.15}$$

In the elliptic case, the Energy equation (1.8) is [17, p.65]:

$$\mathbf{v}^2 = \mu\left(\frac{2}{r} - \frac{1}{a}\right). \tag{1.16}$$

Squaring the angular momentum [17, p.131] we get:

$$\begin{aligned} h^2 &= (\sqrt{\mu p})^2 = \mu a(1-e^2), \\ h^2 &= |\mathbf{r}\times\mathbf{v}|^2 = \mathbf{v}^2\mathbf{r}^2 - (\mathbf{r}\cdot\mathbf{v})^2 = \mathbf{v}^2\mathbf{r}^2 - (rv)^2. \end{aligned}$$

Then,

$$\mu a(1-e^2) = \mathbf{v}^2\mathbf{r}^2 - (rv)^2. \tag{1.17}$$

Substituting the expression of $\mathbf{v}^2$ given in Eq. (1.16) in Eq. (1.17), we obtain:

$$\mu a(1-e^2) = \mu\left(\frac{2}{r} - \frac{1}{a}\right)\mathbf{r}^2 - (rv)^2. \tag{1.18}$$

Define E by

$$r = a(1 - e\cos(E)), \tag{1.19}$$

where E is named the *eccentric anomaly*. As true anomaly φ, already introduced, varies from 0° to 360°, E also varies in the range 0° to 360°. Differentiating Eq. (1.19) we get:

$$\dot{r} = v = ae\dot{E}\sin(E). \tag{1.20}$$

Substituting into Eq. (1.18) and rearranging, we obtain:

$$\frac{a^3}{\mu}\dot{E}^2(1 - e\cos(E))^2 = 1. \tag{1.21}$$

Now the orbit is described so that dE/dt is positive, so that

$$dt = \sqrt{\frac{a^3}{\mu}}(1 - e\cos(E))dE. \tag{1.22}$$

Integrating over a complete revolution we get for the period:

$$T_p = 2\pi\sqrt{\frac{a^3}{\mu}} = \frac{2\pi}{n}, \tag{1.23}$$

where $n = \sqrt{\mu/a^3}$ is the *mean motion*. Thus, Eq. (1.22) can be written, as:

$$n\,dt = (1 - e\cos(E))dE, \tag{1.24}$$

which can be integrated immediately to give:

$$n(t - t_0) = E - e\sin(E), \tag{1.25}$$

where t_0 is the time of passage through the perigee. Eq. (1.25) is named *Kepler's Equation* usually written in the form:

$$M = E - e\sin(E), \tag{1.26}$$

where M is the *mean anomaly*, defined by

$$M = n(t - t_0). \tag{1.27}$$

The relation between the true anomaly (φ) and the eccentric anomaly (E) can be observed in Figure 1.2, and they are related by the formula:

$$\tan\left(\frac{\varphi}{2}\right) = \sqrt{\frac{1+e}{1-e}}\tan\left(\frac{E}{2}\right). \tag{1.28}$$

At this point, the position and velocity of a satellite can be obtained from the following six integrals of motion, called in Astrodynamics the *classical orbital elements*; two of them describe the shape of the orbit, the *semi-major axis* (a) and the *eccentricity* (e). Three of them situate the orbital plane, the *inclination* (i), which is the angular distance between the orbital plane and the plane of reference (Equatorial plane), the *argument of perigee* (ω), which is the angle between the orbit's perigee (the point of closest approach to the Earth) and the orbit's ascending node (the point where the satellite crosses the Equatorial plane from South to North), and the *Right Ascension of the Ascending Node* (Ω), which represents the angular distance between the orbit's ascending node and the reference axis of our inertial system (pointing to Greenwich meridian). Finally, a sixth parameter which determines the position of the body on its orbit. This parameter is one of the three angular variables presented above; *true anomaly*, *mean anomaly* or *eccentric anomaly*. Figure 1.3 illustrates the orbital elements.

1.1.2 Perturbed motion

A conservative force field is one with the property that the work done in moving a particle from a point A to a point B is independent of the path taken. The gravitational field around the Earth is the sum of conservative force field corresponding to each of its particles, hence conservative. It is shown in [5] that any conservative force field can be expressed as:

$$F(\mathbf{r}) = -m_{sat} \cdot \nabla V(\mathbf{r}). \tag{1.29}$$

where $V(\mathbf{r})$ is the potential function [29], which measures how much work has to be done to the satellite from rest in a reference position $\mathbf{r}_0$ close to infinity to rest at position $\mathbf{r}$.

The Earth is not a perfect sphere, it has the shape of an oblate spheroid with an equatorial diameter that exceeds the polar diameter by about $20\,km$. The perturbation

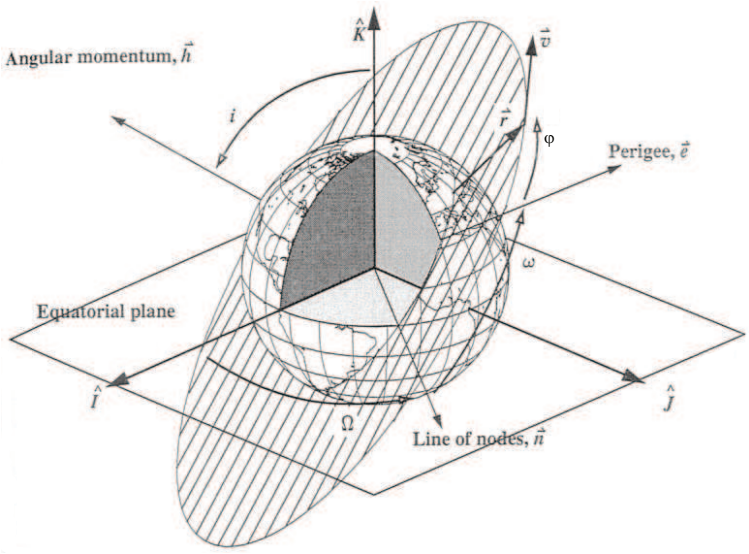

Figure 1.3: Orbital elements.

(**P**) produced by this fact is about three orders of magnitude smaller than the central attraction described before using Newton's law of universal gravitation. Then, Eq. (1.3) can be reformulated as:

$$\ddot{\mathbf{r}} = -\frac{\mu}{r^3}\mathbf{r} + \mathbf{P}, \tag{1.30}$$

which is known in Astrodynamics as the perturbed two-body problem. Then, the key of the particular problem of a satellite orbiting around the Earth consists of determining the potential function that affects to the satellite to determine its acceleration.

The satellite motion represented by the second order equation (1.30) can be expressed as a first order system of equations:

$$\begin{cases} \dot{\mathbf{r}}(t) &= \mathbf{v}(t), \\ \dot{\mathbf{v}}(t) &= -\nabla V(\mathbf{r}(t)), \end{cases} \tag{1.31}$$

where $\mathbf{r}(t)$ and $\mathbf{v}(t)$ represent the position and velocity of the satellite at time t, respectively.

If we consider the Earth as a perfect sphere with constant density (keplerian model), the potential function must be:

$$V_{kep}(\mathbf{r}) = -\frac{\mu}{r}, \tag{1.32}$$

to satisfy Eq. (1.3).

However, if we consider each point of the Earth, then the potential function is [45]:

$$\begin{aligned} V(\mathbf{r}, \phi_{sat}, \lambda_{sat}) = -\frac{\mu}{r}\left[1 - \sum_{l=2}^{\infty} J_l \left(\frac{r_\oplus}{r}\right)^l P_l\left(\sin(\phi_{sat})\right) + \right. \\ \left. + \sum_{l=2}^{\infty}\sum_{m=1}^{l} \left(\frac{r_\oplus}{r}\right)^l P_{l,m}\left(\sin(\phi_{sat})\right)\left[C_{l,m}\cos(m\cdot\lambda_{sat}) + S_{l,m}\sin(m\cdot\lambda_{sat})\right]\right], \end{aligned} \tag{1.33}$$

where $P_l(t)$ is the l-order Legendre Polynomial, $P_{l,m}$ is the l-order, m-degree associated Legendre Polynomial, which are defined from the derivatives of the Legendre Polynomial as follows:

$$P_l(t) = \frac{1}{2^l\, l!}\frac{d^l}{dt^l}(t^2-1)^l, \qquad Q_{l,m}(t) = \frac{d^m}{dt^m}P_l(t), \qquad P_{l,m}(t) = (1-t^2)^{m/2}Q_{l,m}(t),$$

and $(\lambda_{sat}, \phi_{sat}) \in [0, 2\pi] \times [-\pi/2, \pi/2]$ represents the longitude and latitude of the satellite from the center of the Earth, respectively.

Note that, in Eq. (1.33) the potential is inversely proportional with respect to the distance to the Earth. The terms J_l are called zonal harmonics, the terms $C_{l,m}$ and $S_{l,m}$ when $m \neq 0$ and $l \neq m$ are called tesseral harmonics, and the terms $C_{l,m}$ and $S_{l,m}$ when $m \neq 0$ and $l = m$ are called sectorial harmonics. Zonal and tesseral harmonics are illustrated in Figure 1.4, while sectorial harmonics are illustrated in Figure 1.5. See [29] for more precise information.

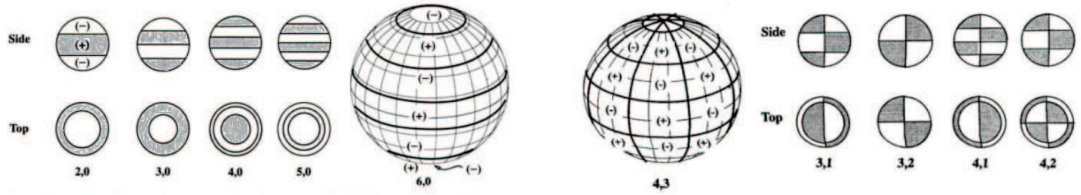

Figure 1.4: Zonal and Tesseral harmonics.

In our study we consider the Earth as a revolution body, then the tesseral and sectorial harmonics will be zero, and the potential will have only zonal harmonics. Table 1.1 shows the values of the zonal harmonics [1, p.228]:

1.1.2.1 Evolution of position and velocity in the perturbed problem

The expression of the potential considering only the zonal harmonics (J_l) is:

$$V(\mathbf{r}) = -\frac{\mu}{r}\left[1 - \sum_{l=2}^{\infty} J_l \left(\frac{r_\oplus}{r}\right)^l P_l\left(\sin(\phi_{sat})\right)\right], \tag{1.34}$$

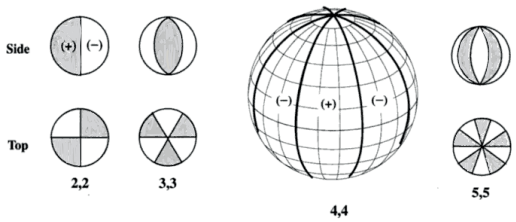

Figure 1.5: Sectorial harmonics.

J_2	$1.08263 \cdot 10^{-3}$
J_3	$-2.53243 \cdot 10^{-6}$
J_4	$-1.61933 \cdot 10^{-6}$
J_5	$-2.27716 \cdot 10^{-7}$
J_6	$5.39648 \cdot 10^{-7}$
$\vdots$	$\vdots$

Table 1.1: Zonal harmonic coefficients for Earth perturbed potential.

and it is usually split in several parts: the Keplerian component V_{kep} and the zonal harmonic components, R_{J_2}, R_{J_3}, etc:

$$\begin{aligned} V(\mathbf{r}) &= V_{kep} + R \\ &= V_{kep} + R_{J_2} + R_{J_3} + \dots \end{aligned} \tag{1.35}$$

We apply the gradient operator to the potential function:

$$\begin{aligned} \nabla V &= \left(\frac{\partial V}{\partial x}, \frac{\partial V}{\partial y}, \frac{\partial V}{\partial z} \right) \\ &= \left(\frac{\partial V_{kep}}{\partial x} + \frac{\partial R_{J_2}}{\partial x} + \frac{\partial R_{J_3}}{\partial x} + \dots, \frac{\partial V_{kep}}{\partial y} + \frac{\partial R_{J_2}}{\partial y} + \frac{\partial R_{J_3}}{\partial y} + \dots \right. \\ &\left. \dots, \frac{\partial V_{kep}}{\partial z} + \frac{\partial R_{J_2}}{\partial z} + \frac{\partial R_{J_3}}{\partial z} + \dots \right). \end{aligned} \tag{1.36}$$

Then, by using Eqs. (1.31) it is possible to derive the state vector of the satellite from the following system of equations:

$$\begin{cases} \dot{x} = v_x, \\ \dot{y} = v_y, \\ \dot{z} = v_z, \\ \dot{v_x} = -\dfrac{\partial V}{\partial x}, \\ \dot{v_y} = -\dfrac{\partial V}{\partial y}, \\ \dot{v_z} = -\dfrac{\partial V}{\partial z}. \end{cases} \tag{1.37}$$

This system of equations can be solved numerically by using a Runge-Kutta Method of order 4. The solution represents the evolution of position and velocity over time. Note that, the more terms we include in the potential function, the more precise the estimation of the position and velocity will be.

1.1.2.2 Evolution of the orbital elements in the perturbed problem

In the keplerian motion, all the orbital elements except M are constant. The evolution of them over time can be represented as a straight line, since M increases linearly:

$M(t) = nt$ where $n = \sqrt{\mu/a^3}$ is the mean motion. When some perturbations appear, the orbital elements are not longer constant. However, the model can be considered instantaneously as a keplerian model, i.e. at each instant of time is possible to describe the movement as a keplerian motion, using six orbital elements which depend on time. These parameters are named *osculating elements*; $a(t)$, $e(t)$, $i(t)$, $\omega(t)$, $\Omega(t)$ and $M(t)$.

Lagrange planetary Equations [45, pg. 585]: are a powerful tool to compute the variation of the osculating elements over time:

$$\begin{cases} \dot{a} = -\dfrac{2}{na}\dfrac{\partial R}{\partial M}, \\ \dot{e} = -\dfrac{1-e^2}{na^2 e}\dfrac{\partial R}{\partial M} + \dfrac{\sqrt{1-e^2}}{na^2 e}\dfrac{\partial R}{\partial \omega}, \\ \dot{i} = \dfrac{1}{na^2\sqrt{1-e^2}\sin(i)}\dfrac{\partial R}{\partial \Omega} - \dfrac{\cos(i)}{na^2\sqrt{1-e^2}\sin(i)}\dfrac{\partial R}{\partial \omega}, \\ \dot{\omega} = -\dfrac{\sqrt{1-e^2}}{na^2 e}\dfrac{\partial R}{\partial e} + \dfrac{\cos(i)}{na^2\sqrt{1-e^2}\sin(i)}\dfrac{\partial R}{\partial i}, \\ \dot{\Omega} = -\dfrac{1}{na^2\sqrt{1-e^2}\sin(i)}\dfrac{\partial R}{\partial i}, \\ \dot{M} = n + \dfrac{2}{na}\dfrac{\partial R}{\partial a} + \dfrac{1-e^2}{na^2 e}\dfrac{\partial R}{\partial e}. \end{cases} \tag{1.38}$$

where R represents the perturbing part of the potential presented in Eq. (1.35).

Note that, Lagrange Planetary Equations only consider the perturbed part of the potential, R. This system of equations can be solved using a Runge-Kutta Method of order 4. The solution represents the evolution of the orbital elements over time. Note that, the more terms we include in the potential function, the more precise the estimation of the position and velocity will be.

1.2 Satellite Constellations

The initial position of a satellite orbiting around the Earth is determined using the classical orbital elements. Then, the first idea to describe a satellite constellation of n satellites, may consist of giving the orbital elements of each one. However, choosing $6n$ independent, continuous parameters is something prohibitive if the constellation has more than 20 satellites. One solution to deal with this curse of dimensionality may consist of having some common orbital parameters for each satellite, thus the number of design variables are strongly reduced.

J.G. Walker developed around 1970s a method to design satellite constellations [47,48]. The satellites in this kind of constellations, called Walker Constellations, have the same semi-major axis (a), the same inclination (i) and they are distributed in circular orbits ($e = 0$). The Right Ascension of the Ascending Node (RAAN) and the true anomaly of each satellite is determined using these three integer parameters:

- T is the total number of satellites in the constellation.
- P is the number of orbital planes.
- F is a phasing parameter.

Walker hypothesized [18, p.12] that optimal constellations would be symmetrical and uniform in their distributions of satellites. Thus, he designs the constellation as follows: the RAAN of the satellites in the P orbital planes are equally distributed around the equator. The satellites within a given orbital plane are also uniformly distributed in mean anomaly. Defining the Pattern Unit (PU) $1PU = 360°/T$, when a satellite on a given plane passes through the ascending node, the satellite on the next adjacent plane to the east has advanced $F \cdot PUs$ past its ascending node. The values of F are limited to the range $[0, P-1]$. Consequently, three integer parameters (T, P, F) and two continuous parameters (a, i) are enough to describe this kind of satellite constellations.

1.2.1 The Flower Constellations

As Draim shows in his work [21], eccentric orbits may be better than circular ones. Thus, another way of designing satellite constellations, without the necessity of having circular orbits, is required. D. Mortari developed around 2004 The Flower Constellations [34, 51] which solve this problem by leaving the eccentricity as a design variable. In this section we briefly describe the evolution of the theory.

The original theory of Flower Constellations has all the satellites in the same repetitive ground-track, or in other words, the same repetitive ground-track relative to the rotating reference frame of the Earth. All the orbits have the same eccentricity (e), inclination (i), and argument of perigee (ω). In order to have all the satellites in the same ground track the compatibility (or resonant) condition must be satisfied:

$$N_p\, T_p = N_d\, T_d, \tag{1.39}$$

where N_p is the number of orbital periods before repetition, T_p is the keplerian orbital period, N_d is the number of revolutions of the rotating reference frame before repetition, and T_d is the period of the rotating reference frame, which in the case of the Earth is a sidereal day. Note that, given the values of N_p, and N_d the value of the semi-major axis (a) is automatically determined. In addition, the effect of J_2 perturbation can be accounted for in the values of T_d and T_p to maintain repeating ground tracks under the J_2 effect [34].

Once the orbit is described the following step is to define the Right Ascension of the Ascending Node (Ω_k) and Mean anomaly (M_k) of the N_{sat} satellites of the constellation. For that purpose three integers (phasing parameters) must be chosen: F_n, F_d and F_h. Finally, the values of Ω_k and M_k are determined using recursively the following equations [35, 50]:

$$\Omega_{k+1} \;=\; \Omega_k + 2\pi \frac{F_n}{F_d}, \qquad k \in [0, N_{sat} - 1].$$

$$M_{k+1} = M_k - 2\pi \frac{N_p F_n + F_d F_h(k)}{F_d N_d}, \qquad k \in [0, N_{sat} - 1]. \tag{1.40}$$

Note that, $F_h(k)$ could be any sequence of numbers from the set $[0, N_d - 1]$ but it is typically chosen to be constant. Then, with the three continuous parameters (e, i, ω) and the six integer parameters $(N_{sat}, N_p, N_d, F_n, F_d, F_h)$ the constellation is completely described. The parameters Ω_0 and M_0 are usually set to zero, but they can be also considered design variables.

The Flower Constellations evolved into the Harmonic Flower Constellations after proving that the number of satellites in a Flower Constellation can not exceed [9]:

$$\frac{N_d F_d}{\gcd(N_d, N_p F_n + F_d F_h)}.$$

This constraint about the maximum number of satellite per orbit allows to reduce one of the integer parameters that defines a Flower Constellation, and reformulate the others to have more understandable and physical parameters. Since the maximum number of satellites is known, and the number of orbits is represented by the parameter F_d, it is possible to infer that the number of satellites per orbit is:

$$N_{so} = \frac{N_d}{\gcd(N_d, N_p F_n + F_d F_h)}.$$

Furthermore, a new parameter called configuration number is defined as [9]:

$$N_c = E_n \frac{N_p F_n + F_d F_h}{\gcd(N_p, N_p F_n + F_d F_h)} \mod (F_d),$$

where E_n and E_d are any integers such that $E_n F_n + E_d F_d = 1$. This parameter is the key to characterize Harmonic Flower Constellations. However, a requirement for the existence of an Harmonic Flower Constellation is,

$$\gcd(F_d, N_{so}, N_c) = 1.$$

The Harmonic Flower Constellations are visualized through the (Ω, M)-space [8], where the admissible locations for the satellites in the constellation are described. The Harmonic Flower Constellations solved the problem of equivalency (two HFC are said to be equivalent if and only if their (Ω, M)-space representations coincide) and similarity, but a simple procedure to compute the (Ω, M)-space from the parameters F_d, N_{so} and N_c is necessary. The extension of the theory into the 2D Lattice Flower Constellation (2D-LFC) [7] solves this problem.

The 2D Lattice Flower Constellations can be described by five integer parameters and three continuous ones. The integer parameters can be broken into two sets, the first describing the phasing of the satellites and the second describing the orbital period (or semi-major axis). The first set is $\{N_o, N_{so}, N_c\}$ where N_o is the number of orbital

planes, N_{so} is the number of satellites per orbit, and N_c is the configuration number. The second set is $\{N_p, N_d\}$ which satisfies the compatibility equation (1.39), which enforces the repeating space-track requirement.

The location of all the satellites of a 2D-LFC corresponds to a Lattice in the (Ω, M)-space [7], which can be regarded as a 3D torus (both axes, M and Ω, are modulo 2π) and coincides with all the solutions of the following system of equations:

$$\begin{pmatrix} N_o & 0 \\ N_c & N_{so} \end{pmatrix} \begin{pmatrix} \Omega \\ M \end{pmatrix} \equiv 0 \mod (2\pi). \tag{1.41}$$

The solutions of Eq. (1.41) can be parameterized as follows:

$$\begin{pmatrix} N_o & 0 \\ N_c & N_{so} \end{pmatrix} \begin{pmatrix} \Omega_{ij} \\ M_{ij} \end{pmatrix} = 2\pi \begin{pmatrix} i \\ j \end{pmatrix}, \tag{1.42}$$

where $i = 0, \cdots, N_o - 1$, $j = 0, \cdots, N_{so} - 1$, and $N_c \in [0, N_o - 1]$. Satellite (i, j) is the j-th satellite on the i-th orbital plane. Consequently, the total number of satellites in the constellation $N_{sat} = N_o N_{so}$.

We represent two different (Ω, M)-spaces to show how the parameter N_c influences the distribution of the satellites. In Figure 1.6 we plot the (Ω, M)-space of a 24-satellite constellation with parameters $N_o = 4, N_{so} = 6, N_c = 0$, while in Figure 1.7 we plot the (Ω, M)-space of a 24-satellite constellation with parameters $N_o = 4, N_{so} = 6, N_c = 2$.

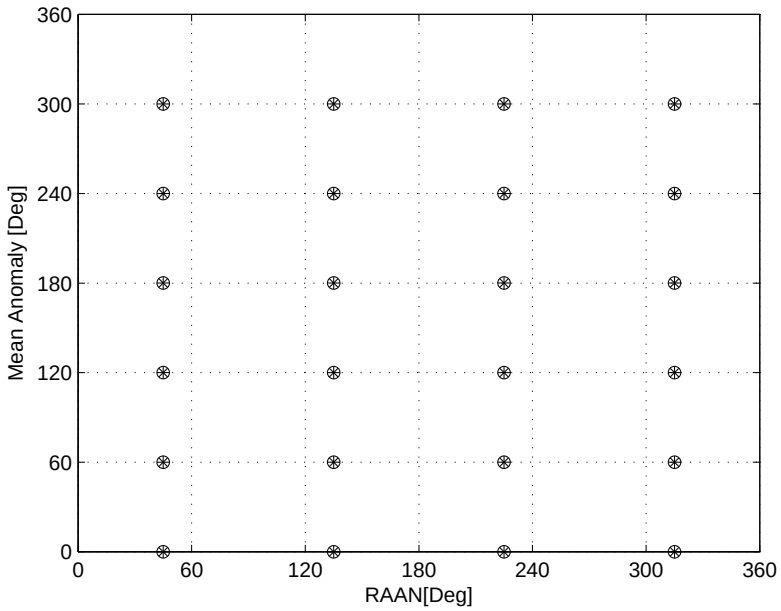

Figure 1.6: 2D-LFC with $N_o = 4$, $N_{so} = 6$, $\mathbf{N_c} = \mathbf{0}$, $\Omega_{00} = 45.0$, and $M_{00} = 0.0$

Note that, the Mean anomalies of the satellites of the second and fourth orbits in Figure 1.7 are shifted with respect to those shown in Figure 1.6 due to the effect of the parameter N_c.

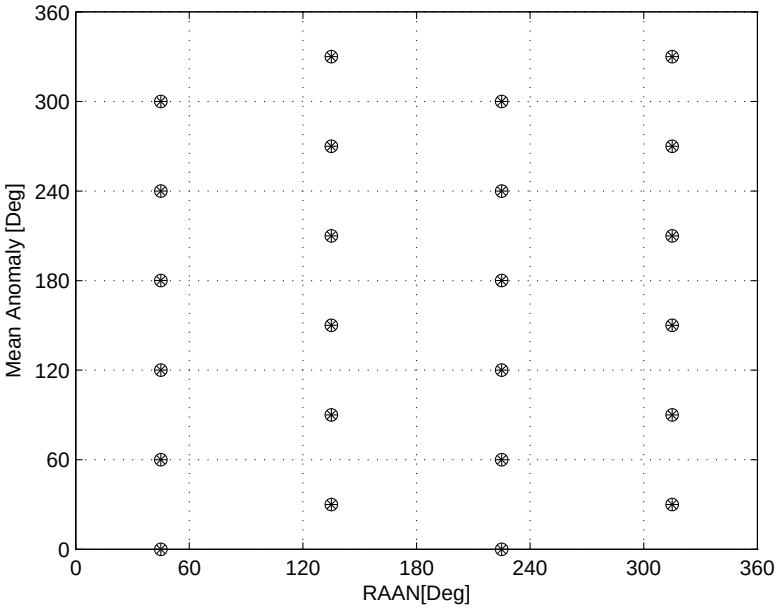

Figure 1.7: 2D-LFC with $N_o = 4$, $N_{so} = 6$, $\mathbf{N_c} = \mathbf{2}$, $\Omega_{00} = 45.0$, and $M_{00} = 0.0$

The remaining parameters required to define the constellation are continuous and the same for all orbits in the constellation: the inclination, the eccentricity, and the argument of perigee. Since all satellites of a 2D-LFC have the same a, e, i, and ω, when the (Ω, M)-space is provided the constellation is completely defined.

To sum up, a 2D-LFC can be viewed as a vector in $\mathbb{N}^3 \times \mathbb{R}^6$ containing the 3 integer parameters (N_o, N_{so}, N_c) describing the layout of the satellites in the (Ω, M)-space, and the 6 continuous orbital parameters (a, e, i, ω, Ω_{00}, M_{00}) of the reference satellite. It can also be regarded as a function $FC(t)$ that gives the position of the $N_{so}N_o$ satellites at time t.

Note that, since the 2D-LFC theory separates the satellite phasing from the orbit size, non-repeating space-tracks can be used without affecting the uniformity of the satellite distribution. However, the condition that all satellites belong to the same repeating ground track can be recovered by choosing any two coprime integers μ and λ, defining:

$$\begin{aligned} N_d &= \lambda N_{so}, \\ N_p &= \mu N_o + \lambda N_c, \end{aligned}$$

and adjusting the semi-major axis according to Eq. (1.39).

For practical applications, we are assuming that the period of the rotational reference frame T_d is constant. Furthermore, the semimajor axis of the satellites is fixed depending on the sort of mission, this means that T_p is known. Thus, the interest of having all the satellites in the same ground-track disappeared, and we can adopt two different points of view. The first case consists of considering that there always exist integers

N_p, N_d such that the ratio N_p/N_d approximates the ratio T_d/T_p. In the second case the constellation may not be compatible with respect to the rotating reference frame (ECEF), since T_p is not necessarily a rational multiple of T_d, but there are infinitely many rotating frames compatible with the constellation. In these rotating frames the trajectory of the satellites is static, but respect to the inertial frame the trajectory rotates with angular velocity:

$$\omega_d = \frac{2\pi N_d}{N_p T_p}. \tag{1.43}$$

As an illustration, the same 2D-LFC is presented in two different rotating reference frames. The phasing parameters are $N_o = 3, N_{so} = 8$, and $N_c = 2$. The continuous parameters are $a = 28000\,km$, $e = 0$, and $i = 55°$. It is possible to observe that the number of relative trajectories followed by the satellites varies depending on the velocity of the rotating reference frame, or in other word, depending on the parameters N_p and N_d.

In Figure 1.8 the 2D-LFC has parameters $N_p = 1$ and $N_d = 0$. Then, using Eq. (1.43) the velocity of the rotating reference frame is $\omega_d = 0$, i.e. the inertial frame (ECI). On the other hand, in Figure 1.9 the 2D-LFC has parameters $N_p = 3$ and $N_d = 12$, and using (1.43) the ground track rotates with angular velocity $\omega_d = 5.39 \cdot 10^{-4}\,rad/sec$. Consequently, none of them is compatible with the Earth rotating reference frame since the angular velocity is $\omega_\oplus = 7.2722 \cdot 10^{-5}\,rad/sec$.

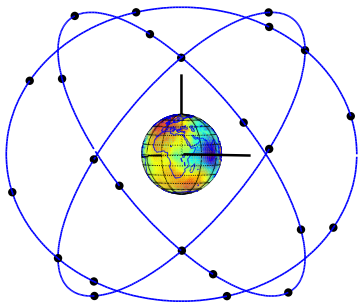

Figure 1.8: A 2D-LFC with three relative trajectories.

In the 2D-LFC theory elliptic orbits are generally avoided due to the rotation of the apsidal line due to Earth's oblateness (the J_2 effect). The 3D Lattice Flower Constellation (3D-LFC) theory [18, 19] utilize, rather than avoid, the J_2 effect to produce uniform constellations of elliptic orbits.

The rotation of the argument of perigee is only meaningful in elliptic orbits. Furthermore, if the critical inclination is considered 63.4° or 116.6° the argument of perigee

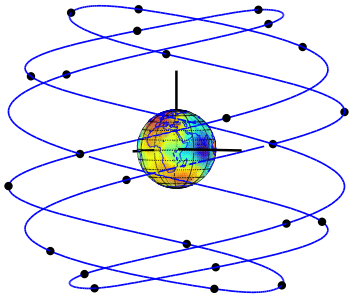

Figure 1.9: A 2D-LFC with all the satellites in the same ground track.

experiences no rotation, but one of the design variables is eliminated. This theory proposes that the satellites within a given orbital plane be placed in multiple orbits with arguments of perigee distributed evenly in the range $[0°, 360°]$. Since all orbits have the same inclination, eccentricity and semi-major axis, their rate of perigee rotation will be approximately equal. Thus, as they each rotate, the relative perigee spacing remains constant, and periodically the constellation resumes its original structure. The concept is illustrated in Figure 1.10.

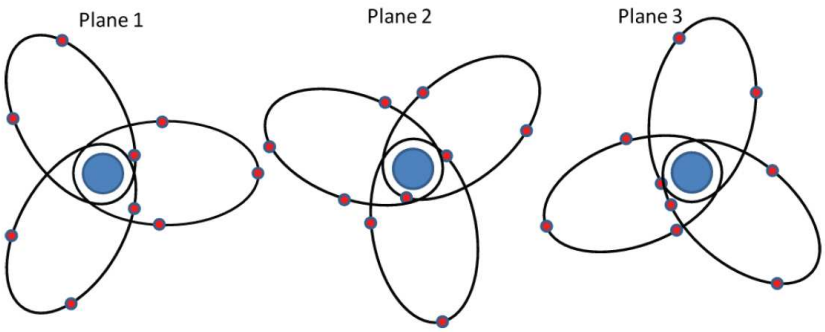

Figure 1.10: 3D-LFC concept.

The mathematical formulation of the 3D-LFC requires six integer parameters and six orbital elements of a reference satellite. We use N_o to represent the number of orbital planes, N_ω to represent the number of unique orbits (with different arguments of perigee) on each plane, and N'_{so} to represent the number of satellites on each of those orbits. Thus, the total number of satellites of the constellation is represented by $N_{sat} = N_o N_\omega N'_{so}$. The remaining three integers are the phasing parameters: N_c^1, N_c^2 and N_c^3.

Following the notes of Davis [19], the distribution of the satellites in the (Ω, ω, M)-space

can be determined solving this system of equations:

$$\begin{pmatrix} N_o & 0 & 0 \\ N_c^3 & N_\omega & 0 \\ N_c^1 & N_c^2 & N_{so}^{'} \end{pmatrix} \begin{pmatrix} \Omega_{ijk} \\ \omega_{ijk} \\ M_{ijk} \end{pmatrix} = 2\pi \begin{pmatrix} i \\ k \\ j \end{pmatrix}, \tag{1.44}$$

where

$$\begin{aligned} i &= 0, \ldots, N_o - 1 & \qquad N_c^1 &\in [0, N_o - 1], \\ j &= 0, \ldots, N_{so}^{'} - 1 & \qquad N_c^2 &\in [0, N_\omega - 1], \\ k &= 0, \ldots, N_\omega - 1 & \qquad N_c^3 &\in [0, N_o - 1]. \end{aligned}$$

Note that, the values outside of those ranges are perfectly valid, but they describe configurations equivalent to ones defined in the specified range, as in modular arithmetic.

The location of all the satellites of a 3D-LFC corresponds to a Lattice in the (Ω, ω, M)-space, which can be regarded as a 4D torus (three axis, Ω, ω, and M, are modulo 2π) and coincides with all the solutions of the system of equations given in (1.44).

The 3D-LFC theory not only shares many properties with 2D-LFC. This theory generalizes the 2D-LFC and other existing satellite constellations, such as Walker constellations or Draim constellations.

1.3 Dilution of Precision

The Global Positioning System [38] (GPS) determines the user position using the concept Time-Of-Arrival (TOA), which consists of determining the user position measuring the time-of-arrival for a signal transmitted by a satellite at a known location to reach the user location. Multiplying the TOA by the speed of the signal transmitted, it is possible to determine the user's position. In order to understand this problem, it will be useful solve first the two-dimensional case [28].

The two-dimensional position determination problem can be presented through the well known problem of a mariner at sea determining his or her vessel's position from a foghorn. First of all, assume that the vessel's and foghorn's clocks are perfectly synchronized. And also, assume that the mariner has an approximate idea of the vessel's position. The mariner has to take note of the time that the foghorn whistle needs to travel from the foghorn to the mariner's ear. Then, the distance can be easily computed multiplying the measured time by the speed of sound.

For example, if we consider that the speed of sound is $335\,m/sec$, and the propagation time measured by the mariner is $2\,sec$, the circumference of radio $R1 = 670\,m$, illustrated in Figure 1.11, represents all the possible mariner's locations.

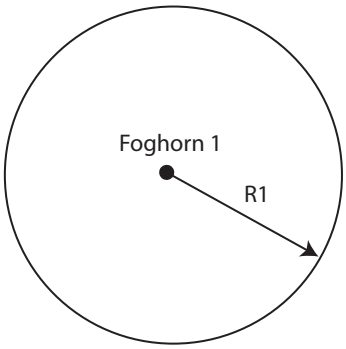

Figure 1.11: Possible vessel's position.

If the mariner, at the same time, computes the propagation time of a second foghorn whistle, for example $1\,sec$. The vessel will be at range $R1 = 670\,m$ from the foghorn 1 and range $R2 = 335\,m$ from the foghorn 2, as we can see in Figure 1.12. As we mention before, the mariner has an approximate idea of the vessel's position and it is possible to discard one of the intersection points. If not, a third range measurement $R3$ from a third foghorn can be used to solve this ambiguity.

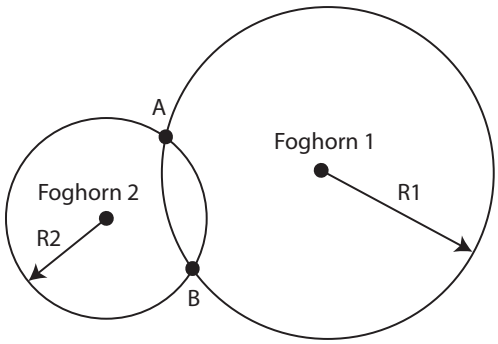

Figure 1.12: Two possible vessel's position.

The previous problem has been solved assuming that the clocks were perfectly synchronized. But, this fact does not happen in a real case. On the other hand, all measurements will have the same time offsets, because the mariner's clock is the same for all the time measurements and all the foghorns clocks are synchronized. Then, the time offset is reflected as an error in the ranges $R1$, $R2$, and $R3$. As an example, if the time offset between the mariner's clock and the foghorn's clock is $0.1\,sec$ the ranges must add an error of $\epsilon = 33.5\,m$. This concept is illustrated in Figure 1.13. Obviously, the true vessel position is a function of the vessel's clock offset, if this offset could be removed the vessel's position will be completely precise. In the real case, must be considered other delay effects such as: atmospheric effects, interfering sounds, etc.

The three-dimensional position determination problem [28] consists of determining the user position (x_u, y_u, z_u) using the location of three satellites, whose coordinates are well known. The idea is exactly the same as in the vessel's problem, but instead of using two foghorns three satellites are used, and instead of intersecting circumferences, spheres

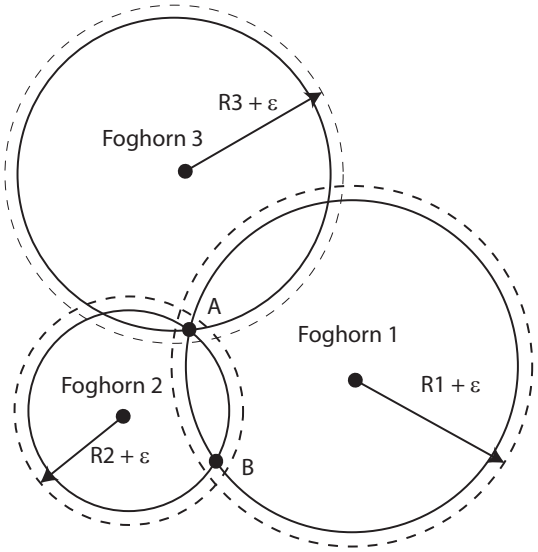

Figure 1.13: Effect of time offset on the measurements.

will be intersected. In this case, the speed of light will be used, as opposed to the speed of sound used in the foghorn problem. Furthermore, the time offset (t_u), which represents the difference in time between the clocks of the receiver and the satellite, will be another unknown. Then, four visible satellites are needed to completely determine the four unknowns; the user position coordinates and the time offset. We explain carefully this problem [28].

Let $\mathbf{s}$ be the vector from the Earth's center to the j-th satellite and be $\mathbf{u}$ the vector from the Earth's center to the user position. These vectors are illustrated in Figure 1.14.

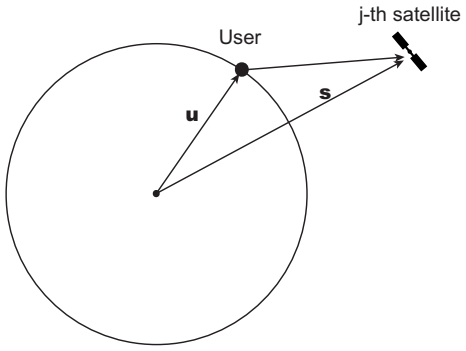

Figure 1.14: User and j-th satellite position vectors from the Earth's center.

The distance between j-th satellite and the user position can be computed by measuring the time between the emission of a signal from the satellite, and the reception of that signal by the receiver. If the satellite clock and the receiver clock were perfectly synchronized, the time Δt, which represents the time between emitting and receiving the signal, would be the propagation time. Then, the range satellite-user can be

computed from the velocity equation:

$$c = \frac{||\mathbf{s} - \mathbf{u}||}{\Delta t}. \tag{1.45}$$

However, the receiver and satellite clocks will generally have a bias error from system time. The distance between the user and the satellite, which is computed multiplying the signal propagation velocity by the measured propagation time, is not the real distance and it is called pseudorange measurement. The measurement contains: (1) the geometric satellite-user range. (2) an offset attributed to the difference between system time and user clock. (3) an offset attributed to the difference between system time and satellite clock. (4) other sources of error that corrupt the measurements such as the atmosphere, because it makes the pseudorange larger than it would be if the signal were propagated in a vacuum, the troposphere, that delays the reception time, and the ionosphere, that advances the reception of the signal. Furthermore, reflections (i.e multipath) and hardware effects during the codification of the signal may advance or delay the signal transmission. δt_D resumes all the errors described in (4),

$$\delta t_D = \delta t_{atm} + \delta t_{noise\&int} + \delta t_{mp} + \delta t_{hw}, \tag{1.46}$$

where:

$\delta t_{atm} =$ delays due to the atmosphere.

$\delta t_{noise\&int} =$ delays due to receiver noise and interference.

$\delta t_{mp} =$ delays due to the multipath offset.

$\delta t_{hw} =$ delays due to the hardware offset.

The relation between times are expressed in Figure 1.15 where:

$\Delta t =$ geometric range time equivalent.

$T_s =$ system time at which the signal left the satellite.

$T_u =$ system time at which the signal would have reached the ground station without δt_D.

$T'_u =$ system time at which the signal reach the user receiver considering δt_D.

$\delta t =$ offset of the satellite clock from the system time. Advance is positive, delay is negative.

$t_u =$ offset of the receiver clock from the system time.

$T_s + \delta t =$ satellite clock reading at time which the signal left the satellite.

$T'_u + t_u =$ user receiver clock reading at time when the signal reach the user receiver.

$c =$ speed of light.

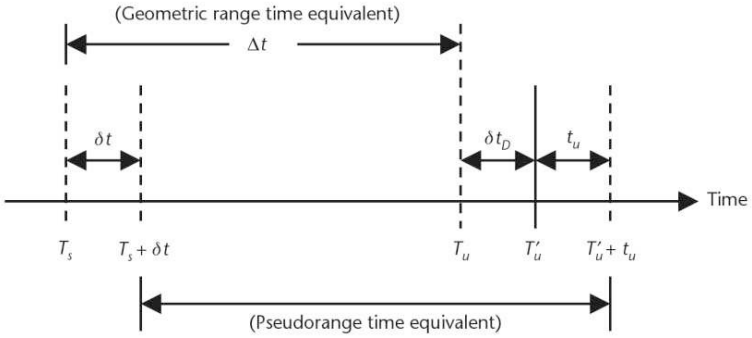

Figure 1.15: Pseudorange time measurement.

Then, the pseudorange measurement is:

$$\begin{aligned} \rho &= c[(T'_u + t_u) - (T_s + \delta t)] \\ &= c(T'_u - T_s) + c(t_u - \delta t) \\ &= c(T_u + \delta t_D - T_s) + c(t_u - \delta t) \\ &= c(T_u - T_s) + c(t_u - \delta t + \delta t_D) \\ &= ||\mathbf{s} - \mathbf{u}|| + c(t_u - \delta t + \delta t_D). \end{aligned} \tag{1.47}$$

The offset δt, which represents the offset of the satellite clock from the system clock is no longer considered because the GPS ground-monitoring network applied the necessary corrections within the user receiver in order to synchronize the satellite clock with the system clock of each signal, meaning that $\delta t = 0$. In our study, we consider that the value $\delta t_D = 0$. Thus, Eq. (1.47) can be rewritten as:

$$\rho = ||\mathbf{s} - \mathbf{u}|| + ct_u. \tag{1.48}$$

where $\mathbf{s} = (x_j, y_j, z_j)$ represents the coordinates of the j-th satellite, $\mathbf{u} = (x_u, y_u, z_u)$ represents the coordinates of the user's position, and the amount t_u represents the advance of the receiver clock with respect to the satellite clock.

At this point, our problem has four unknowns (x_u, y_u, z_u) and t_u, that is why at least four visible satellites will be necessary to determine the unknowns. Eq. (1.48) can be expanded into the following set of equations in the unknowns x_u, y_u, z_u, and t_u.

$$\begin{aligned} \rho_1 &= \sqrt{(x_1 - x_u)^2 + (y_1 - y_u)^2 + (z_1 - z_u)^2} + ct_u, \\ \rho_2 &= \sqrt{(x_2 - x_u)^2 + (y_2 - y_u)^2 + (z_2 - z_u)^2} + ct_u, \\ \rho_3 &= \sqrt{(x_3 - x_u)^2 + (y_3 - y_u)^2 + (z_3 - z_u)^2} + ct_u, \\ \rho_4 &= \sqrt{(x_4 - x_u)^2 + (y_4 - y_u)^2 + (z_4 - z_u)^2} + ct_u. \end{aligned} \tag{1.49}$$

We expand Eqs. (1.49) using Taylor series about an approximate user position denoted by $(\hat{x}_u, \hat{y}_u, \hat{z}_u)$ in order to linearized them. Now, we express the offset of the true position (x_u, y_u, z_u) from the approximate position $(\hat{x}_u, \hat{y}_u, \hat{z}_u)$ by a displacement

$(\Delta x_u, \Delta y_u, \Delta z_u)$. It is also considered a time bias estimate $\hat{t}_u$ from the time estimate t_u. Then, we have the following relation:

$$\begin{aligned} x_u &= \hat{x}_u + \Delta x_u, \\ y_u &= \hat{y}_u + \Delta y_u, \\ z_u &= \hat{z}_u + \Delta z_u, \\ t_u &= \hat{t}_u + \Delta t_u. \end{aligned} \tag{1.50}$$

The pseudorrange measurements from the user position (x_u, y_u, z_u) to the j-th satellite with time estimate t_u, and from the approximation user position $(\hat{x}_u, \hat{y}_u, \hat{z}_u)$ to the j-th satellite with time bias estimate $\hat{t}_u$ can be described using a function f:

$$\begin{aligned} \rho_j &= \sqrt{(x_j - x_u)^2 + (y_j - y_u)^2 + (z_j - z_u)^2} + ct_u = f(x_u, y_u, z_u, t_u), \\ \hat{\rho}_j &= \sqrt{(x_j - \hat{x}_u)^2 + (y_j - \hat{y}_u)^2 + (z_j - \hat{z}_u)^2} + c\hat{t}_u = f(\hat{x}_u, \hat{y}_u, \hat{z}_u, \hat{t}_u). \end{aligned} \tag{1.51}$$

It is possible to relate ρ_j and $\hat{\rho}_j$ by using Eqs (1.50). Then, we expand this expression about the approximate point $(\hat{x}_u, \hat{y}_u, \hat{z}_u)$ and time bias estimate $\hat{t}_u$ using Taylor series expansion:

$$\begin{aligned} f(x_u, y_u, z_u, t_u) &= f(\hat{x}_u + \Delta x_u, \hat{y}_u + \Delta y_u, \hat{z}_u + \Delta z_u, \hat{t}_u + \Delta t_u) \\ &= f(\hat{x}_u, \hat{y}_u, \hat{z}_u, \hat{t}_u) + \frac{\partial f(\hat{x}_u, \hat{y}_u, \hat{z}_u, \hat{t}_u)}{\partial \hat{x}_u}\Delta x_u + \\ &+ \frac{\partial f(\hat{x}_u, \hat{y}_u, \hat{z}_u, \hat{t}_u)}{\partial \hat{y}_u}\Delta y_u + \frac{\partial f(\hat{x}_u, \hat{y}_u, \hat{z}_u, \hat{t}_u)}{\partial \hat{z}_u}\Delta z_u + \\ &+ \frac{\partial f(\hat{x}_u, \hat{y}_u, \hat{z}_u, \hat{t}_u)}{\partial \hat{t}_u}\Delta t_u + \dots \end{aligned} \tag{1.52}$$

The partial derivatives of Eq. (1.52) have been truncated after the first-order to eliminate nonlinear terms as follows:

$$\begin{aligned} \frac{\partial f(\hat{x}_u, \hat{y}_u, \hat{z}_u, \hat{t}_u)}{\partial \hat{x}_u} &= -\frac{x_j - \hat{x}_u}{\hat{r}_j}, \\ \frac{\partial f(\hat{x}_u, \hat{y}_u, \hat{z}_u, \hat{t}_u)}{\partial \hat{y}_u} &= -\frac{y_j - \hat{y}_u}{\hat{r}_j}, \\ \frac{\partial f(\hat{x}_u, \hat{y}_u, \hat{z}_u, \hat{t}_u)}{\partial \hat{z}_u} &= -\frac{z_j - \hat{z}_u}{\hat{r}_j}, \\ \frac{\partial f(\hat{x}_u, \hat{y}_u, \hat{z}_u, \hat{t}_u)}{\partial \hat{t}_u} &= c, \end{aligned} \tag{1.53}$$

where

$$\hat{r}_j = \sqrt{(x_j - \hat{x}_u)^2 + (y_j - \hat{y}_u)^2 + (z_j - \hat{z}_u)^2}.$$

Finally, substituting Eqs. (1.51) and Eqs. (1.53) into Eq. (1.52) we obtain:

$$\rho_j = \hat{\rho}_j - \frac{x_j - \hat{x}_u}{\hat{r}_j}\Delta x_u - \frac{y_j - \hat{y}_u}{\hat{r}_j}\Delta y_u - \frac{z_j - \hat{z}_u}{\hat{r}_j}\Delta z_u + c\Delta t_u. \tag{1.54}$$

We have a linearized expression of the pseudorange measurement ρ_j, given in Eq. (1.51), with respect to the unknowns $\Delta x_u, \Delta y_u, \Delta z_u$, and Δt_u.
Now, we define the direction cosines of the unit vector pointing from the approximate user position to the j-th satellite:

$$\begin{aligned} a_{x_j} &= \frac{x_j - \hat{x}_u}{\hat{r}_j}, \\ a_{y_j} &= \frac{y_j - \hat{y}_u}{\hat{r}_j}, \\ a_{z_j} &= \frac{z_j - \hat{z}_u}{\hat{r}_j}. \end{aligned} \tag{1.55}$$

We also define the variable $\Delta\rho_j = \hat{\rho}_j - \rho_j$. Then, Eq. (1.54) can be rewritten as:

$$\Delta\rho_j = a_{x_j}\Delta x_u + a_{y_j}\Delta y_u + a_{z_j}\Delta z_u - c\Delta t_u. \tag{1.56}$$

The unknowns of our problem can be determined by solving the following set of linear equations:

$$\begin{aligned} \Delta\rho_1 &= a_{x_1}\Delta x_u + a_{y_1}\Delta y_u + a_{z_1}\Delta z_u - c\Delta t_u, \\ \Delta\rho_2 &= a_{x_2}\Delta x_u + a_{y_2}\Delta y_u + a_{z_2}\Delta z_u - c\Delta t_u, \\ \Delta\rho_3 &= a_{x_3}\Delta x_u + a_{y_3}\Delta y_u + a_{z_3}\Delta z_u - c\Delta t_u, \\ \Delta\rho_4 &= a_{x_4}\Delta x_u + a_{y_4}\Delta y_u + a_{z_4}\Delta z_u - c\Delta t_u. \end{aligned}$$

These equations can be set in matrix notation:

$$\Delta\rho = \begin{pmatrix} \Delta\rho_1 \\ \Delta\rho_2 \\ \Delta\rho_3 \\ \Delta\rho_4 \end{pmatrix}, \qquad H = \begin{pmatrix} a_{x_1} & a_{y_1} & a_{z_1} & 1 \\ a_{x_2} & a_{y_2} & a_{z_2} & 1 \\ a_{x_3} & a_{y_3} & a_{z_3} & 1 \\ a_{x_4} & a_{y_4} & a_{z_4} & 1 \end{pmatrix}, \qquad \Delta x = \begin{pmatrix} \Delta x_u \\ \Delta y_u \\ \Delta z_u \\ -c\Delta t_u \end{pmatrix}.$$

Finally, we obtain the equation:

$$\Delta\rho = H\Delta x. \tag{1.57}$$

Since the elements of H are linearly independent, the matrix is invertible,

$$\Delta x = H^{-1}\Delta\rho. \tag{1.58}$$

In some cases, we have a $n \times 4$ dimension matrix instead of a 4×4 dimension matrix because we have more than four visible satellites. In this case we use the method of least squares. By multiplying Eq. (1.57) by H^T we obtain:

$$H^T\Delta\rho = H^T H\Delta x. \tag{1.59}$$

Now, we multiply by $(H^T H)^{-1}$ and we get:

$$\Delta x = (H^T H)^{-1} H^T \Delta\rho. \tag{1.60}$$

Note that, we have solved the error-free problem, in which we only consider the offset between the satellite clock and the receiver clock. But, as we have already mention,

this problem has other source errors. Thus, the pseudorange measurements can be viewed as a linear combination of the following three terms:

$$\Delta\rho = \rho_T - \rho_L + d\rho, \tag{1.61}$$

where ρ_T is the vector of error-free pseudorange values, ρ_L is the vector of pseudorange values computed at the linearization point, and $d\rho$ represents the net error in the pseudorange values. In the same way, the vector Δx can be viewed as a linear combination of three terms,

$$\Delta x = x_T - x_L + dx, \tag{1.62}$$

where x_T is the error-free position and time, x_L is the position and time defined as the linearization point, and dx is the error in the position and time estimate.

From the free-error equation (1.58), in which $dx = 0$ and $d\rho = 0$ is possible obtain the following relation,

$$(x_T - x_L) = (H^T H)^{-1} H^T (\rho_T - \rho_L). \tag{1.63}$$

By substituting Eq. (1.61) and Eq. (1.62) in Eq. (1.60), and using the relation (1.63) is possible to obtain:

$$\begin{aligned} \Delta x &= (H^T H)^{-1} H^T \Delta\rho, \\ (x_T - x_L + dx) &= (H^T H)^{-1} H^T (\rho_T - \rho_L + d\rho), \\ (H^T H)^{-1} H^T (\rho_T - \rho_L) + dx &= (H^T H)^{-1} H^T (\rho_T - \rho_L) + (H^T H)^{-1} H^T d\rho, \\ dx &= (H^T H)^{-1} H^T d\rho. \end{aligned} \tag{1.64}$$

This relation gives the functional relationship between the errors in the pseudorange values and the induced errors in the computed position and time. The matrix $(H^T H)^{-1} H^T$ is a $4 \times n$ matrix, and it depends only on the relative geometry between the user and the satellites, meaning that it is possible to determine the error in the computed position and time from the geometry of the constellation.

The covariance of a vector is frequently of interest to asses how strongly two variables of the vector change together [30]. Then, we compute $\mathrm{cov}(dx)$ as:

$$\begin{aligned} \mathrm{cov}(dx) &= E[dx dx^T] \\ &= E[((H^T H)^{-1} H^T) d\rho (((H^T H)^{-1} H^T) d\rho)^T] \\ &= ((H^T H)^{-1} H^T) E[d\rho d\rho^T] ((H^T H)^{-1} H^T)^T \\ &= ((H^T H)^{-1} H^T) \mathrm{cov}(d\rho) ((H^T H)^{-1} H^T)^T. \end{aligned} \tag{1.65}$$

The usual assumption of the vector $d\rho$ is that its components has a Gaussian distribution and zero mean. With the geometry considered fixed, it follows that dx is also Gaussian and zero mean. The components of $d\rho$ are identically distributed, independent and have a variance equal to the square of the satellite UERE (User Equivalent Range Error), which is considered to be the statistical sum of the contributions from each of the error sources associated with the satellite. Usually, the error components are considered independent, and the composite UERE for a satellite is approximated

as a zero mean Gaussian random variable, where its variance is determined as the sum of the variance of each of its components. UERE is usually assumed to be independent, and identically distributed from satellite to satellite. Then, the covariance of the vector $d\rho$ is:

$$\text{cov}(d\rho) = I_n \sigma^2_{UERE}. \tag{1.66}$$

Using Eq. (1.66) in Eq. (1.65) we obtain:

$$\begin{aligned} \text{cov}(dx) &= (H^T H)^{-1} H^T I_n \sigma^2_{UERE} ((H^T H)^{-1} H^T)^T \\ &= (H^T H)^{-1} H^T H ((H^T H)^{-1})^T \sigma^2_{UERE} \\ &= (H^T H)^{-1} \sigma^2_{UERE}. \end{aligned} \tag{1.67}$$

However, $\text{cov}(dx)$ can be computed as follows:

$$cov(dx) = \begin{pmatrix} \sigma^2_{x_u} & \sigma_{x_u y_u} & \sigma_{x_u z_u} & \sigma_{x_u t_u} \\ \sigma_{y_u x_u} & \sigma^2_{y_u} & \sigma_{y_u z_u} & \sigma_{y_u t_u} \\ \sigma_{z_u x_u} & \sigma_{z_u y_u} & \sigma^2_{z_u} & \sigma_{z_u t_u} \\ \sigma_{t_u x_u} & \sigma_{t_u y_u} & \sigma_{t_u z_u} & \sigma^2_{t_u} \end{pmatrix}.$$

Then, as we mention before, the geometry of the constellation plays an important role since the components of $(H^T H)^{-1}$ quantify how pseudorange errors translate into components of the covariance of dx, meaning that, it is possible to determine how accurate the computed position is from the geometry of the constellation.

Dilution Of Precision [31, 52, 54] (DOP) parameters in GPS are defined in terms of the ratio of combinations of the components of the $\text{cov}(dx)$ and σ^2_{UERE}. It is implicitly assumed in the DOP definitions that the user/satellite geometry is considered fixed. It is also assumed that local user coordinates are being used in the specification of $\text{cov}(dx)$ and dx. The positive x-axis points east, the y-axis points north, and the z-axis points up. The most general parameter is termed Geometric Dilution Of Precision (GDOP) and it is defined by:

$$GDOP = \frac{\sqrt{\sigma^2_{x_u} + \sigma^2_{y_u} + \sigma^2_{z_u} + \sigma^2_{t_u}}}{\sigma_{UERE}}. \tag{1.68}$$

An expression for GDOP is obtained in terms of the components of $(H^T H)^{-1}$ by expressing $(H^T H)^{-1}$ in component form:

$$(H^T H)^{-1} = \begin{pmatrix} D_{11} & D_{12} & D_{13} & D_{14} \\ D_{21} & D_{22} & D_{23} & D_{24} \\ D_{31} & D_{32} & D_{33} & D_{34} \\ D_{41} & D_{42} & D_{43} & D_{44} \end{pmatrix}.$$

Then, GDOP can be computed as the square root of the trace of the $(H^T H)^{-1}$ matrix:

$$GDOP = \sqrt{D_{11} + D_{22} + D_{33} + D_{44}}. \tag{1.69}$$

If we assume that there are no errors in the synchronization of the clocks, the value D_{44} can be disregarded. The DOP computed without D_{44} is called Position Dilution of

Precision (PDOP). Similarly, we obtain other DOP values such as; Horizontal Dilution of Precision (HDOP), Vertical Dilution of Precision (VDOP), and Time Dilution of Precision (TDOP). They can be expressed in terms of the components of $(H^T H)^{-1}$ as follows:

$$\begin{aligned} PDOP &= \sqrt{D_{11} + D_{22} + D_{33}}, \\ HDOP &= \sqrt{D_{11} + D_{22}}, \\ VDOP &= \sqrt{D_{33}}, \\ TDOP &= \sqrt{D_{44}}. \end{aligned} \tag{1.70}$$

At this point, it is obvious that the geometry of the constellations has a direct role on positioning accuracies [53]. Several tools are defined to describe the accuracy error, but Geometric Dilution of Precision (GDOP) used by GPS it is the most powerful accuracy indicator since it consider all possible sources of errors. The GDOP will show how well the constellation is organized geometrically. It is a quantity varying between 1 and ∞, while 1 means that the constellation presents a perfect distribution of satellites, a large value (greater than 6) means that presents a really poor geometrical distribution.

1.4 Evolutive Algorithms

An optimization problem consists of finding the best solution within a search space, which is the set of all possible candidate solutions. This space has the same dimension as the number of variables that the problem has and, depending on the problem type, the variables can be discrete or continuous.

For a search space with only a small number of possible solutions, all of them can be examined in a reasonable amount of time and the optimal one will be eventually found. This technique is called brute-force search or exhaustive search. Basically, it consists of enumerating all possible candidates for the solution and selecting the most suitable. It has an easy implementation, and it always finds the optimal solution if it exists. However, the cost of this algorithm grows exponentially with the dimension of the search space.

Instead of using the brute-force search algorithm, evolutionary algorithms [23] have been developed. These kind of algorithms abstract biological evolution or biological behaviors to search an optimal solution to a problem. Two different algorithms are considered [22, 26]: Genetic Algorithm and the Particle Swarm Optimization Algorithm.

1.4.1 Genetic Algorithms

Charles Darwin's *On the Origin of Species*, in his *Principles of Biology* (1864) proposed the idea that over several generations, biological organisms evolve based on the principle of natural selection "survival of the fittest". This idea works well in nature. An individual in a population competes with each other for different resources like food, shelter, etc. Due to the selection, the most adapted to the environment and the

stronger ones have more chance to survive and reproduce, while the less adapted have less chance to survive and reproduce. Continuously improving the individual characteristics of the species, since the new generations take the good characteristics of their antecessors and will improve them at each generation. They will become more and more adapted to their environment. Note that, sometimes in nature it will occur a crazy or random fact, that consists of taking random characteristics and create an individual completely new with different characteristics that sometimes are better, sometimes worse than the existing individuals.

The idea of solving different optimization problems using evolutive techniques started in 1954 with the work of Nils Aall Barricelli. However, Genetic Algorithms became popular through the work of John Holland in 1975 in his book *Adaptation in Natural and Artificial Systems*. It will be very useful a brief introduction to biology to understand Genetic Algorithms. Genetics is a science that study all the differences and similarities in the individuals of a specie. The genetic information of an individual, which has all the characteristics of itself, is stored in the chromosomes. The chromosomes are divided in several parts called genes. These genes code the properties of the individuals of the specie. In the reproduction process, the new individuals will select the genes between all the available possibilities of their antecessors. Note that, individuals with better characteristics have a greater chance to reproduce its genes, while the ones which are less adapted or have worst characteristics have a fewer chance to reproduce its genes. In this reproduction process, all the genes of the new individuals may suffer small variations.

Genetic Algorithms [44] mimic the process of natural evolution described above. It is a search technique to find optimal solutions to a problem. Genetic Algorithms have an initial population represented by a group of individuals, each of these individuals represents a solution to the optimization problem and they are considered as the chromosomes. After evaluating all the initial population with the fitness function, to know how good the solutions are, a number of individuals are selected to create the next generation combining their genes. In the reproduction process, different reproduction operators are used, such as, recombination and mutation. The first one consists of recombining different chromosomes of two different individuals (parents) to generate a new individual (child). The second one is a factor that randomly generates completely new genes for the new individual. When the new generation is built, we evaluate the population with the fitness function and start again the process until the stopping criteria is reached. It can be a finite number of generations, the convergence toward the optimal solution, etc.

The following procedure shows how the Genetic Algorithm works;

Step 1: Select randomly an initial population of n individuals from the search space, i.e. select randomly n solutions of the optimization problem.

Step 2: Evaluate the individuals of the population with the fitness function.

Step 3: Create a new population following these steps:

Step 3.1: Select two individuals (parents), the better the fitness is, the bigger the chance to get selected.

Step 3.2: Crossover the genes of the two parents to create a new individual (child).

Step 3.3: With a mutation probability, mutate randomly the genes of the new individual (child).

Step 3.4: Repeat the process until have a population of n new individuals.

Step 4: If the stopping criteria is satisfied, evaluate the new generation and select the most suitable individual. If not, go to Step 2.

1.4.2 Particle Swarm Optimization Algorithm

Particle Swarm Optimization Algorithm [44] (PSO) is a population based stochastic optimization method, i.e. a method that generate and use random variables to find the optimal solution. PSO was developed by Dr. Eberhart and Dr. Kennedy in 1995, inspired by the social behavior of bird flocking or fish schooling. The basic idea is to simulate these behaviors with an algorithm. In both cases, if a bird or a fish sees a good path to go (because they find food, protection or good weather), the rest of the swarm will be able to follow that path even if they were going in the opposite way. However, there is a "craziness factor" or random factor that makes some of the particles move away from the flock in order to explore new paths.
It is possible to translate this behavior into an algorithm. Each different bird or fish is considered as an initial particle in the search space. These particles are flying through the search space and have two essential capabilities: remembering their own best position (individual factor) and knowing the best position of the entire swarm (social factor). The basic idea is that individuals communicate good positions to each other and adjust their own position and velocity depending on the social and individual factors.

During the simulation, each particle has a position and velocity. Additionally, each particle keeps track of the position of the best solution it has visited so far (*pbest*) and the position of the best solution visited by any other particle (*gbest*). At each step, the velocity is updated at each iteration taking into account *pbest* and *gbest*.
Changing the position and velocity of each particle at each iteration works as follows. Assume that the i-th particle has position vector $x_i(t)$ and velocity vector $v_i(t)$. Then, the updated velocity will be:

$$v_i(t+1) = \alpha v_i(t) + c_1 \cdot rand_1 \cdot (pbest_i - x_i(t)) + c_2 \cdot rand_2 \cdot (gbest(t) - x_i(t)) \quad (1.71)$$

where α is the inertia weight that controls the exploration of the search space. The constants c_1 and c_2, which in our simulation are taken between 0 and 1, determine how the individual and social factor affects the velocity of the particle. Finally, $rand_1$, $rand_2$ are random numbers chosen uniformly in [0,1]. Note that without the second and third terms of the expression (1.71) the particle will keep in the same direction until it hits the boundary.

The position is updated as follows:

$$x_i(t+1) = x_i(t) + v_i(t+1) \tag{1.72}$$

This process is repeated for each particle until the best optimal solution is obtained or the stopping criteria is reached.

The PSO can be implemented as follows:

Step 1: Initialize randomly an initial swarm of n particles from the search space.

- **Step 1.1:** Initialize randomly the initial positions, i.e. the solutions of the problem, $x_i(0)$.
- **Step 1.2:** Initialize randomly the velocities of the initial particles, $v_i(0)$.
- **Step 1.3:** Update the *pbest* and *gbest* values thought the fitness function.

Step 2: Update the new velocities for the particles, $v_i(t+1)$, according to Eq. (1.71).

Step 3: Calculate the new positions of the particles, $x_i(t+1) = x_i(t) + v_i(t+1))$.

Step 4: Update the *pbest* and *gbest* values thought the fitness function.

Step 5: Go to step 2, and repeat until convergence or stopping criteria.

Both methods are included in the evolutionary computation, and offers practical advantages to several optimization problems. They are conceptually simple and highly parallelizable.

Chapter 2

Optimizing Flower Constellations for Global and Regional Coverage

2.1 Introduction

The design of optimal satellite constellations is the key problem in all kind of applications such as global navigation, global/regional coverage, telecommunications, Earth observation, radio-occultation, etc.
The purpose of this chapter is to determine the best 2D-LFC for certain global coverage problems using evolutionary algorithms. In particular, we are interested in the problem of Global Positioning, with a minimum of four satellites in view from any point on the Earth at any time as a constraint. The geometry of these four or more satellites with respect to a ground station should ideally minimize the Geometric Dilution of Precision (GDOP).
The metric defining our optimality is the maximum value of the GDOP experienced over the propagation time for 30,000 ground stations randomly distributed on the Earth surface. In this chapter the reason for choosing 30,000 ground stations randomly distributed on the Earth surface, the optimal propagation time needed for computing the GDOP amongst other things will be discussed. Evolutive algorithms are used to carry out a search among all possible configurations, to find the parameters that minimize the maximum GDOP experienced. One of the original parts of this chapter is that we extend the search space to include eccentric orbits using the 2D Lattice theory.

2.2 Optimization problem

Given the total number of satellites of a 2D-LFC (N_{sat}), it is possible to obtain all the different possible configurations for the phasing parameters (N_o, N_{so}, N_c). The number of different configurations can be obtained from the divisors of N_{sat}. For each divisor d, we select $N_o = d$, $N_{so} = N_{sat}/d$ and the configuration number N_c varying between 0 and $d-1$. Consequently, the number of different configurations is given by the formula,

$$f(N_{sat}) = \sum_{d|N_{sat}} d. \tag{2.1}$$

As an example, given $N_{sat} = 27$ satellites, following Eq. (2.1) the different possibilities for the phasing parameters are 40, and they are shown in Table 2.1.

N_{sat}	27	27	27	27	27	27	27	...	27	27	27	...	27
N_o	1	3	3	3	9	9	9	...	9	27	27	...	27
N_{so}	27	9	9	9	3	3	3	...	3	1	1	...	1
N_c	0	0	1	2	0	1	2	...	8	0	1	...	26

Table 2.1: Possible phasing parameters.

All satellite missions have a fixed semi-major axis, meaning that the orbital period is known (T_p). Since our missions are around the Earth, the rotating period of our ECEF frame, which is the Earth rotating period, is also known (T_d). Therefore, it is possible to select parameters N_p and N_d in such a way that they satisfy Eq. (1.39).

2.2.1 Fitness function

In this problem it is necessary to determine which satellites are visible from a ground station. For this purpose, a *grazing angle* or spacecraft elevation angle of a satellite is required. This is the angle between the horizon and the position vector of a satellite. Another way to refer to this angle is using the *angle of incidence* which is the angle between the normal vector to the surface of the Earth at the ground station and the position vector. Due to the existence of buildings, mountains, and other visibility obstacles a reference grazing angle is considered in the formulation of all global positioning problems. In our problem, we consider a reference grazing angle $\alpha = 10°$, or in other words, a reference angle of incidence $\beta = 80°$. Figure 2.1 illustrates the reference grazing angle (α) and the reference angle of incidence (β). Also it is illustrated when a satellite is or is not visible.

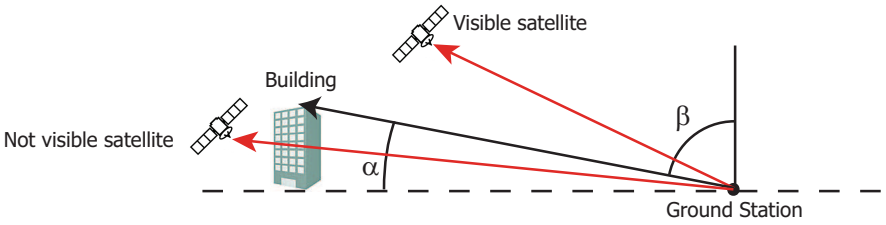

Figure 2.1: The grazing angle α and the angle of incidence β.

As we illustrate in Figure 2.2, a satellite will be visible if the angle ε is smaller than the reference angle of incidence ($\beta = 80°$). This is equivalent to $\cos(\varepsilon) > cos(\beta)$, or using the dot product to express $\cos(\varepsilon)$, to the following condition:

$$\frac{(\mathbf{r}_{sat} - \mathbf{r}_{gs}) \cdot \mathbf{r}_{gs}}{||(\mathbf{r}_{sat} - \mathbf{r}_{gs})|| \cdot ||\mathbf{r}_{gs}||} > cos(\beta).$$

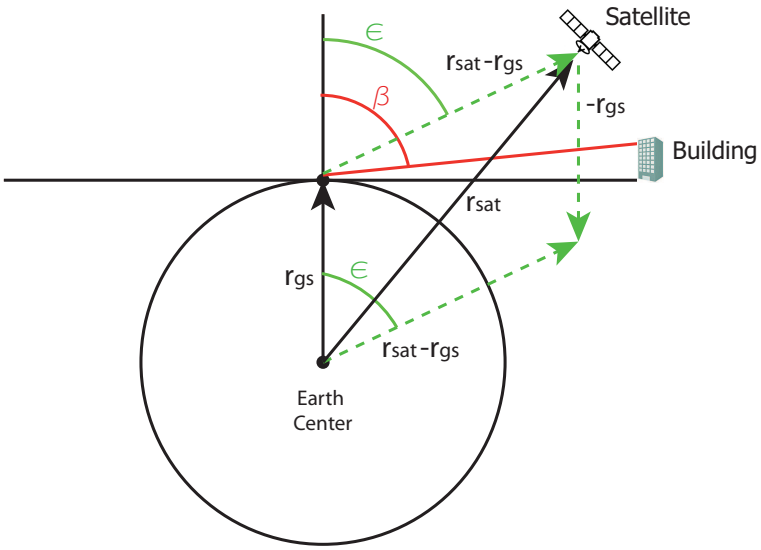

Figure 2.2: A visible satellite in the ECEF frame.

Definition 1. Let FC be a Flower Constellation and let $\mathbf{r}_{gs}$ be the location of a ground station. The *Geometric Dilution Of Precision* is a function:

$$\begin{aligned} GDOP : \mathbb{N}^3 \times \mathbb{R}^6 \times \mathbb{R}^3 \times \mathbb{R} &\rightarrow \mathbb{R}_{\geq 1} \\ (FC, \mathbf{r}_{gs}, t) &\mapsto GDOP(FC, \mathbf{r}_{gs}, t). \end{aligned} \tag{2.2}$$

See preliminaries for an explicit formula.

Definition 2. Let FC be a Flower Constellation and let T_{prop} be a propagation time. We define the maximum value of the GDOP experienced by the FC during the time interval $[0, T_{prop}]$ for all the points of the Earth surface as Ground Stations:

$$\begin{aligned} \max GDOP : \mathbb{N}^3 \times \mathbb{R}^6 \times \mathbb{R}_{\geq 0} &\rightarrow \mathbb{R}_{\geq 1} \\ (FC, T_{prop}) &\mapsto \max GDOP(FC, T_{prop}). \end{aligned}$$

$$\max GDOP(FC, T_{prop}) = \max_{t \in [0, T_{prop}]} \max_{\mathbf{r}_{gs} \in \text{Earth}} GDOP(FC, \mathbf{r}_{gs}, t). \tag{2.3}$$

In the case where T_{prop} is the repetition time of the constellation $T = N_p T_p$, which is the time that the constellation needs to return to its original configuration, the function above is the *theoretical fitness function*:

$$\begin{aligned} fitness : \mathbb{N}^3 \times \mathbb{R}^6 &\rightarrow \mathbb{R}_{\geq 1} \\ FC &\mapsto fitness(FC). \end{aligned}$$

$$\begin{aligned} fitness(FC) &= \max GDOP(FC, N_p T_p) \\ &= \max_{t \in [0, N_p T_p]} \max_{\mathbf{r}_{gs} \in \text{Earth}} GDOP(FC, \mathbf{r}_{gs}, t). \end{aligned} \tag{2.4}$$

2.2.2 Evolutive Algorithms

Given the total number of satellites of a 2D-LFC, for each possible configuration of the phasing parameters, and the values for N_p and N_d already selected; evolutive algorithms are used to carry out a search to find the best orbital parameters (e, i, ω), which completely define the constellation, and minimize the fitness function.

In the case of the Genetic Algorithm an initial population of $n = 60$ individuals is taken, i.e. 60 possible values for the orbital parameters (e, i, ω). Then, each constellation is evaluated with the fitness function. After that, a new generation of 60 individuals is created. The new individuals are created with 10 fittest ones from the previous generation, and 50 others obtained by crossover and mutation. The crossover consists of selecting a father (e_f, i_f, ω_f) and a mother (e_m, i_m, ω_m) from the previous generation at random and creating a son

$$(e_f x_1 + e_m(1 - x_1), i_f x_2 + i_m(1 - x_2), \omega_f x_3 + \omega_m(1 - x_3)),$$

where $x_1, x_2, x_3 \in \{0, 1\}$ are chosen at random with 0.5 probability each. After the son is created, we decide with probability 0.05 whether it mutates or not. Mutation consists of choosing all three coordinates e, i, ω at random within their allowed ranges. The process is repeated 60 generations and, at that point, the best individual found provides the solution to the optimization process.

In the case of the Particle Swarm Optimization an initial swarm of $n = 60$ particles is taken, i.e. 60 possible values for the orbital parameters (e, i, ω) which are the positions, and 60 possible velocities for them. Both positions and velocities are chosen randomly within the search space. It should be noted that neither position or velocity correspond with the actual motion of the satellites; these quantities are unitless. Then, we evaluate each constellation with the fitness function and update the new velocities and positions according to Eq. (1.71) and Eq. (1.72). We are using an inertia factor $\alpha = 0.95$, individual factor $c_1 = 0.75$, social factor $c_2 = 0.35$, and the process is repeated 60 iterations.

We show how the Particle Swarm Optimization algorithm works with the following example. Given a 27 satellite constellation with parameters $N_o = 3$, $N_{so} = 9$, and $N_c = 2$. We find the optimal parameters (e, i, ω) which minimizes the fitness function. The behavior of the different particles (e, i, ω) of the swarm is presented in Figure 2.3. We show different plots in where we illustrate the position of each particle (e, i, ω) in different generations. In particular, we plot the generation number 1, 5, 10, 20, 30, 40, 50, and 60 from the top to the bottom and from the left to the right, respectively. We observe how the particles converge to the optimal solution, which is $e = 0.0$, $i = 54.057°$, and $\omega = 173.707°$.

2.2.3 Search Space Reduction

Evolutive algorithms have an initial population of 60 individuals, meaning that we have to propagate 60 constellations and compute the maximum value experienced for the

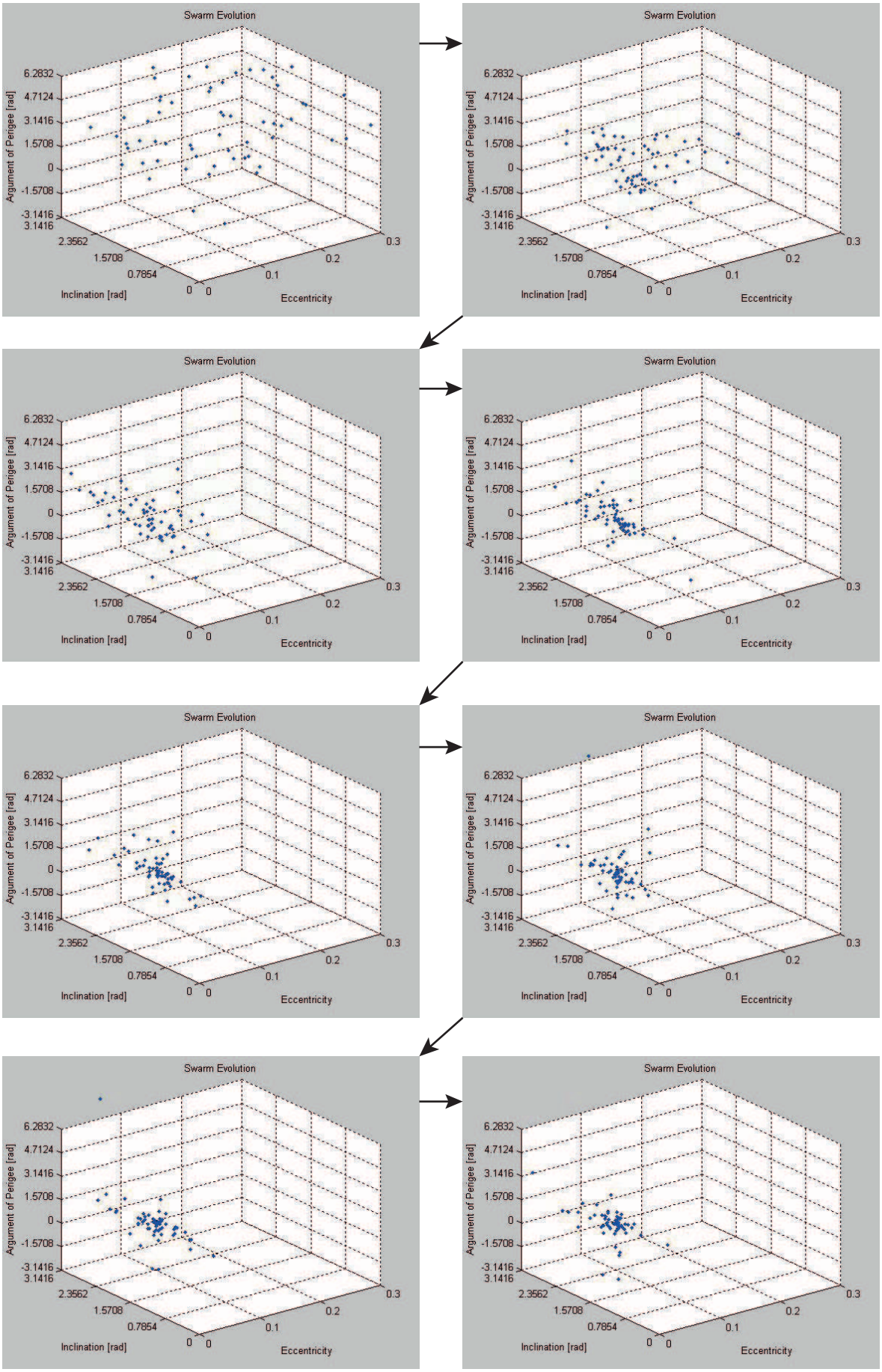

Figure 2.3: Swarm of particles searching the optimal solution.

Figure 2.4: Counterclockwise and clockwise direction.

GDOP over the 30,000 ground stations. This process is repeated 60 times, because the number of generations is 60. Consequently, we need to propagate 3,600 constellations and compute the maximum value of the GDOP experienced in each case. Furthermore, this process needs to be repeated as many times as different configurations the constellation has, that can be derived from N_{sat} by Eq. (2.1).
In the following discussion, we will see a few results that allow us to reduce the propagation time T, and also the search range of some variables of our search space. Note that, each reduction translates into a significant reduction in the computational cost.

2.2.3.1 Propagation time reduction

Definition 3. A counterclockwise rotation around the z-axis through angle α is a function:

$$\begin{aligned} Rot_z(\alpha) : \mathbb{R}^3 &\rightarrow \mathbb{R}^3 \\ \mathbf{x} &\mapsto Rot_z(\alpha)\mathbf{x} = \begin{pmatrix} \cos\alpha & -\sin\alpha & 0 \\ \sin\alpha & \cos\alpha & 0 \\ 0 & 0 & 1 \end{pmatrix} \mathbf{x}. \end{aligned}$$

As we illustrate in Figure 2.4, when the angle α is positive the rotation is called counterclockwise. When the angle α is negative the rotation is called clockwise.

Let FC be a Flower Constellation. $FC' = Rot_z(\alpha)FC$ is the constellation obtained by a rotation around the z-axis through angle α of the position vector of each satellite. The parameters of FC' and FC are exactly the same except $\Omega_0' = \Omega_0 + \alpha$.

Lemma 4. Let FC be a Flower Constellation. Then, in the ECEF frame,

$$FC(t) = Rot_z(\mp\frac{2\pi}{T_d}T_p)FC(t + T_p). \tag{2.5}$$

Proof. In the ECEF frame the inertial orbits rotate with angular velocity equal to the Earth rotating velocity $\frac{2\pi}{T_d}\, rad/sec$ as we illustrate in Figure 2.5. After T_p seconds, the orbits have rotated around the z-axis an angle $\pm\frac{2\pi}{T_d}T_p\, rad$. The position of the satellites in the inertial orbits at time $t + T_p$ seconds will be the same as at time t, and the configuration of the constellation is exactly the same but rotated. Then, by rotating the FC around the z-axis an angle $\mp\frac{2\pi}{T_d}T_p\, rad$ the position of the satellites at time t and at time $t + T_p$ will be exactly the same. Consequently, Eq. (2.5) is satisfied. □

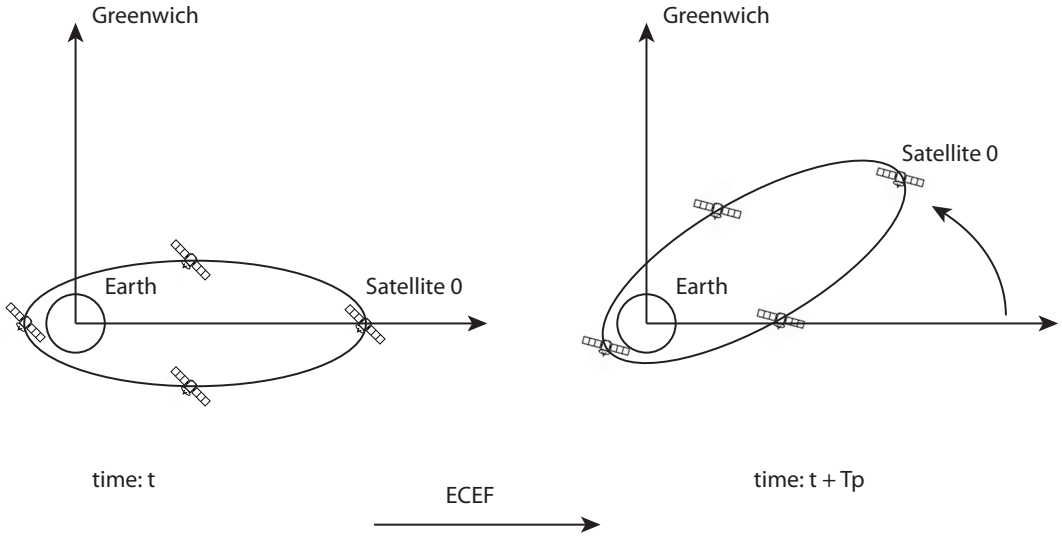

Figure 2.5: First orbit of the FC at time t, and at time $t + T_p$.

Lemma 5. Let FC be a Flower Constellation. Let $\mathbf{r}_{gs}$ be a ground station. Then, in the ECEF frame,

$$GDOP(FC, \mathbf{r}_{gs}, t) = GDOP(FC, Rot_z(\pm\frac{2\pi}{T_d}T_p)\mathbf{r}_{gs}, t + T_p). \tag{2.6}$$

Proof. After T_p seconds, as we show in lemma 4, the position of the satellites is the same but rotated an angle $\pm\frac{2\pi}{T_d}T_p\, rad$. The ground station $\mathbf{r}_{gs}$ after T_p seconds will be in the same position since we are in the ECEF frame. Consequently, if we rotate the ground station an angle $\pm\frac{2\pi}{T_d}T_p\, rad$ the relative position of the satellites and the ground station is the same at time t and at time $t + T_p$ and the GDOP will be the same as the lemma states. □

Theorem 6. Let FC be a Flower Constellation. Then,

$$\text{maxGDOP}(FC, N_pT_p) = \text{maxGDOP}(FC, T_p).$$

Proof. In the ECEF frame,

$$\begin{aligned}
\text{maxGDOP}(FC, N_pT_p) &= \max_{t\in[0,N_pT_p]} \max_{\mathbf{r}_{gs}\in\text{Earth}} GDOP(FC, \mathbf{r}_{gs}, t) \\
&= \max_{i=0,\ldots,N_p-1} \max_{t\in[iT_p,(i+1)T_p]} \max_{\mathbf{r}_{gs}\in\text{Earth}} GDOP(FC, \mathbf{r}_{gs}, t) \\
&= \max_{i=0,\ldots,N_p-1} \max_{t\in[0,T_p]} \max_{\mathbf{r}_{gs}\in\text{Earth}} GDOP(FC, \mathbf{r}_{gs}, t + iT_p) \\
&= \max_{i=0,\ldots,N_p-1} \max_{t\in[0,T_p]} \max_{\mathbf{r}_{gs}\in\text{Earth}} GDOP(FC, Rot_z(\pm\frac{2\pi}{T_d}iT_p)\mathbf{r}_{gs}, t) \\
&= \max_{i=0,\ldots,N_p-1} \max_{t\in[0,T_p]} \max_{\mathbf{r}'_{gs}\in\text{Earth}} GDOP(FC, \mathbf{r}'_{gs}, t) \\
&= \max_{t\in[0,T_p]} \max_{\mathbf{r}'_{gs}\in\text{Earth}} GDOP(FC, \mathbf{r}'_{gs}, t)
\end{aligned}$$

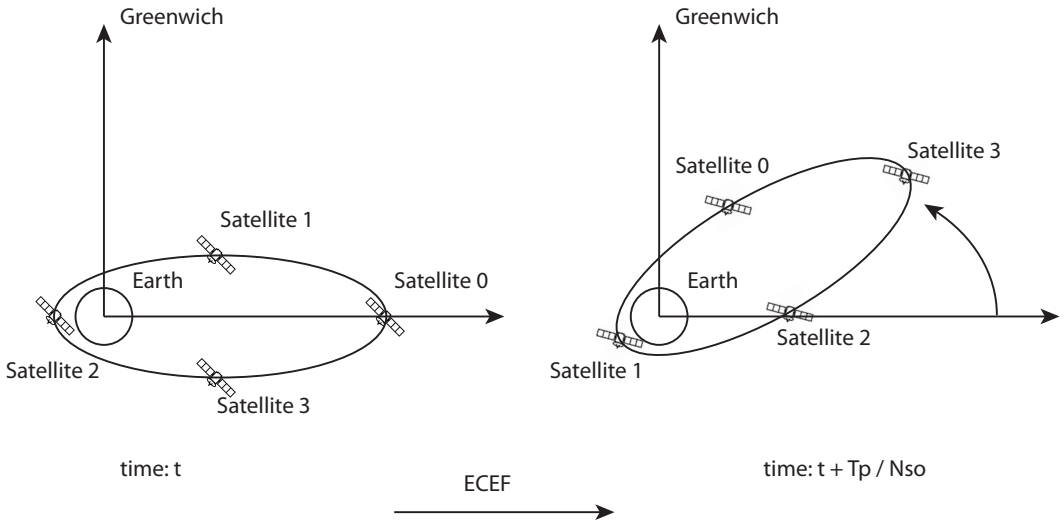

Figure 2.6: First orbit of the FC at time t, and at time $t + \frac{T_p}{N_{so}}$.

$$= \quad \text{maxGDOP}(FC, T_p).$$

The first and the last equalities are true by definition. The second equality consists of dividing the time interval $[0, N_p T_p]$ into smaller intervals of length T_p. The fourth equality is by using lemma 5. The fifth equality is true since the Earth is a solid of revolution (spheroid), and it has a rotational symmetry with respect to the z-axis, the points $\mathbf{r}'_{gs}$ cover all the Earth surface as the points $\mathbf{r}_{gs}$. □

Lemma 7. Let FC be a Flower Constellation. Then, in the ECEF frame,

$$FC(t) = Rot_z(\mp\frac{2\pi}{T_d}\frac{T_p}{N_{so}})FC(t + \frac{T_p}{N_{so}}). \tag{2.7}$$

Proof. In the ECEF frame the inertial orbits rotate with angular velocity equal to the Earth rotating velocity $\frac{2\pi}{T_d}\, rad/sec$. After $\frac{T_p}{N_{so}}$ seconds, the orbits have rotated around the z-axis an angle $\pm\frac{2\pi}{T_d}\frac{T_p}{N_{so}}$ rad. as we illustrate in Figure 2.6. Note that, after $\frac{T_p}{N_{so}}\, sec$ the satellites in the inertial orbit will occupy the position that the following satellite occupied at time t, for example, satellite 0 after $\frac{T_p}{N_{so}}\, sec$ will occupy the position that the satellite 1 occupied at time t. This means, that the distribution of the satellites in the inertial orbits at time $t + \frac{T_p}{N_{so}}$ seconds will be the same as at time t, but each satellite will occupy the position that its following neighbor occupied at time t, so the configuration of the constellation will be exactly the same, but rotated. Then, by rotating the FC around the z-axis an angle $\mp\frac{2\pi}{T_d}\frac{T_p}{N_{so}}\, rad$ the position of the satellites at time t and at time $t + \frac{T_p}{N_{so}}$ will be exactly the same. Consequently, Eq. (2.7) is satisfied. □

Lemma 8. Let FC be a Flower Constellation. Let $\mathbf{r}_{gs}$ be a ground station. Then, in the ECEF frame,

$$GDOP(FC, \mathbf{r}_{gs}, t) = GDOP(FC, Rot_z(\pm\frac{2\pi}{T_d}\frac{T_p}{N_{so}})\mathbf{r}_{gs}, t + \frac{T_p}{N_{so}}). \tag{2.8}$$

Proof. Similar to Lemma 5. □

Theorem 9. Let FC be a Flower Constellation. Then,

$$\text{maxGDOP}(FC, T_p) = \text{maxGDOP}(FC, \frac{T_p}{N_{so}}).$$

Proof. In the ECEF frame,

$$\begin{aligned}
\text{maxGDOP}(FC, T_p) &= \max_{t\in[0,T_p]} \max_{\mathbf{r}_{gs}\in\text{Earth}} GDOP(FC, \mathbf{r}_{gs}, t) \\
&= \max_{j=0,\ldots,N_{so}-1} \max_{t\in[j\frac{T_p}{N_{so}},(j+1)\frac{T_p}{N_{so}}]} \max_{\mathbf{r}_{gs}\in\text{Earth}} GDOP(FC, \mathbf{r}_{gs}, t) \\
&= \max_{j=0,\ldots,N_{so}-1} \max_{t\in[0,\frac{T_p}{N_{so}}]} \max_{\mathbf{r}_{gs}\in\text{Earth}} GDOP(FC, \mathbf{r}_{gs}, t + j\frac{T_p}{N_{so}}) \\
&= \max_{j=0,\ldots,N_{so}-1} \max_{t\in[0,\frac{T_p}{N_{so}}]} \max_{\mathbf{r}_{gs}\in\text{Earth}} GDOP(FC, Rot_z(\pm\frac{2\pi}{T_d}j\frac{T_p}{N_{so}})\mathbf{r}_{gs}, t) \\
&= \max_{j=0,\ldots,N_{so}-1} \max_{t\in[0,\frac{T_p}{N_{so}}]} \max_{\mathbf{r}'_{gs}\in\text{Earth}} GDOP(FC, \mathbf{r}'_{gs}, t) \\
&= \max_{t\in[0,\frac{T_p}{N_{so}}]} \max_{\mathbf{r}'_{gs}\in\text{Earth}} GDOP(FC, \mathbf{r}'_{gs}, t) \\
&= \text{maxGDOP}(FC, \frac{T_p}{N_{so}}).
\end{aligned}$$

The first and the last equalities are true by definition. The second consists of dividing the time interval $[0, T_p]$ into smaller intervals of length $\frac{T_p}{N_{so}}$. The fourth equality is by using lemma 8. The fifth equality is true since the Earth is a solid of revolution (spheroid), and it has a rotational symmetry with respect to the z-axis, the points $\mathbf{r}'_{gs}$ cover all the Earth surface as the points $\mathbf{r}_{gs}$. □

Lemma 10. Let $a, b \geq 1$ be integers. The sequence $\{ia \mod (b)\}$ with $i = 0, 1, \ldots, b-1$ contains only the multiples of $\gcd(a, b)$ between 0 and $b-1$ inclusive.

Proof. ($\Rightarrow$) Let α be an integer in the sequence $\{ia \mod (b)\}$ with $i = 0, 1, \ldots, b-1$. α is the remainder of dividing ia by b for some i. Then, $\alpha = ia - bq$. Since a is divisible by $\gcd(a, b)$, b is divisible by $\gcd(a, b)$. Then, $\alpha = ia - bq$ is divisible by $\gcd(a, b)$ and α is a multiple of $\gcd(a, b)$ between 0 and and $b-1$ inclusive.

($\Leftarrow$) Let $\beta = \gcd(a, b)r$ be a multiple of $\gcd(a, b)$ between 0 and $b-1$. For some $m, n \in \mathbb{Z}$, we have $\gcd(a, b) = an + bm$. Then, $\beta = (an + bm)r = anr + bmr$. If we divide nr by b we have $nr = bq + i$ with $i = 0, 1, \ldots, b-1$. Then, $\beta = abq + ai + bmr$. Finally, the remainder of dividing ai by b is β and we conclude that β belongs to the sequence $\{ia \mod (b)\}$ with $i = 0, 1, \ldots, b-1$ □

Lemma 11. Let $a, b, c \geq 1$ be integers. The sequence $\{jc - ia \mod (bc)\}$ with $i = 0, 1, \ldots, c-1$ and $j = 0, 1, \ldots, b-1$ contains only the multiples of $\gcd(a, c)$ between 0 and $bc - 1$ included.

Proof. ($\Rightarrow$) Let α be an integer in the sequence $\{jc-ia \mod (bc)\}$ with $i = 0, 1, \ldots, c-1$ and $j = 0, 1, \ldots, b-1$. α is the remainder of dividing $jc - ia$ by bc. Then, $\alpha = jc - ia - bcq$. Since c is divisible by $\gcd(a, c)$, a is divisible by $\gcd(a, c)$ and bcq is divisible by $\gcd(a, c)$. Then, α is divisible by $\gcd(a, c)$. Consequently, α is a multiple of $\gcd(a, c)$ and it is between 0 and $bc - 1$.

($\Leftarrow$) Let β be a multiple of $\gcd(a, c)$ between 0 and $bc - 1$. We have two cases:

Case 1: $\beta = 0$. $\beta \in \{jc - ia \mod (bc)\}$ with $i = 0, 1, \ldots, c-1$ and $j = 0, 1, \ldots, b-1$ by choosing $i = j = 0$.

Case 2: $\beta \geq 1$ and $\beta \leq bc-1$. We know that β and c are multiples of $\gcd(a, c)$. Then, $bc - \beta$ is also a multiple of $\gcd(a, c)$. Furthermore, $bc - \beta \in [1, 2, \ldots, bc - 1]$. Dividing $bc-\beta$ by c we have $bc-\beta = cQ+r$ with $r \in [0, 1, \ldots, c-1]$ and $Q \in \mathbb{Z}$. Note that, r is multiple of $\gcd(a, c)$. Applying Theorem 10 to r, we have that $r = ia \mod (c)$ with $i = 0, 1, \ldots, c-1$. Then, $r = ia + c\tilde{Q}$ with $\tilde{Q} \in \mathbb{Z}$. Then, $bc - \beta = c(Q + \tilde{Q}) + ia$. Consequently, $\beta = c(b - Q - \tilde{Q}) - ia$. Now, we divide $b - Q - \tilde{Q}$ by b obtaining $b - Q - \tilde{Q} = bw + j$ with $j = 0, 1, \ldots, b-1$. Finally, $\beta = cbw + jc - ia$, which is the remainder of dividing $jc - ia$ by bc. This proves that β belongs to the sequence $\{jc - ia \mod (bc)\}$ with $i = 0, 1, \ldots, c-1$ and $j = 0, 1, \ldots, b-1$.

□

Lemma 12. Let FC be a Flower Constellation. Then, in the ECEF frame,

$$FC(t) = Rot_z(\mp\Delta\Omega \mp \Delta\alpha)FC(t + \Delta t), \tag{2.9}$$

where

$$\Delta t = \frac{T_p}{N_o N_{so}} \gcd(N_c, N_o), \qquad \Delta\Omega = \frac{2\pi\Delta t}{T_d}, \qquad \Delta\alpha = \frac{2\pi i}{N_o}.$$

for some integer $i \in [0, \ldots, N_o - 1]$.

Proof. The mean anomaly of the satellites in a Flower Constellation is given by,

$$M_{ij} = \frac{2\pi j}{N_{so}} - \frac{N_c}{N_{so}}\frac{2\pi}{N_o} = \frac{2\pi}{N_{so}N_o}(jN_o - iN_c),$$

where $i = 0, 1, \ldots, N_o - 1$ and $j = 0, 1, \ldots, N_{so} - 1$.

Note that, since coordinates in the (Ω, M)-space are modulus 2π:

$$\begin{aligned}
\frac{2\pi}{N_{so}N_o}(jN_o - iN_c) &= \frac{2\pi}{N_{so}N_o}(jN_o - iN_c) + 2\pi(jN_o - iN_c) \\
&= \frac{2\pi}{N_{so}N_o}[(jN_o - iN_c) + N_{so}N_o(jN_o - iN_c)] \\
&= \frac{2\pi}{N_{so}N_o}[(jN_o - iN_c) \mod (N_{so}N_o)] \\
&= \frac{2\pi}{N_{sat}}[(jN_o - iN_c) \mod (N_{sat})].
\end{aligned}$$

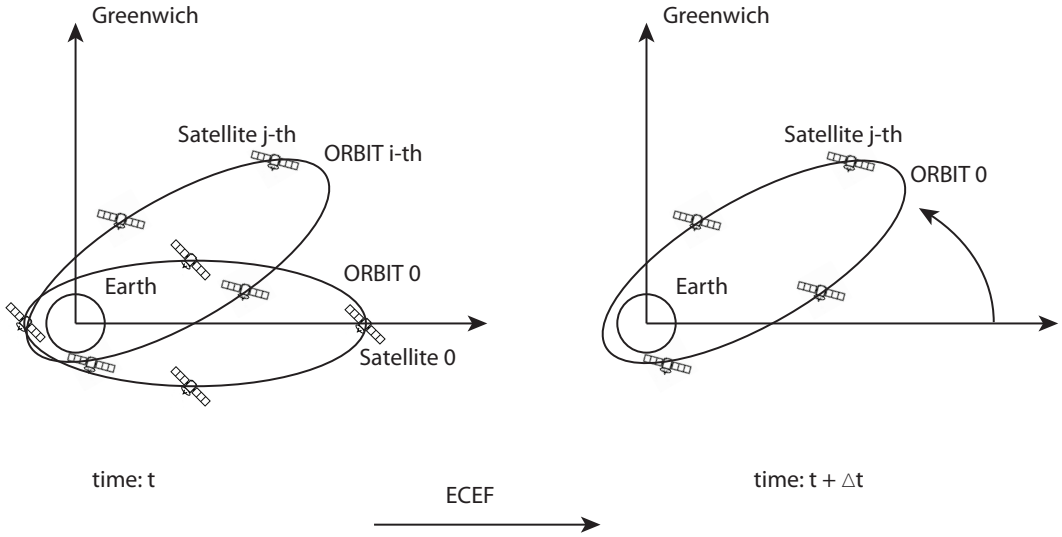

Figure 2.7: First orbit of the FC at time t, and at time $t + \Delta t$.

Our goal is to minimize the quantity M_{ij} for any pair (i, j). By using Lemma 11 with values $a = N_c$, $b = N_{so}$ and $c = N_o$. The sequence $\{jN_o - iN_c \mod (N_{so}N_o)\}$ contains the multiples of $\gcd(N_c, N_o)$ that are between 0 and $N_{so}N_o - 1$. Consequently,

$$\min_{>0}\{jN_o - iN_c \mod (N_{sat})\} = \gcd(N_c, N_o).$$

Thus, the quantity that minimizes the value M_{ij} over all pairs (i, j) is $\frac{2\pi}{N_{sat}} \gcd(N_c, N_o)$. Since the satellite needs T_p seconds to reach its initial position in the inertial orbit, to sweep $\frac{2\pi}{N_{sat}} \gcd(N_c, N_o)$ radians the satellite needs $\Delta t = \frac{T_p}{N_{sat}} \gcd(N_c, N_o)$ seconds.

In the ECEF frame the inertial orbits rotate with angular velocity equal to the Earth rotating velocity $\frac{2\pi}{T_d} rad/sec$. Then, after Δt seconds, the orbits have rotated an angle $\Delta\Omega = \pm\frac{2\pi}{T_d}\Delta t\, rad$.

Furthermore, the pair (i, j), previously computed, indicates where the first satellite of the orbit 0 at time t will be after Δt seconds. Thus, the satellite 0 of the zero orbit, as we illustrate in Figure 2.7, after Δt sec. will occupy the position that the satellite $j-th$ in the $i-th$ inertial orbit occupied at time t. Note that, the distance between the first orbit and the $i-th$ orbit is $\Delta\alpha = \frac{2\pi i}{N_{so}}$. Consequently, by rotating the FC around the z-axis firstly an angle $\mp\Delta\Omega\, rad$ and secondly an angle $\mp\Delta\alpha\, rad$, the constellation will have the same configuration at time t and at time $t + \Delta t$. This is a rotation around the z-axis of angle $\mp\Delta\Omega \mp \Delta\alpha$, then Eq. (2.9) is satisfied as theorem states. □

Lemma 13. Let FC be a Flower Constellation. Let $\mathbf{r}_{gs}$ be a ground station. Then, in the ECEF frame,

$$GDOP(FC, \mathbf{r}_{gs}, t) = GDOP(FC, Rot_z(\pm\Delta\Omega \pm \Delta\alpha)\mathbf{r}_{gs}, t + \Delta t), \tag{2.10}$$

where

$$\Delta t = \frac{T_p}{N_o N_{so}} \gcd(N_c, N_o), \qquad \Delta\Omega = \frac{2\pi\Delta t}{T_d}, \qquad \Delta\alpha = \frac{2\pi i}{N_o}.$$

for some integer $i \in [0, \ldots, N_o - 1]$.

Proof. After Δt seconds, as we show in lemma 12, the distribution of the satellites is the same but rotated an angle $(\pm\Delta\Omega \pm \Delta M)\, rad$. The ground station $\mathbf{r}_{gs}$ after Δt seconds will be in the same position since we are in the ECEF frame. Consequently, if we rotate the ground station an angle $(\pm\Delta\Omega \pm \Delta M)\, rad$ the relative position of the satellites and the ground station is the same at time t and at time $t + \Delta t$ and the GDOP will be the same as the lemma states. □

Theorem 14. Let FC be a Flower Constellation. Then,

$$\text{maxGDOP}(FC, \frac{T_p}{N_{so}}) = \text{maxGDOP}(FC, \Delta t),$$

where $\Delta t = \frac{T_p}{N_o N_{so}} \gcd(N_c, N_o)$.

Proof. Define $n = \frac{N_o}{\gcd(N_c, N_o)}$. In the ECEF frame,

$$\begin{aligned}
\text{maxGDOP}(FC, \frac{T_p}{N_{so}}) &= \max_{t\in[0,\frac{T_p}{N_{so}}]} \max_{\mathbf{r}_{gs}\in\text{Earth}} GDOP(FC, \mathbf{r}_{gs}, t) \\
&= \max_{k=0,\ldots,n-1} \max_{t\in[k\Delta t,(k+1)\Delta t]} \max_{\mathbf{r}_{gs}\in\text{Earth}} GDOP(FC, \mathbf{r}_{gs}, t) \\
&= \max_{k=0,\ldots,n-1} \max_{t\in[0,\Delta t]} \max_{\mathbf{r}_{gs}\in\text{Earth}} GDOP(FC, \mathbf{r}_{gs}, t + k\Delta t) \\
&= \max_{k=0,\ldots,n-1} \max_{t\in[0,\Delta t]} \max_{\mathbf{r}_{gs}\in\text{Earth}} GDOP(FC, Rot_z((\pm\Delta\Omega \pm \Delta M)k)\mathbf{r}_{gs}, t) \\
&= \max_{k=0,\ldots,n-1} \max_{t\in[0,\Delta t]} \max_{\mathbf{r}'_{gs}\in\text{Earth}} GDOP(FC, \mathbf{r}'_{gs}, t) \\
&= \max_{t\in[0,\Delta t]} \max_{\mathbf{r}'_{gs}\in\text{Earth}} GDOP(FC, \mathbf{r}'_{gs}, t) \\
&= \text{maxGDOP}(FC, \Delta t).
\end{aligned}$$

The first and the last equalities are true by definition. The second consists of dividing the time interval $[0, \frac{T_p}{N_{so}}]$ into smaller intervals of length Δt. The fourth equality is by using lemma 13. The fifth equality is true since the Earth is a solid of revolution (spheroid), and it has a rotational symmetry with respect to the z-axis, the points $\mathbf{r}'_{gs}$ cover all the Earth surface as the points $\mathbf{r}_{gs}$. □

Corollary 15. Let FC be a Flower Constellation. Then, the fitness function can be reformulated as:

$$fitness(FC) = \text{maxGDOP}(FC, \Delta t),$$

where $\Delta t = \frac{T_p}{N_o N_{so}} \gcd(N_c, N_o)$.

Proof.

$$\begin{aligned}
fitness(FC) &= \text{maxGDOP}(FC, T_p N_p) \\
&= \text{maxGDOP}(FC, T_p) \\
&= \text{maxGDOP}(FC, \frac{T_p}{N_{so}})
\end{aligned}$$

$$= \quad \text{maxGDOP}(FC, \Delta t).$$

The first equality is true by definition. The second, third and fourth equalities are true by using Theorem 6, Theorem 9, and Theorem 14, respectively. □

Note that, the fitness function as defined in (2.4) is not computationally feasible since it is not possible to compute the value of the GDOP at each point of the Earth surface. Therefore, an accurate approximate fitness function is required. For that purpose we select n ground stations randomly distributed over the Earth surface $\mathbf{r}_{gs_1}, \mathbf{r}_{gs_2}, \ldots, \mathbf{r}_{gs_n}$ that will remain fixed throughout this section.

Definition 16. Let FC be a Flower Constellation, let T_{prop} be a propagation time and let $\mathbf{r}_{gs_1}, \mathbf{r}_{gs_2}, \ldots, \mathbf{r}_{gs_n}$ be the position vector of the n ground stations. We define the maximum value of the GDOP experienced by the FC during the time interval $[0, T_{prop}]$ for the n ground stations over the Earth surface:

$$\begin{aligned} \overline{\max GDOP} : \mathbb{N}^3 \times \mathbb{R}^6 \times \mathbb{R}_{\geq 0} &\rightarrow \mathbb{R}_{\geq 1} \\ (FC, T_{prop}) &\mapsto \overline{\max GDOP}(FC, T_{prop}). \end{aligned}$$

$$\overline{\max GDOP}(FC, T_{prop}) = \max_{t \in [0, T_{prop}]} \max_{i=1,\ldots,n} GDOP(FC, \mathbf{r}_{gs_i}, t). \tag{2.11}$$

In the case where T_{prop} is the repetition time of the constellation $T = N_p T_p$, the function above is the *approximate fitness function*:

$$\begin{aligned} \overline{fitness} : \mathbb{N}^3 \times \mathbb{R}^6 &\rightarrow \mathbb{R}_{\geq 1} \\ FC &\mapsto \overline{fitness}(FC). \end{aligned}$$

$$\begin{aligned} \overline{fitness}(FC) &= \overline{\max GDOP}(FC, N_p T_p) \\ &= \max_{t \in [0, N_p T_p]} \max_{i=1,\ldots,n} GDOP(FC, \mathbf{r}_{gs_i}, t). \end{aligned}$$

Remark 17. When the number of ground stations approaches infinity the approximate fitness function converges to the theoretical function.

$$\overline{fitness}(FC) \rightarrow fitness(FC).$$

We will decide below what is the minimum number of ground stations needed to have an acceptable approximation of the theoretical fitness function. For that purpose we take a Flower Constellation of 27 satellites distributed in three orbital planes $N_o = 3$, with nine satellites per orbit $N_{so} = 9$, and configuration number $N_c = 2$. The semi-major axis equal to $27,000\ km$, eccentricity equal to 0.05, inclination equal to 56°, argument of perigee, Right Ascension of the Ascending Node and mean anomaly equal to zero. Table 2.2 shows how the value of the approximate fitness function changes as the number n of ground stations increases, and how the different seeds, which set the starting point for generating the n ground stations, influence to get the optimal value of the fitness function.

We observe that this is a sensitive procedure that depends on the initial seed to generate the n ground stations and also on the number of ground stations. We must reduce

	seed = 1	seed = 2	seed = 3	seed = 4
n	$\overline{fitness}(FC)$	$\overline{fitness}(FC)$	$\overline{fitness}(FC)$	$\overline{fitness}(FC)$
100	3.605398276568	3.628921099334	3.583989218822	3.639154163226
500	3.674101015200	3.650307182435	3.656458212953	3.647322709899
1000	3.674180285547	3.650307182435	3.670664296126	3.684728030781
2000	3.678746975526	3.669673852604	5.090641658212	5.116533527851
5000	5.097846349537	3.680194764103	5.090641658212	5.116533527851
10000	5.120664103384	5.121797474482	5.090641658212	5.116533527851
15000	5.120664103384	5.121797474482	5.090641658212	5.116533527851
20000	5.120664103384	5.121797474482	5.090641658212	5.116533527851
25000	5.121846132055	5.121797474482	5.090641658212	5.116533527851
30000	5.121846132055	5.121797474482	5.090641658212	5.116533527851
35000	5.121846132055	5.121797474482	5.090641658212	5.116533527851
40000	5.121846132055	5.121797474482	5.090641658212	5.116533527851
45000	5.121846132055	5.121797474482	5.090641658212	5.116533527851
50000	5.121846132055	5.121797474482	5.090641658212	5.116533527851
60000	5.121846132055	5.121797474482	5.090641658212	5.116533527851
70000	5.121846132055	5.121797474482	5.090641658212	5.133762521059
100000	5.126021072346	5.130243646165	5.133643131118	5.120944798524
200000	5.126491285036	5.130243646165	5.133643131118	5.126593590013
500000	5.136021085303	5.135772602892	5.133643131118	5.135591784229
1000000	5.136021085303	5.135772602892	5.137804209605	5.135591784229
5000000	5.137970170756	5.135918682806	5.137961423302	5.137972091420
10000000	5.137970170756	5.137956261401	5.137961423302	5.137972091420
50000000	5.137970170756	5.135918682806	5.137961423302	5.137972091420
100000000	5.137975421252	5.137987828576	5.137962103239	5.137986488673

Table 2.2: Value of the fitness function depending on the number of ground stations and seed number.

the number of ground stations as much as possible since the computational cost of determining the optimal value of the fitness function increases linearly as the number of ground stations raises. If we consider 30,000 ground stations, the different GDOP values obtained vary no more than 0.03. Although that difference is not meaningless, we decided that 30,000 ground stations were enough to keep certain accuracy while keeping a feasible computational time cost. Thus, we conclude that using 30,000 ground stations randomly selected over the Earth surface the *approximate fitness function* satisfies:

$$\overline{fitness}(FC) \cong fitness(FC).$$

Corollary 18. Let FC be a Flower Constellation. Then, the fitness function can be approximated by:

$$fitness(FC) \cong \overline{fitness}(FC) \cong \overline{\max GDOP}(FC, \Delta t),$$

where $\Delta t = \frac{T_p}{N_o N_{so}} \gcd(N_c, N_o)$.

Proof.

$$\begin{aligned}
\overline{fitness}(FC) &= \overline{\max GDOP}(FC, T_p N_p) \\
&\cong \max GDOP(FC, T_p N_p) \\
&= \max GDOP(FC, T_p) \\
&= \max GDOP(FC, \frac{T_p}{N_{so}}) \\
&= \max GDOP(FC, \Delta t) \\
&\cong \overline{\max GDOP}(FC, \Delta t).
\end{aligned}$$

The first equality is true by definition. The second and the last equalities are true by Remark 17. The third, fourth, and fifth equalities are based on Corollary 15. □

2.2.3.2 Symmetries in a 2D-LFC

We have decreased the computational cost by reducing the propagation time to compute the GDOP of the constellation. Another way to decrease the computational cost is by reducing the search space. By selecting the inclination in a range $0° \leq i \leq 90°$ (instead of $0° \leq i \leq 180°$) or choosing the parameter N_c in a range $[0, \ldots, \frac{N_o}{2}]$ (instead of $[0, \ldots, N_o - 1]$) it is possible to reduce considerably the computational cost. The following theorems show that either of these two reductions of the search space do not skip any possible configuration.

The values of the configuration number, N_c, and the index i are considered modulo N_o, i.e. we always reduce to the representative value in the interval $[0, N_o - 1]$. Similarly, the index j is considered modulo N_{so}. Thus, the value $-N_c$ represents $-N_c \mod (N_o)$, and the value $-j$ represents $-j \mod (N_{so})$.

Proposition 19. Let M_1, M_2 be the mean anomalies and φ_1, φ_2 the true anomalies of two satellites. If $M_2 = -M_1$ then, $\varphi_2 = -\varphi_1$.

Proof. The function that converts the eccentric anomaly to the mean anomaly (see Eq. (1.26)),

$$\begin{aligned} M : [0, 2\pi] &\rightarrow [0, 2\pi] \\ E &\mapsto M(E) = E - e\sin(E), \end{aligned}$$

is an odd function. The inverse of an odd function (M^{-1}) is also an odd function. The function that converts the eccentric anomaly to the true anomaly (see Eq. (1.28)),

$$\begin{aligned} \Phi : [0, 2\pi] &\rightarrow [0, 2\pi] \\ E &\mapsto \Phi(E) = 2\arctan\left(\sqrt{\frac{1+e}{1-e}}\tan\left(\frac{E}{2}\right)\right), \end{aligned}$$

is an odd function since it is the composition of odd functions. Consequently, the function that converts the mean anomaly to the true anomaly, which is the composition of M^{-1} with the function Φ, is an odd function:

$$\begin{aligned} \Phi \circ M^{-1} : [0, 2\pi] &\rightarrow [0, 2\pi] \\ M &\mapsto \Phi \circ M^{-1}(M). \end{aligned}$$

In this particular case,

$$\varphi_2 = \Phi \circ M^{-1}(M_2) = \Phi(M^{-1}(-M_1)) = -\Phi(M^{-1}(M_1)) = -\varphi_1.$$

□

Proposition 20. Let α be an angle, the following property is satisfied:

$$Rot_z(-\alpha) = \begin{pmatrix} 1 & 0 & 0 \\ 0 & -1 & 0 \\ 0 & 0 & 1 \end{pmatrix} Rot_z(\alpha) \begin{pmatrix} 1 & 0 & 0 \\ 0 & -1 & 0 \\ 0 & 0 & 1 \end{pmatrix}. \tag{2.12}$$

The same also applies changing z by x.

Proof.

$$\begin{aligned} Rot_z(-\alpha) &= \begin{pmatrix} \cos(-\alpha) & -\sin(-\alpha) & 0 \\ \sin(-\alpha) & \cos(-\alpha) & 0 \\ 0 & 0 & 1 \end{pmatrix} \\ &= \begin{pmatrix} \cos(\alpha) & \sin(\alpha) & 0 \\ -\sin(\alpha) & \cos(\alpha) & 0 \\ 0 & 0 & 1 \end{pmatrix} \\ &= \begin{pmatrix} 1 & 0 & 0 \\ 0 & -1 & 0 \\ 0 & 0 & 1 \end{pmatrix} \begin{pmatrix} \cos(\alpha) & -\sin(\alpha) & 0 \\ \sin(\alpha) & \cos(\alpha) & 0 \\ 0 & 0 & 1 \end{pmatrix} \begin{pmatrix} 1 & 0 & 0 \\ 0 & -1 & 0 \\ 0 & 0 & 1 \end{pmatrix} \\ &= \begin{pmatrix} 1 & 0 & 0 \\ 0 & -1 & 0 \\ 0 & 0 & 1 \end{pmatrix} Rot_z(\alpha) \begin{pmatrix} 1 & 0 & 0 \\ 0 & -1 & 0 \\ 0 & 0 & 1 \end{pmatrix}. \end{aligned}$$

The case with x is proved similarly. □

Theorem 21. Let $FC_1(N_o, N_{so}, N_c, a, e, i, \omega, \Omega_{00}, M_{00})$ and $FC_2(N_o, N_{so}, -N_c, a, e, \pi - i, -\omega, \Omega_{00}+\pi, -M_{00})$ be two Flower Constellations. Then, the position of the satellites satisfies,

$$\mathbf{r}^1_{ij}(t) = -\mathbf{r}^2_{i(-j)}(-t), \tag{2.13}$$

where $\mathbf{r}^1_{ij}(t)$ represents the position of the satellite (i,j) at time t of the Flower Constellation FC_1, and $\mathbf{r}^2_{i(-j)}(-t)$ represents the position of the satellite $(i,(-j))$ at time $-t$ of the Flower Constellation FC_2.

Proof. The RAAN and the Mean anomaly of the constellations FC_1 and FC_2 satisfy:

$$\begin{aligned}
\Omega^2_{i(-j)} &= \Omega_{00} + \pi + \frac{2\pi i}{N_o} = \Omega^1_{ij} + \pi, \\
M^2_{i(-j)}(-t) &= -M_{00} + \frac{2\pi}{N_o N_{so}}(-jN_o + i(-N_c)) + \frac{2\pi(-t)}{T_p} = -M^1_{ij}(t).
\end{aligned}$$

Using Proposition 19, we get $\varphi^2_{i(-j)}(-t) = -\varphi^1_{ij}(t)$. Consequently,

$$\frac{p}{1+e\cos(\varphi^2_{i(-j)}(-t))}\begin{pmatrix}\cos(\varphi^2_{i(-j)}(-t))\\ \sin(\varphi^2_{i(-j)}(-t))\\ 0\end{pmatrix} = \begin{pmatrix}1&0&0\\0&-1&0\\0&0&1\end{pmatrix}\mathbf{u},$$

where

$$\mathbf{u} = \frac{p}{1+e\cos(\varphi^1_{ij}(t))}\begin{pmatrix}\cos(\varphi^1_{ij}(t))\\ \sin(\varphi^1_{ij}(t))\\ 0\end{pmatrix}.$$

Thus, the position of the satellite $(i,-j)$ at time $-t$ in the Flower Constellation FC_2 is given by:

$$\begin{aligned}
\mathbf{r}^2_{i(-j)}(-t) &= Rot_z(\Omega^2_{i(-j)})Rot_x(i^2)Rot_z(\omega^2)\frac{p}{1+e\cos(\varphi^2_{i(-j)}(-t))}\begin{pmatrix}\cos(\varphi^2_{i(-j)}(-t))\\ \sin(\varphi^2_{i(-j)}(-t))\\ 0\end{pmatrix} \\
&= Rot_z(\Omega^1_{ij}+\pi)Rot_x(\pi-i)Rot_z(-\omega)\begin{pmatrix}1&0&0\\0&-1&0\\0&0&1\end{pmatrix}\mathbf{u} \\
&= Rot_z(\Omega^1_{ij})\begin{pmatrix}-1&0&0\\0&-1&0\\0&0&1\end{pmatrix}\begin{pmatrix}1&0&0\\0&-1&0\\0&0&-1\end{pmatrix}Rot_x(-i) \\
&\quad \begin{pmatrix}1&0&0\\0&-1&0\\0&0&1\end{pmatrix}\begin{pmatrix}1&0&0\\0&-1&0\\0&0&1\end{pmatrix}Rot_z(-\omega)\begin{pmatrix}1&0&0\\0&-1&0\\0&0&1\end{pmatrix}\mathbf{u} \\
&= Rot_z(\Omega^1_{ij})\begin{pmatrix}-1&0&0\\0&1&0\\0&0&-1\end{pmatrix}Rot_x(-i)\begin{pmatrix}1&0&0\\0&-1&0\\0&0&1\end{pmatrix}Rot_z(\omega)\mathbf{u} \\
&= Rot_z(\Omega^1_{ij})\begin{pmatrix}-1&0&0\\0&1&0\\0&0&-1\end{pmatrix}\begin{pmatrix}1&0&0\\0&-1&0\\0&0&1\end{pmatrix}
\end{aligned}$$

$$\begin{pmatrix} 1 & 0 & 0 \\ 0 & -1 & 0 \\ 0 & 0 & 1 \end{pmatrix} Rot_x(-i) \begin{pmatrix} 1 & 0 & 0 \\ 0 & -1 & 0 \\ 0 & 0 & 1 \end{pmatrix} Rot_z(\omega)\mathbf{u}$$
$$= -Rot_z(\Omega^1_{ij})Rot_x(i)Rot_z(\omega)\mathbf{u}.$$
$$= -\mathbf{r}^1_{ij}(t).$$

The first equality is true by definition. The second equality consists of expressing the parameters of FC_2 in terms of the parameters of FC_1. The third equality consist of splitting $Rot_z(\Omega^1_{ij}+\pi)$ into $Rot_z(\Omega^1_{ij})Rot_z(\pi)$, and $Rot_x(\pi - i)$ into $Rot_x(\pi)Rot_x(-i)$, and introducing the identity matrix. The fourth equality is obtained by applying Proposition 20 to $Rot_z(\omega)$. The fifth equality is true by introducing the identity matrix. The sixth equality is true by applying Proposition 20 to $Rot_x(i)$. □

Theorem 22. Let $FC_1(N_o, N_{so}, N_c, a, e, i, \omega, \Omega_{00}, M_{00})$ and $FC_2(N_o, N_{so}, -N_c, a, e, \pi - i, -\omega, \Omega_{00}+\pi, -M_{00})$ be two Flower Constellations. Then,

$$\max GDOP(FC_2, T_p) = \max GDOP(FC_1, T_p). \tag{2.14}$$

Proof.

$$\begin{aligned} \max GDOP(FC_2, T_p) &= \max_{t\in[0,T_p]} \max_{\mathbf{r}_{gs}\in \text{Earth}} GDOP(FC_2, \mathbf{r}_{gs}, t) \\ &= \max_{t\in[0,T_p]} \max_{\mathbf{r}_{gs}\in \text{Earth}} GDOP(FC_2, \mathbf{r}_{gs}, -t) \\ &= \max_{t\in[0,T_p]} \max_{\mathbf{r}_{gs}\in \text{Earth}} GDOP(FC_1, -\mathbf{r}_{gs}, t) \\ &= \max_{t\in[0,T_p]} \max_{\mathbf{r}'_{gs}\in \text{Earth}} GDOP(FC_1, \mathbf{r}'_{gs}, t) \\ &= \max GDOP(FC_1, T_p). \end{aligned}$$

The first and the last equalities are true by definition. Whether the time goes positive or the time goes negative, after T_p seconds all the inertial orbits have been swept by the satellites and considering all the points of the Earth surface, the maximum GDOP experienced will be the same in both cases. Consequently, the second equality is true. The third equality is true by using Theorem 21. The fourth equality is true since the Earth is a solid of revolution (spheroid), and it has a symmetry with respect to the center of the Earth, the points $\mathbf{r}'_{gs}$ cover all the Earth surface as the points $\mathbf{r}_{gs}$. □

Corollary 23. Given a Flower Constellation (FC_1) with the inclination in the range $[0°, 180°]$. There always exists another Flower Constellation (FC_2) with the inclination in the range $[0°, 90°]$ that has the same maximum value for the GDOP experienced as $(FC1)$.

Proof. By using Theorem 22, given a Flower Constellation (FC_1) whose inclination is in the range $[0°, 180°]$ exists a Flower Constellation (FC_2), symmetric with respect to the center of the Earth, whose inclination is in the range $[0°, 90°]$ with identical value for the fitness function. □

Corollary 24. Given a Flower Constellation (FC_1) with the configuration number in the range $N_c \in [0, 1, \ldots, N_o]$. There always exist another Flower Constellation (FC_2) such that the value for N_c is in the region $[0, 1, \ldots, \frac{N_o}{2}]$ and both of them have identical value for the fitness function.

Proof. By using Theorem 22, given a Flower Constellation (FC_1) whose parameter N_c is in the range $[0, 1, \ldots, N_o]$ there always exists a Flower Constellation (FC_2), symmetric with respect to the center of the Earth, whose value of the parameter $N_c \in [0, 1, \ldots, \frac{N_o}{2}]$ and both of them have identical value for the fitness function. □

2.2.3.3 Summary

In this subsection we have reduced the computational cost of our algorithm through two different techniques. The first one by reducing the propagation time needed to compute the maximum value of the GDOP experienced by the constellation. Instead of propagating each constellation $T = N_p T_p$ seconds we propagate them Δt seconds, and this technique can be applied to our three algorithms. The second one by narrowing down the domain of the fitness function. In particular, it is possible to reduce the range of the inclination into $[0°, 90°]$ instead of $[0°, 180°]$ in the brute force search algorithm, as Corollary 23 states. Also it is possible to reduce the range of the parameter $N_c \in [0, \ldots, N_o]$ to the region $[0, \ldots, \frac{N_o}{2}]$ in the Genetic Algorithm and Particle Swarm Optimization algorithm as Corollary 24 states.

2.3 Results

2.3.1 Method comparison

In this research three different algorithms have been used: a brute force search or exhaustive search to have an approximate idea of the optimal solution and two evolutive algorithms. These last two are the Genetic Algorithm and Particle Swarm Optimization algorithm, which improve substantially the brute force search, as we show below.

For a given a number of satellites N_{sat}, according to the 2D-LFC theory, the number of different constellations, is given by the Eq. (2.1). Thus, the total number of constellations with $18 \leq N_{sat} \leq 40$ is equal to:

$$\sum_{n=18}^{40} f(n) = 1104. \tag{2.15}$$

Each of these 1104 cases has been analyzed to find the best parameters (e, i, ω) that minimize the GDOP with the three methods. Figure 2.8 shows the number of times in which one method is better than the others, considering a reference grazing angle equal to 10°. The PSO algorithm is the best method followed by the Genetic Algorithm and the exhaustive search algorithm. In certain configurations, it is impossible to find a constellation with GDOP better than 99. For instance, when $N_o = 1$ the satellites are always on the same orbit plane, hence the maximum GDOP is 99. Those cases have

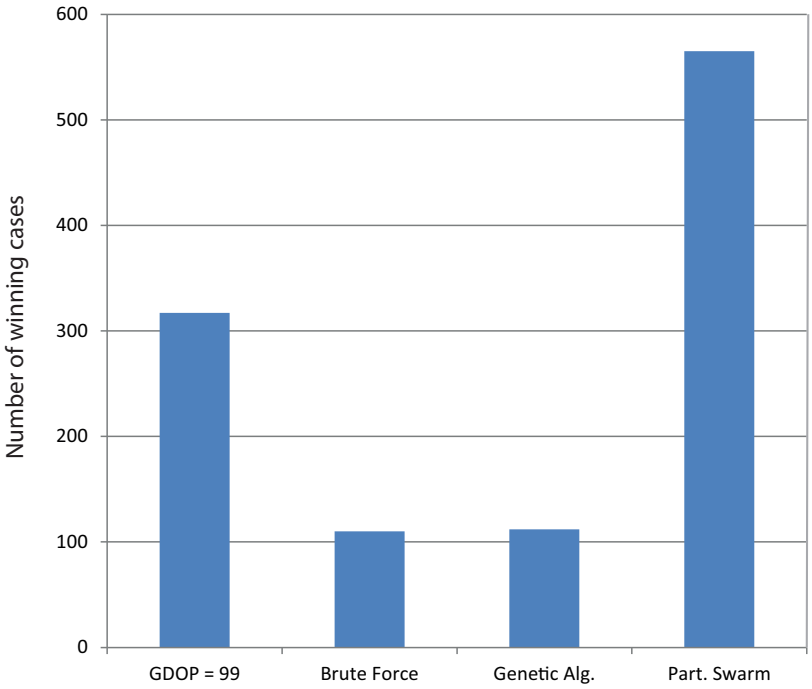

Figure 2.8: Comparison of the three methods.

been excluded from the comparison between methods, and they are represented with a separate bar in Figure 2.8.

Another interesting result consist of comparing the Genetic Algorithm and the exhaustive or brute force search algorithm. We count the number of times in which Genetic Algorithm is better than the exhaustive search, excluding in this case the Particle Swarm algorithm. In Figure 2.9 we observe that in 64.45% of the cases the Genetic Algorithm is better than the exhaustive search algorithm.

Finally, we compare the evolutive algorithms. In Figure 2.10 we plot three bars; the first one represents the cases in which the GDOP is equal to 99. The second and third bars represent the cases in which the Genetic Algorithm and the Particle Swarm Algorithm win, respectively. In this case we observe that in 82.03% of the cases the Particle Swarm wins the Genetic algorithm.

Note that the comparison between the three methods is fair because they evaluate the cost function (i.e. the maximum GDOP) the same number of times, as we show below:

- Genetic Algorithm has 60 generations with 60 individuals. Each individual represents a 3-tuple (e, i, ω). For each individual the maximum GDOP of the constellation is computed. In one generation the maximum GDOP is computed 60 times. Thus, in 60 generations the maximum GDOP is calculated 3,600 times.

- Particle Swarm Optimization has 60 generations of 60 particles. As the Genetic Algorithm the maximum value of the GDOP is computed 3,600 times.

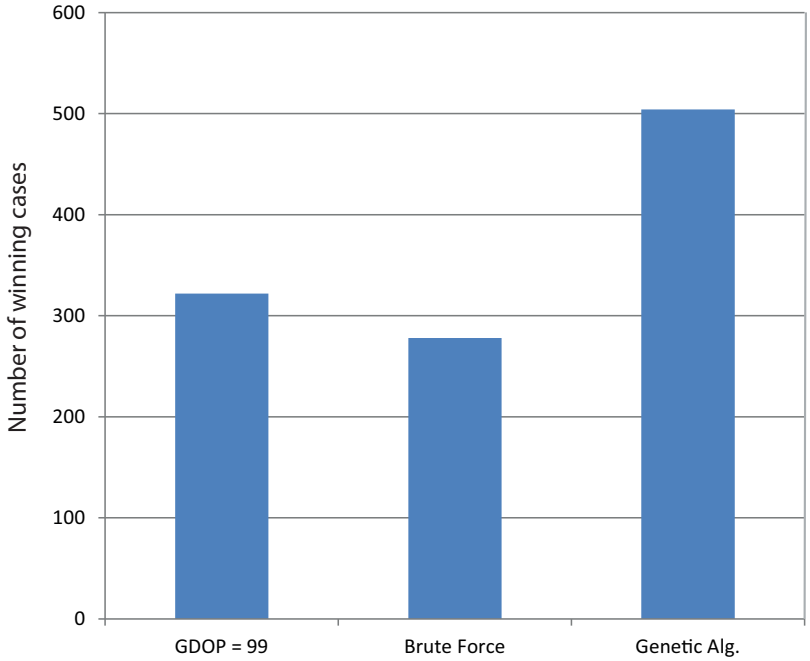

Figure 2.9: Comparison of the Genetic Algorithm and the exhaustive search.

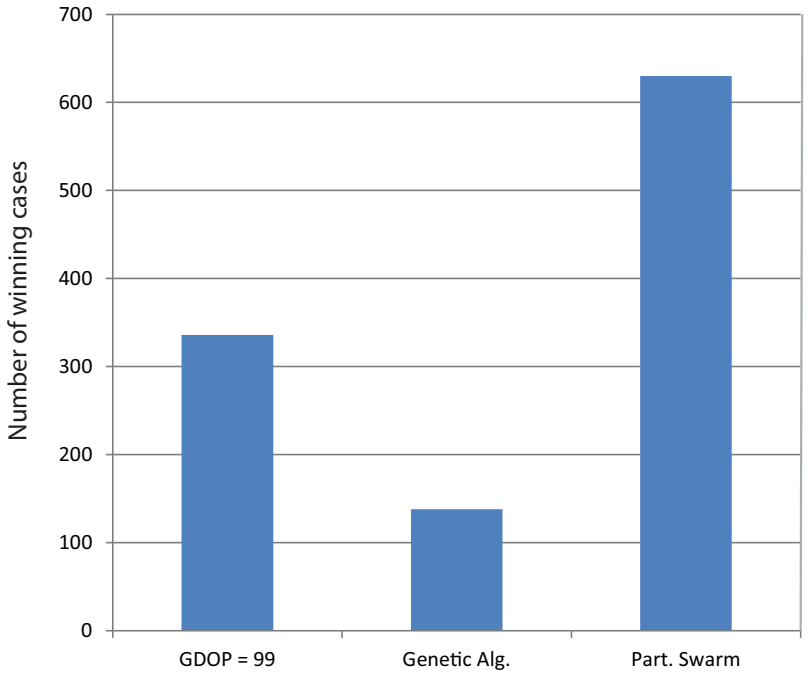

Figure 2.10: Comparison of the Genetic Algorithm and the Particle Swarm algorithm.

Method	N_{sat}	N_o	N_{so}	N_c	e	i	ω	max GDOP
BF	27	3	9	2	0.0300	55.0000	0.0000	3.63983
GA	27	3	9	2	0.0389	55.5870	177.9400	3.64860
PSO	27	3	9	2	0.0000	54.0572	173.7075	3.61023

Table 2.3: Optimal configurations with three different methods.

- Brute Force search algorithms has 20 different values for the eccentricity, that is $e \in [0, 0.3]$ and with step of 0.015. The inclination has 36 different possibilities, that is $i \in [0, 180°]$ with step of 5°. Finally, the argument of perigee $\omega \in [0, 360°]$ with step of 72°, so it assumes only 5 different values. Thus, the maximum value of the GDOP is calculated $20 \cdot 36 \cdot 5 = 3,600$ times.

For example, if we have $N_{sat} = 27$, the time that PSO (60 generations of 60 particles) takes to find the optimal constellation with one core is approximately 3,200 seconds. There are 40 possible configurations for the phasing parameters (N_{so}, N_o, N_c), so the total computational cost would be about $40 \cdot 3,200 = 128,000$ seconds, which are around 1.5 days. When the number of satellites is larger, not only we have more possible configurations, but also the computational time per configuration increases, since there are more satellites to evaluate. That is why some parallelization techniques, some reductions on the search space and optimization in the propagation time are necessary to reduce significantly the computational cost.

2.3.2 Optimal configurations

Consider first a constellation with $N_{sat} = 27$ satellites. As we can see in Table 2.1, there are 40 possible configurations for the phasing parameters. For each of those configurations, the three algorithms were used to determine the best parameters (e, i, and ω) that minimize the maximum value of the GDOP along the propagation time. These optimal parameters are shown in Table 2.3.

It can be clearly seen that the best constellation found depends on the method. We kept track of the results with different grazing angles, but for practical purposes, only the case where the reference grazing angle is equal to 10° is relevant. Regarding the sensitivity to the method, we decided to continue using the three methods, and use the best solution found by any of them. The solutions found by the other two are used to provide some confidence on the optimality of the GDOP.

Now, we do the same for any number of satellites $18 \leq N_{sat} \leq 40$. The GDOP of the best configuration found by each of the three methods is shown in the Figure 2.11. We only show the configurations with more than 23 satellites, since the cases with $N_{sat} \leq 23$ have GDOP above 5, which is considered not good for solving a global positioning problem.

Intuitively, the more satellites the constellation has, the better results for the GDOP value should be obtained. However, this is not always true, because with 27 satellites

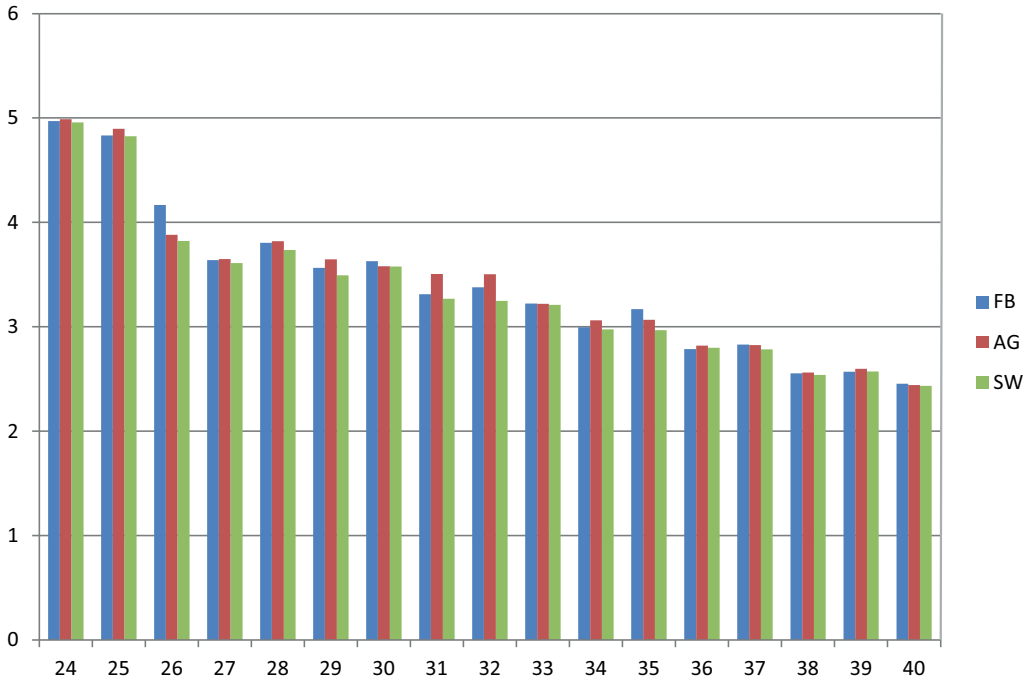

Figure 2.11: Maximum GDOP experienced for constellation with satellites between 24 and 40 satellites.

we obtained better results than with 28 satellites. A similar behaviour is observed with 29 and 30 satellites and also with 38 and 39 satellites.

It seems that the number of configurations is a potential factor to find good constellations, i.e. the more configurations are possible, the more possibilities to find a good constellation for global coverage. But this is not always true as we can observe with 29 and 30 satellites, because the 29 satellites constellation has fewer configurations than the 30 satellites constellation and we obtain better results.

The best configurations found for $N_{sat} \in [24, 40]$ are summarized in Table 2.4.

2.3.3 Eccentric orbits

One of the innovative results, thanks to the 2D-LFC theory, is that eccentric orbits are considered in the searching process. As we can see in Table 2.4, in many occasions the optimal configuration has a highly eccentric orbit. For instance, when $N_{sat} = 35$, the optimal constellation has $e = 0.3$. This case is shown in Figure 2.12.

2.3.4 Comparison

Galileo Constellation [40] is currently being built by the European Union to have an alternative navigation system to the existing GPS System [27,39] (US), the GLONASS

N_{sat}	N_o	N_{so}	N_c	e	i	ω	max GDOP
24	24	1	2	0.000	125.187	88.611	4.96074
25	25	1	2	0.000	127.492	236.480	4.82628
26	26	1	10	0.000	61.104	492.410	3.82216
27	3	9	2	0.000	54.057	173.707	3.61023
28	7	4	2	0.000	127.535	150.965	3.73561
29	29	1	11	0.023	61.518	100.863	3.49341
30	10	3	4	0.036	57.836	263.915	3.57843
31	31	1	4	0.000	71.774	256.259	3.27212
32	16	2	7	0.253	63.514	179.549	3.24969
33	11	3	4	0.006	59.795	94.0092	3.21361
34	34	1	12	0.000	120.478	229.407	2.97527
35	35	1	8	0.300	63.005	0.084	2.95912
36	12	3	4	0.075	60.000	0.000	2.78647
37	37	1	5	0.000	60.637	82.5934	2.79373
38	38	1	14	0.000	59.039	184.670	2.53557
39	13	3	4	0.065	60.000	0.000	2.57115
40	10	4	7	0.000	58.009	25.722	2.43542

Table 2.4: Optimal configurations with reference grazing angle $\alpha = 10°$.

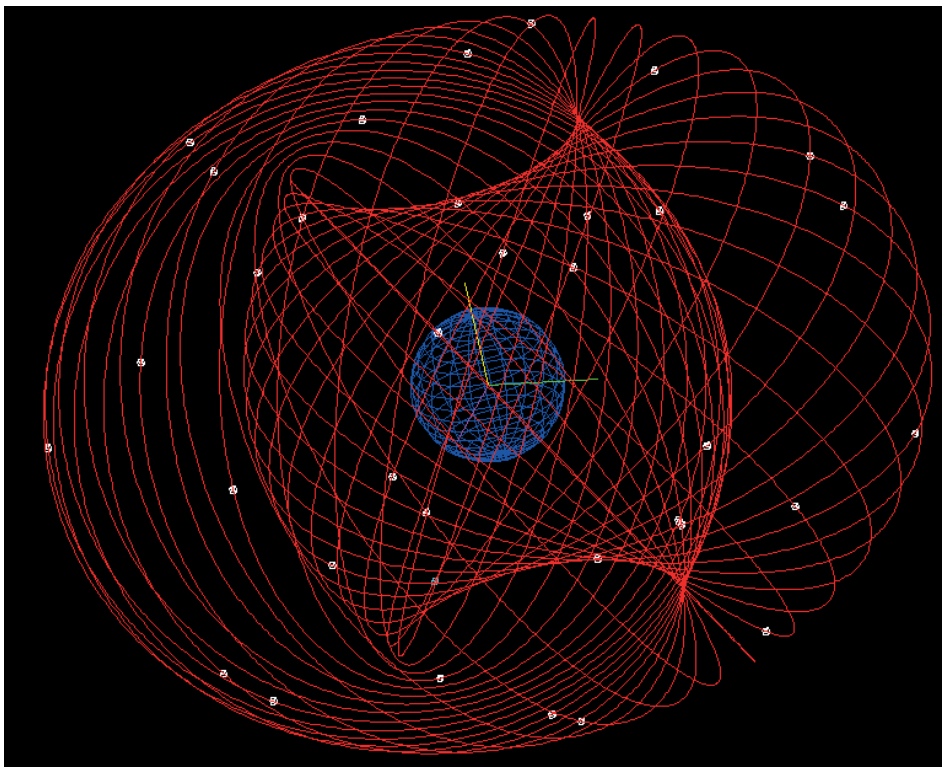

Figure 2.12: A $(N_o = 35, N_{so} = 1, N_c = 8, N_p = 17, N_d = 10, e = 0.3, i = 63.005, \omega = 0.084)$ 2D-LFC.

N_{sat}	N_o	N_{so}	N_c	e	i	ω	max GDOP
24	3	8	1	0.106	55.60	22.90	5.97224

Table 2.5: Parameters and GDOP of a 24 2D-LFC with a reference angle of incidence of 80°.

N_{sat}	N_o	N_{so}	N_c	e	i	ω	max GDOP
24	3	8	1	0.0	63.124	151.444	3.79882

Table 2.6: Parameters and GDOP of a 24 2D-LFC with a reference angle of incidence of 85°.

(Russian), and the Chinese Compass System. This constellation has 27 satellites moving in three circular orbits with an inclination of 56°. This corresponds to the 2D-LFC with parameters $N_o = 3$, $N_{so} = 9$, $N_c = 2$, $e = 0$, and $i = 56°$. The semi-major axis is determined by the compatibility ratio $N_p/N_d = 17/10$.

Using a reference grazing angle $\alpha = 10°$ and our algorithms, the original Galileo Constellation has a $GDOP = 3.77602$. Table 2.3 shows that the three methods were able to find constellations with $N_{sat} = 27$ that are marginally better than Galileo. The best of these three constellations, which was found by the Particle Swarm Algorithm, is also shown in Table 2.4 and it has $GDOP = 3.61023$.

The GLobal NAvigation Satellite System (GLONASS) corresponds to the 2D-LFC with parameters $N_o = 3$, $N_{so} = 8$, and $N_c = 1$. The eccentricity is equal to 0.0, and the inclination is 64.8°. The semi-major axis is about $25,478.137\,km$. The ratio $N_p/N_d \cong 2.13$. Then, we select $N_p = 21$ and $N_d = 10$. With a reference angle of incidence of 80° and propagating the satellites with a time step equal to 60.0 seconds, with our algorithms the GDOP of the GLONASS constellation is 99, while our best result for the 2D-LFC is shown in Table 2.5.

However, if we consider a reference angle of incidence equal to 85° the GDOP of GLONNAS with our algorithms is 3.92058. By using the evolutionary algorithms with the GLONNAS configuration, our results, which slightly improves the GLONASS ones, are shown in Table 2.6.

2.3.5 Time-evolution of the GDOP

While our algorithms compare constellations based on the worst GDOP value seen by any of the ground stations at any instant of time, it would be interesting to see the evolution in time of the maximum GDOP, average GDOP, and minimum GDOP experienced by the 30,000 ground stations. These three values of the GDOP are shown in Fig. 2.13 for our optimal constellation with 27 satellites. For clarity, Fig. 2.14 shows only the evolution of the maximum value of the GDOP over time.

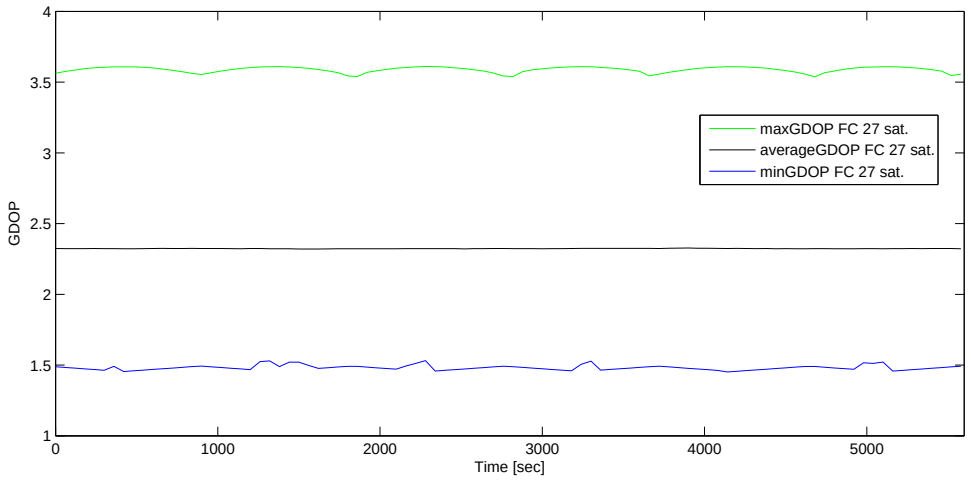

Figure 2.13: Maximum, minimum and average GDOP value of our 27 satellite constellation.

In the first of these figures, we can see that the maximum GDOP experienced by the 30,000 stations is around 3.6 at any time, meaning that there is always a ground station where the GDOP is about 3.6, and that no ground station has a GDOP worse than that. Similarly, we can see that the minimum GDOP is aproximately 1.5, so there is always a point on the Earth where the GDOP is as good as 1.5. Finally, the average moves around 2.3, so we can expect half of the ground stations to have a GDOP between 1.5 and 2.3, and the other half in the interval [2.3, 3.6]. Intuitively, this means that about half of the surface of the Earth would experience a GDOP better than 2.3.
In the next figure, we can see that the maximum GDOP oscillates between 3.58 ± 0.04. The deviation from the center value is less than 1.2%. This indicates that the performance of the constellation remains almost constant over time.

Finally, we provide in Fig. 2.15 a comparison between Galileo and the 27 satellite optimal constellation, which we already know has better maximum GDOP. In Figure 2.16 and Figure 2.17 we illustrate the average and minimum GDOP experienced during the propagation time of Galileo constellation and our 27 FC, respectively. With respect to the average metric, Galileo seems to be better than our constellation, except during some small intervals of time. However with respect to the minimum GDOP, we observe that none of the constellations are better than the other.

Now we compare the 24 satellite Flower Constellation with the existing GLONASS constellation. In this case we compare the maximum GDOP values experienced over time. As we illustrate in Figure 2.18 our constellation is better at any time.

As we observe in Table 2.4 there exist some configurations that obtain better results with less satellites. For example with 27 satellites we obtain better results than with 28 satellites. The same thing occurs with 29 and 30 satellites, and also with 38 and 39 satellites. Figure 2.19 and Figure 2.20 show the maximum GDOP of the constellations

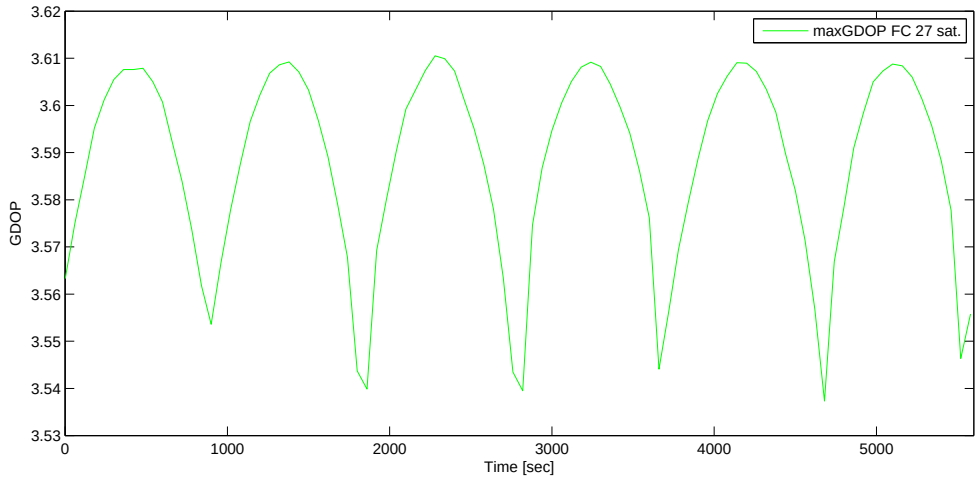

Figure 2.14: Maximum GDOP value of our 27 satellite constellation over time.

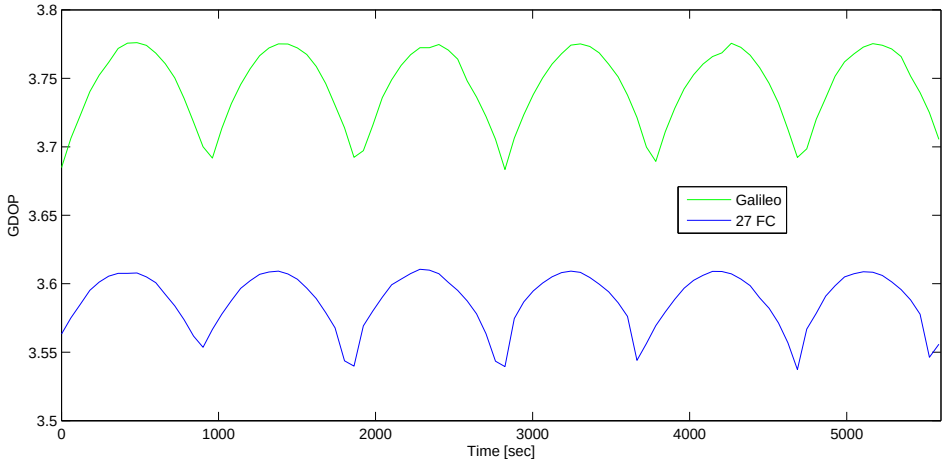

Figure 2.15: Maximum GDOP of Galileo Constellation and our 27 satellite constellation.

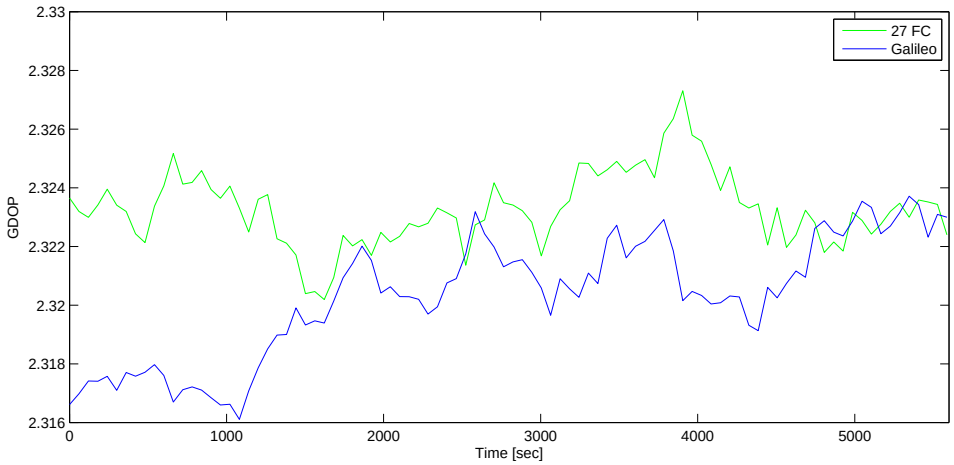

Figure 2.16: Average GDOP of Galileo Constellation and our 27 satellite constellation.

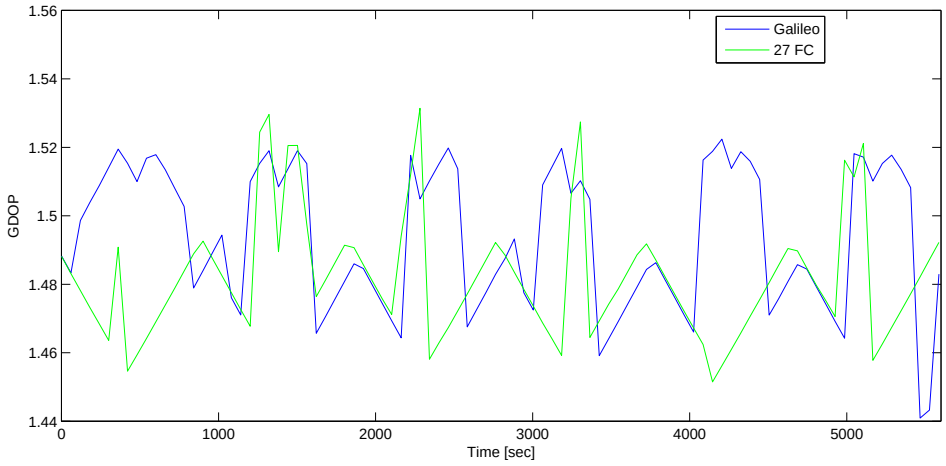

Figure 2.17: Minimum GDOP of Galileo Constellation and our 27 satellite constellation.

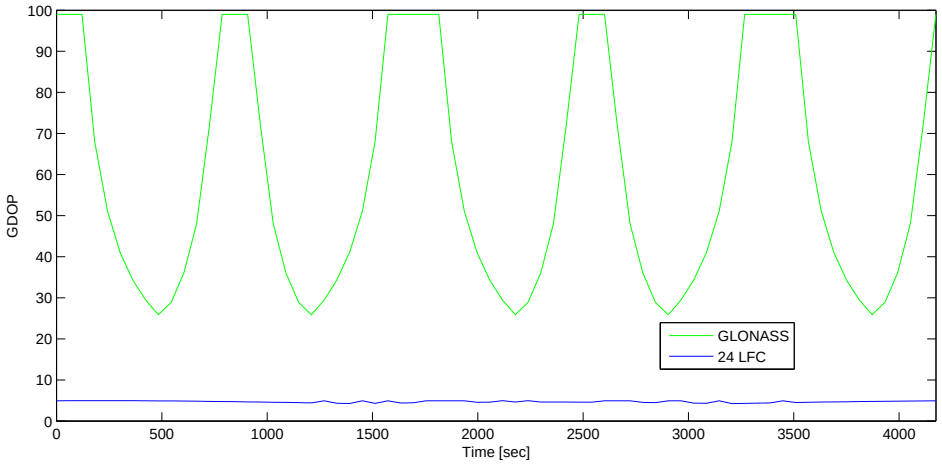

Figure 2.18: Maximum GDOP experienced over time of GLONASS constellation and our 24 satellites 2D-LFC.

experienced over time that confirms that sometimes with less satellites it is possible to obtain better results.

2.4 Conclusions

Through this work we found optimal configurations for solving a global positioning problem. To search among all possible design variables we use evolutive algorithms. Due to the high computational cost of the evolutive algorithms in this work, we found several ways to reduce the computational cost, such as; the search space reduction or the propagation time reduction. The computational time has been also reduced by using parallelization techniques.

In this study, the problem of the collision between satellites is completely ignored, since a constellation with a low GDOP value means that all satellites are never align and always far away from each other, while a bad GDOP means that the satellites are almost align and consequently there exist risk of collision.

Note that, most of the optimal configurations have one satellite per orbit and we know that launch a constellation with more than three orbital planes has a high monetary cost. However, we also have configurations with a small number of orbital planes.

An interesting line of research would be studying the low thrust needed to maintain the configuration of the constellation under the J_2 effect. A first step in this direction is done in the next chapter. We try to obtain parameters of a FC, in such a way that all the satellites are perturbed in the same way and consequently the relative position of the satellites in the osculating elements space remains almost constant, what we call Rigid Constellation.

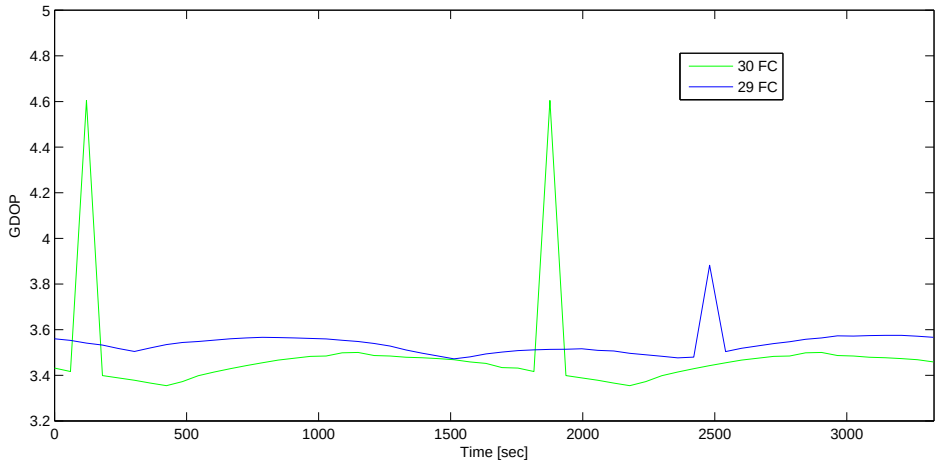

Figure 2.19: Maximum GDOP experienced over time of our 29 satellites 2D-LFC and our 30 satellites 2D-LFC.

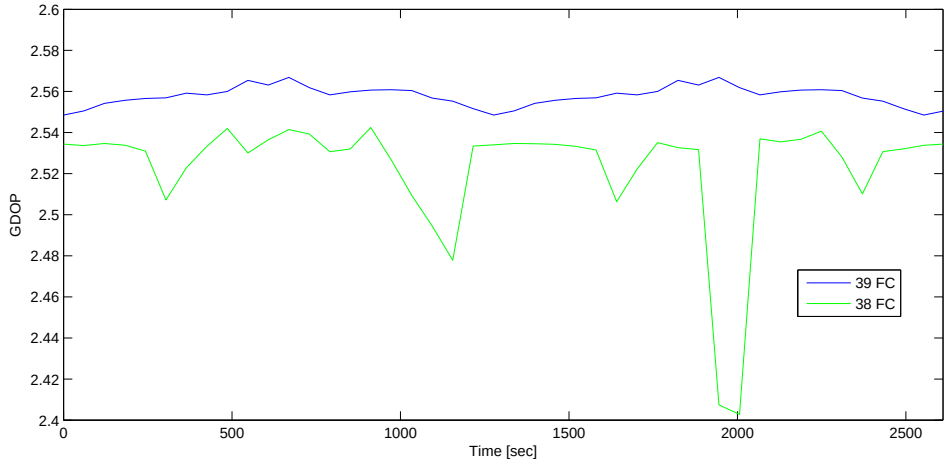

Figure 2.20: Maximum GDOP experienced over time of our 38 satellites 2D-LFC and our 39 satellites 2D-LFC.

Chapter 3

Flower Constellations under the J_2 effect

3.1 Introduction

The instantaneous position (and velocity) of a satellite orbiting about the Earth is determined by six orbital parameters; semi-major axis (a), eccentricity (e), inclination (i), argument of perigee (ω), Right Ascension of the Ascending Node (Ω), and Mean anomaly (M). In a 2D-LFC all the satellites have the same a, e, i, ω, and the pairs (Ω, M) lie on a lattice given by three integer parameters N_o, N_{so}, N_c, see section 1.2.1. The configuration determined by these parameters is denoted $FC(N_o, N_{so}, N_c, a, e, i, \omega, \Omega, M)$.

In the keplerian model, the evolution of the orbital parameters of the satellites of a Flower Constellation is very simple, because all the parameters remain constant, except for the mean anomaly M that increases linearly at the same rate $n = \sqrt{\mu/a^3}$ for all the satellites.

$$FC(N_o, N_{so}, N_c, a, e, i, \omega, \Omega, M) \overset{t/\text{Kepler}}{\longrightarrow} FC(N_o, N_{so}, N_c, a, e, i, \omega, \Omega, M + nt). \quad (3.1)$$

Hidden in Eq. (3.1) is a remarkable fact about Flower Constellations in the keplerian model that motivates part of this work: FCs remain FCs!

In this chapter we investigate whether something similar happens when the keplerian potential is perturbed with the J_2 term. Note that, the only way that FCs, when propagated under the effect of J_2, remain being FCs, is when J_2 perturbs all the satellites in the FC in exactly the same way. More precisely, we ask for the existence of functions $a(t)$, $e(t)$, $i(t)$, $\omega(t)$, $\Omega(t)$, $M(t)$, such that

$$FC(N_o, N_{so}, N_c, a, e, i, \omega, \Omega, M) \overset{t/J_2}{\longrightarrow} FC(N_o, N_{so}, N_c, a(t), e(t), i(t), \omega(t), \Omega(t), M(t)). \quad (3.2)$$

Constellations satisfying Eq. (3.2), named Rigid Constellations, are our main subject of interest.

3.2 Dynamics of the satellites

As we have shown in the preliminaries, the motion of a satellite under any conservative force field is determined by the potential function and the initial conditions. Once the potential function is determined, we apply the gradient operator and solve the system of equations of order one given in (1.31).

Given an initial position $\mathbf{r}_0$ and velocity $\mathbf{v}_0$, the solution of Eqs. (1.31) describes the motion completely. The instantaneous position $\mathbf{r}(t)$ and velocity $\mathbf{v}(t)$ are called state vectors. Another way of describing the motion of the satellite is using the osculating elements $a(t)$, $e(t)$, $i(t)$, $\omega(t)$, $\Omega(t)$ and $M(t)$ as we explained in subsection 1.1.2.2.

In subsection 1.1.2.2 we mentioned that in the keplerian motion, all the orbital elements except M are constant. The evolution of them over time can be represented as a straight line, since M increases linearly: $M(t) = M_0 + nt$ where $n = \sqrt{\mu/a^3}$ is the mean motion. When some perturbations appear, the potential can be split as:

$$V(\mathbf{r}) = V_{kep} + R, \tag{3.3}$$

and the orbital elements are not longer constant, whose evolution follow Lagrange Planetary Equations (1.38). The osculating elements have three different kind of terms [1], illustrated in Figure 3.1:

- Polynomial terms in the variable t. These terms produce a secular displacement from the constant behavior of the orbital elements that take place in the keplerian motion.
- Terms of sine and cosine of the variables ω, Ω, and i. Due to the slowly variation of these angular variables, they cause a periodic oscillation with long period. This terms are named long periodic terms.
- Terms of sine and cosine of the variable M, which has the same period as the orbit. They cause small oscillations around the secular perturbation and the long period perturbation. They are named short periodic terms.

In this thesis, we only make a distinction between the first kind of terms (secular) $a_{sec}(t), e_{sec}(t), \ldots, M_{sec}(t)$ and the sum of the last two terms (non-secular). When the potential is perturbed only with the J_2 term, the secular components of the osculating elements show a linear secular behavior.

3.3 Problem formulation

We assume that the Earth is a revolution body, consequently, the tesseral harmonic terms of the potential function are zero, and the potential function have only zonal harmonic terms. As a first approximation, we consider only the J_2 effect since it is almost 1000 times larger than the next coefficient J_3. Then, our potential function becomes:

$$V(\mathbf{r}) = V_{kep} + R_{J_2}. \tag{3.4}$$

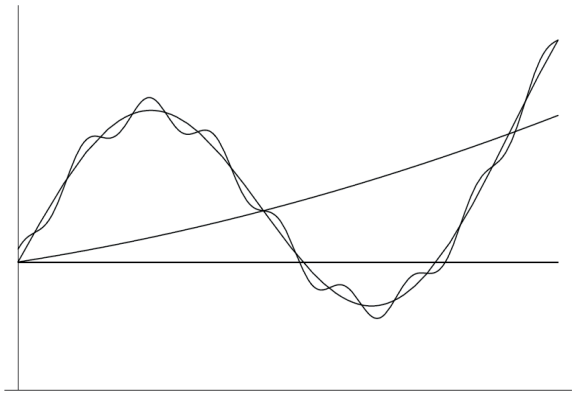

Figure 3.1: Secular and non-secular perturbations.

We need the expression of the potential function in terms of the position and velocity and in terms of the orbital elements, in order to obtain the motion of a satellites through Eqs. (1.37) and Eqs. (1.38).

3.3.1 Potential as a function of position and velocity

Following Eq. (1.34), the expression of the potential in terms of the position and velocity, considering only the zonal harmonic (J_2) is,

$$\begin{aligned} V(\mathbf{r}) &= V_{kep} + R_{J_2} \\ &= -\frac{\mu}{r} + \frac{\mu}{r} J_2 \left(\frac{r_\oplus}{r}\right)^2 P_2\left(\sin(\phi_{sat})\right) \\ &= -\frac{\mu}{r} + \frac{\mu}{r} J_2 \left(\frac{r_\oplus}{r}\right)^2 \frac{1}{2}\left(3\left(\frac{z}{r}\right)^2 - 1\right). \end{aligned}$$

The last equality is true since ϕ_{sat} represents the latitude of the satellite, thus $\sin(\phi_{sat}) = z/r$. We apply the gradient operator to the previous expression of the potential,

$$\begin{aligned} \frac{\partial V}{\partial x} &= \frac{\partial V_{kep}}{\partial x} + \frac{\partial R_{J_2}}{\partial x} = \mu\frac{x}{r^3} + \frac{\mu J_2 r_\oplus^2 x}{r^7}\frac{3}{2}(x^2 + y^2 - 4z^2), \\ \frac{\partial V}{\partial y} &= \frac{\partial V_{kep}}{\partial y} + \frac{\partial R_{J_2}}{\partial y} = \mu\frac{y}{r^3} + \frac{\mu J_2 r_\oplus^2 y}{r^7}\frac{3}{2}(x^2 + y^2 - 4z^2), \\ \frac{\partial V}{\partial z} &= \frac{\partial V_{kep}}{\partial y} + \frac{\partial R_{J_2}}{\partial y} = \mu\frac{z}{r^3} + \frac{\mu J_2 r_\oplus^2 z}{r^7}\frac{3}{2}(3x^2 + 3y^2 - 2z^2). \end{aligned}$$

Finally, the first order system of equations given in (1.37) can be expressed as follows:

$$\begin{cases} \dot{x} = v_x, \\ \dot{y} = v_y, \\ \dot{z} = v_z, \\ \dot{v_x} = -\frac{\partial V}{\partial x} = -\mu\frac{x}{r^3} - \frac{\mu J_2 r_\oplus^2 x}{r^7}\frac{3}{2}(x^2+y^2-4z^2), \\ \dot{v_y} = -\frac{\partial V}{\partial y} = -\mu\frac{y}{r^3} - \frac{\mu J_2 r_\oplus^2 y}{r^7}\frac{3}{2}(x^2+y^2-4z^2), \\ \dot{v_z} = -\frac{\partial V}{\partial z} = -\mu\frac{z}{r^3} - \frac{\mu J_2 r_\oplus^2 z}{r^7}\frac{3}{2}(3x^2+3y^2-2z^2). \end{cases} \tag{3.5}$$

3.3.2 Potential as a function of the orbital elements

In order to use Lagrange Planetary Equations we should determine the potential function in terms of the orbital elements. For that purpose, the latitude of the satellite can be rewritten as $\sin(\phi_{sat}) = z/r$, where $z = r\sin(i)\sin(\omega+\varphi)$ and φ represents the true anomaly. Thus, the potential function in terms of the orbital elements is:

$$\begin{aligned} V(\mathbf{r}) &= V_{kep} + R_{J_2} \\ &= -\frac{\mu}{r} + \frac{\mu}{r} J_2 \left(\frac{r_\oplus}{r}\right)^2 \frac{1}{2}\left(3\sin^2(i)\sin^2(\omega+\varphi) - 1\right). \end{aligned}$$

The standard approach is to consider an averaged perturbed potential $\overline{R_{J_2}}$ over an orbital period, instead of the full expression of R_{J_2}, in order to focus on the non-periodic variations (short periodic terms) of the orbital parameters [10].

$$\overline{R_{J_2}} = \frac{1}{2\pi}\int_0^{2\pi} R_{J_2}(a,e,i,\omega,\Omega,M)dM = \frac{\mu J_2 r_\oplus^2 (2-3\sin^2 i)}{4a^3(1-e^2)^{\frac{3}{2}}}. \tag{3.6}$$

In this case, Lagrange Planetary Equations show that the osculating orbital parameters of any satellite are linear functions whose slopes are given by:

$$\begin{aligned} \dot{a} &= 0, & \dot{\omega} &= \frac{3}{4} J_2 \left(\frac{r_\oplus}{p}\right)^2 n\left(5\cos^2 i - 1\right), \\ \dot{e} &= 0, & \dot{\Omega} &= -\frac{3}{2} J_2 \left(\frac{r_\oplus}{p}\right)^2 n\cos i, \\ \dot{i} &= 0, & \dot{M} &= n\left[1 + \frac{3}{4}\sqrt{1-e^2} J_2 \left(\frac{r_\oplus}{p}\right)^2 \left(3\cos^2 i - 1\right)\right]. \end{aligned} \tag{3.7}$$

Applying these formulas to the case of FCs, we see that all the satellites suffer exactly the same perturbation due to $\overline{R_{J_2}}$, since all the satellites have the same a, e, i, and ω. Note that, in this case there is no non-secular component of the osculating elements. This shows that, for the case of the averaged perturbed potential, the conclusion of Eq. (3.2) is valid.

It is important to note that Eqs. (3.7) are the main assumption of the theory of 3D-LFC [18, 19]. In this thesis, we will analyze whether the same happens under the

full expression of the potential, considering only the zonal harmonic (J_2). When the propagation is done with the full expression of R_{J_2}, the osculating elements show a slightly different behavior: each parameter has a secular component (a linear function) and a non-secular component (small oscillations with average zero). Using Lagrange Planetary Equations and the full expression of R_{J_2}, it is possible to obtain the variation of the orbital elements over time [25]:

$$\begin{cases} \dot{a} = -\dfrac{6b\sqrt{1-e^2}}{na^4}\left\{\dfrac{-e}{(1-e^2)}\dfrac{a^4}{r^4}\sin\varphi\left[\dfrac{3}{2}\sin^2 i(1-\cos 2u)-1\right]+\dfrac{a^5}{r^5}\left[\sin^2 i\sin 2u\right]\right\}, \\ \dot{e} = -\dfrac{3b(1-e^2)^{\frac{3}{2}}}{na^5e}\left\{\dfrac{-e}{(1-e^2)}\dfrac{a^4}{r^4}\sin\varphi\left[\dfrac{3}{2}\sin^2 i(1-\cos 2u)-1\right]+\dfrac{a^5}{r^5}\left[\sin^2 i\sin 2u\right]\right\}+ \\ \quad +\dfrac{3b\sqrt{1-e^2}}{na^5e}\dfrac{a^3}{r^3}\sin^2 i\sin 2u, \\ \dot{i} = -\dfrac{3b}{2na^5\sqrt{1-e^2}}\dfrac{a^3}{r^3}\sin 2i\sin 2u, \\ \dot{\omega} = -\dfrac{3b\sqrt{1-e^2}}{na^5e}\left\{\dfrac{a^4}{r^4}\cos\varphi\left[\dfrac{3}{2}\sin^2 i(1-\cos 2u)-1\right]+\dfrac{a^3}{r^3}\left[\sin^2 i\sin 2u\dfrac{2+e\cos\varphi}{1-e^2}\sin\varphi\right]\right\}+ \\ \quad +\dfrac{3b}{na^5\sqrt{1-e^2}}\dfrac{a^3}{r^3}\left[\cos^2 i(1-\cos 2u)\right], \\ \dot{\Omega} = -\dfrac{3b}{na^5\sqrt{1-e^2}}\dfrac{a^3}{r^3}\left[\cos i(1-\cos 2u)\right], \\ \dot{M} = n-\dfrac{6b}{na^5}\dfrac{a^3}{r^3}\left[\dfrac{3}{2}\sin^2 i(1-\cos 2u)-1\right]+ \\ \quad +\dfrac{3b(1-e^2)}{na^5e}\left\{\dfrac{a^4}{r^4}\cos\varphi\left[\dfrac{3}{2}\sin^2 i(1-\cos 2u)-1\right]+\dfrac{a^3}{r^3}\left[\sin^2 i\sin 2u\dfrac{2+e\cos\varphi}{1-e^2}\sin\varphi\right]\right\}. \end{cases} \tag{3.8}$$

Where $b=\frac{\mu J_2 r_\oplus^2}{2}$ and $u=\omega+\varphi$. In this situation, the only way we can obtain Eq. (3.2) for a FC, would be by showing that:

(a) The slopes of $a_{sec}(t)$, $e_{sec}(t)$, $i_{sec}(t)$, $\omega_{sec}(t)$, $\Omega_{sec}(t)$, $M_{sec}(t)$ depend only on the initial a, e, i, ω, hence the same for all satellites.

(b) The non-secular component is negligible (within a certain tolerance).

In the following section we show that the slopes of $a_{sec}(t)$, $e_{sec}(t)$, $i_{sec}(t)$, $\omega_{sec}(t)$, $\Omega_{sec}(t)$, $M_{sec}(t)$ do not depend on Ω. However, they depend on the initial Mean anomaly of each satellite, which is a major problem since the satellites in a FC have different values of M. We propose a method to correct this problem for a FC, by changing the semi-major axis of the satellites by a few kilometers, in such a way that the secular part of the osculating elements of each satellite will have the same slope. Thus, the secular part can be controlled in a FC.

We also describe the non-secular component of a satellite and we study its dependency with respect to the initial orbital elements of the satellite. We will find different regions where the non-secular component of a satellite is minimized. Finally, by providing a good set of initial conditions we will have 2D-LFCs which stay as 2D-LFCs even under the J_2 effect, and therefore Eq. (3.2) will be valid up to a given tolerance.

3.4 Secular and non-secular perturbations of the osculating elements

In this section we analyze how the J_2 term affects a satellite orbiting about the Earth. As an example we select random initial orbital elements for a satellite; $a = 26,544.2976\,km$, $e = 0.1046$, $i = 36.3356°$, $\omega = \Omega = M = 0.0$. This satellite has an orbital period of approximately 12 hours. We integrate the system of Eqs. (3.8) applying a Runge Kutta method of order 4, with fixed step $\delta t = 1.0\,sec$ during 432,000 seconds (i.e. five days).

Figure 3.2, Figure 3.3, and Figure 3.4 show the evolution of the semi-major axis, eccentricity and inclination over time, respectively. It is possible to observe that the secular perturbation of these parameters are equal to zero. However, the non-secular perturbation makes them oscillate. The semi-major axis oscillates about $2.5\,km$, the eccentricity about 10^{-4} and the inclination around $0.0034°$ each orbital period. Figure 3.5 and Figure 3.6 show the evolution of the argument of perigee and the RAAN, respectively. In these cases we observe a secular and non-secular behavior in each parameter. Finally, Figure 3.7 shows the evolution of the Mean anomaly over time and we observe a small oscillation besides a secular behavior. Note that, instead of a line, the plot has a sawtooth shape due to the modular nature of angular values. For clarity, the non-secular component of M during an orbital period has been plotted separately in Figure 3.10

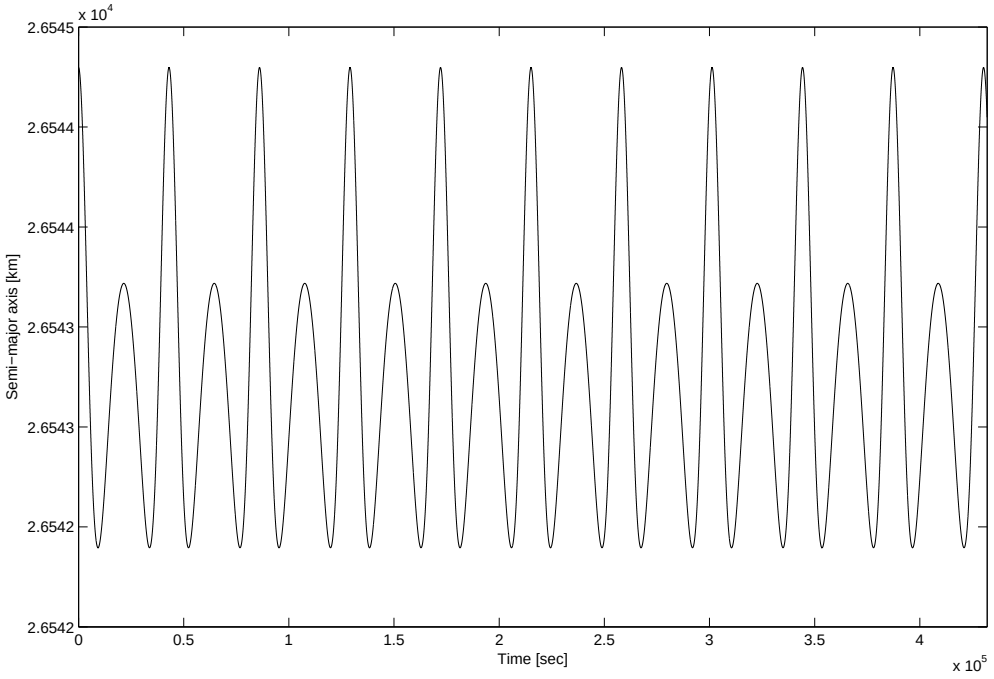

Figure 3.2: Evolution of the semi-major axis.

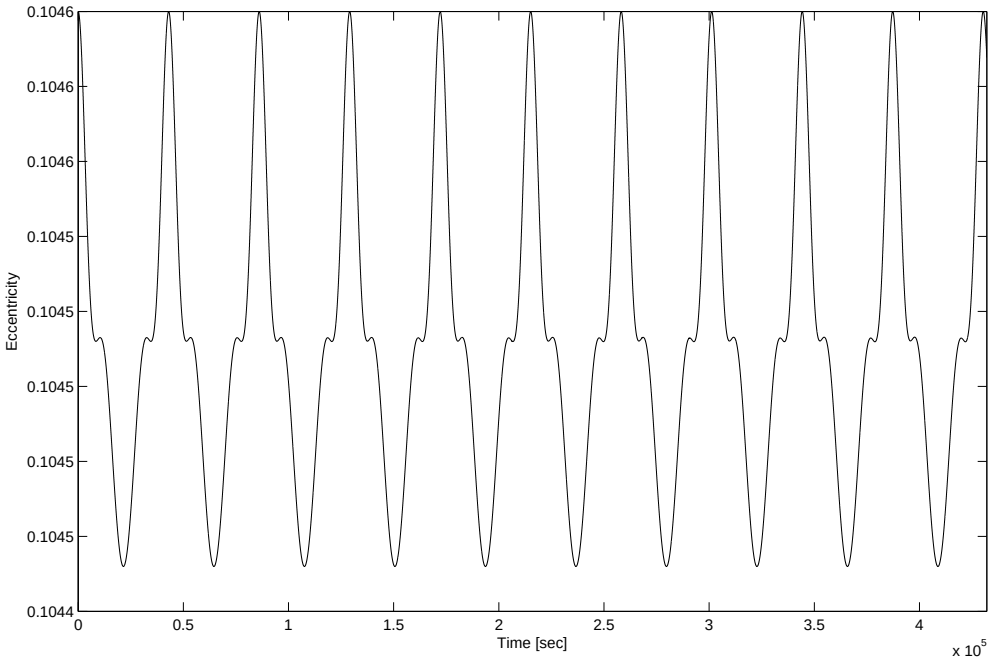

Figure 3.3: Evolution of the eccentricity.

In order to determine the secular component of an osculating element $q \in \{a, e, i, \omega, \Omega, M\}$, we use linear interpolation over the data set consisting of the pairs $(t, q(t))$ obtained by propagating with the full expression of the potential R_{J_2}. For the angular parameters ω, Ω, and M, we add or subtract multiplies of 2π before the linear interpolation, to handle the non-linearity created by their modulus 2π behavior. In Table 3.1, we compare the slopes of the secular components of the osculating elements computed with our linear interpolation and the ones that would be obtained if the propagation were done using the averaged potential $\overline{R_{J_2}}$. The difference between both propagations is very small in one orbital period but it is not bounded for a long time period propagation. Since we are interested in highly accurate results, we disregard the averaged potential in favor of the full expression of R_{J_2}.

There are cases that require a special treatment. For instance, when the eccentricity approaches zero, there is a large variation in ω. Actually, when $e = 0.0$ the argument of perigee is undefined. In the previous example, we observe that the argument of perigee oscillates around $10^{-3}\,rad$ (see Figure 3.5) due to the non-secular component. Now, we consider the same example but we change the eccentricity ($e = 0.0001$). In this case, as we illustrate in Figure 3.8 the secular and non-secular components of the argument of perigee are extremely high. Besides, in Figure 3.9 we plot the non-secular component of the argument of perigee in one orbital period. It has been obtained by removing the secular component. In this example, the non-secular component of the argument of perigee oscillates about $2\,rad$ in one orbital period, thus proving the large variation that ω presents in near-circular orbits. An analysis of near-circular orbits, showing that ω behaves this way is given in [11].

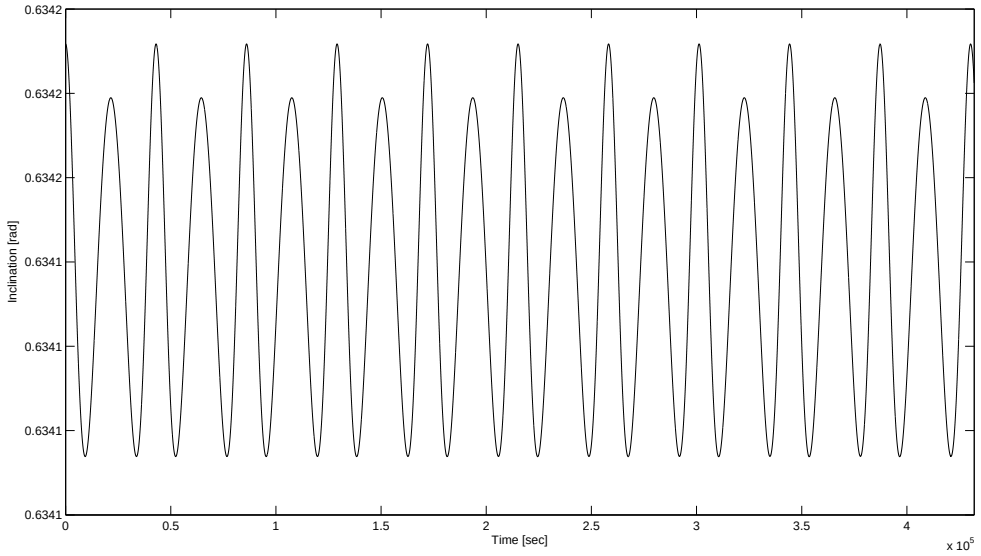

Figure 3.4: Evolution of the inclination.

	$\overline{R_{J_2}}$	R_{J_2}
$\dot{a}_{sec}\,(km{\cdot}sec^{-1})$	0.0	$7.734381692{\cdot}10^{-8}$
$\dot{e}_{sec}\,(sec^{-1})$	0.0	$4.486699948{\cdot}10^{-12}$
$\dot{i}_{sec}\,(rad{\cdot}sec^{-1})$	0.0	$1.336085298{\cdot}10^{-12}$
$\dot{\omega}_{sec}\,(rad{\cdot}sec^{-1})$	$1.570708925{\cdot}10^{-8}$	$1.551532370{\cdot}10^{-8}$
$\dot{\Omega}_{sec}\,(rad{\cdot}sec^{-1})$	$-1.127357777{\cdot}10^{-8}$	$-1.127143934{\cdot}10^{-8}$
$\dot{M}_{sec}\,(rad{\cdot}sec^{-1})$	$1.460054338{\cdot}10^{-4}$	$1.460055229{\cdot}10^{-4}$

Table 3.1: Comparison of the slopes of the secular components of the osculating elements propagating with $\overline{R_{J_2}}$ and R_{J_2}.

Note that, we may think that Figure 3.7 and Figure 3.8 present a similar behavior. Both of them have a huge secular component and the plots have a sawtooth shape. However, in the case of the Mean anomaly (Figure 3.7), we plot its non-secular component in one orbital period in Figure 3.10 and we observe that it is rather small (order $\approx 10^{-4}$), while in the case of the argument of perigee, as we observe in Figure 3.9, the non-secular component is 10,000 times larger.

Another situation that requires special treatment is when $i \approx 0$ or $i \approx \pi$. All these cases are excluded in our research because it is not possible to control or even define the secular part of these parameters [11].

3.4.1 The secular component of the osculating elements

The expression for the gravitational potential including only the J_2 term is symmetric with respect to rotations about the z-axis. Consequently, two satellites with same orbital parameters except the value of the RAAN have an identical evolution over time

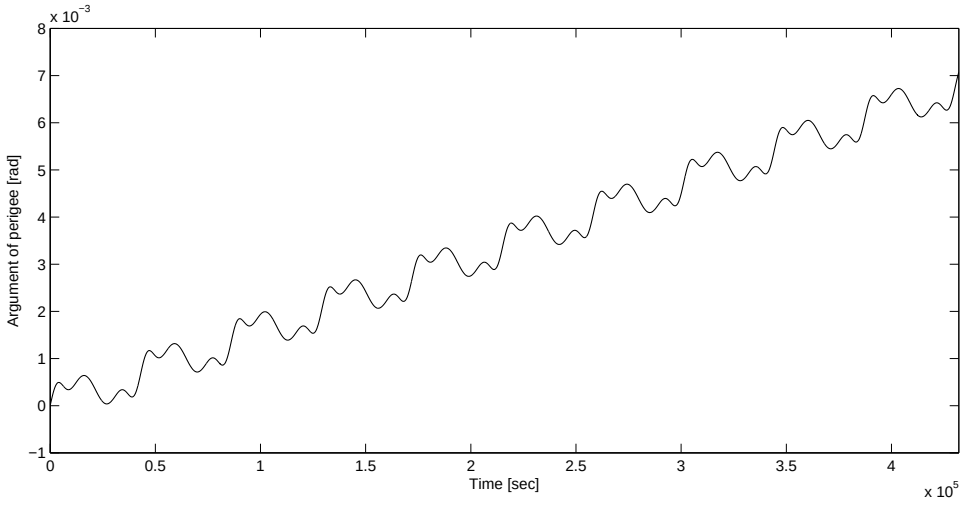

Figure 3.5: Evolution of the argument of perigee.

	$a\,(km)$	e	$i\,(deg)$	$\omega\,(deg)$	$\Omega\,(deg)$	$M\,(deg)$
Sat_1	29000.0	0.35	20.0	130.0	0.0	0.0
Sat_2	29000.0	0.35	20.0	130.0	57.0	0.0
Sat_3	29000.0	0.35	20.0	130.0	125.0	0.0
Sat_4	29000.0	0.35	20.0	130.0	170.0	0.0

Table 3.2: Orbital elements of four satellites.

but rotated about the z-axis. Meaning that, the slopes of $a_{sec}(t)$, $e_{sec}(t)$, $i_{sec}(t)$, $\omega_{sec}(t)$, $\Omega_{sec}(t)$, $M_{sec}(t)$ do not depend on Ω, or in other words, they depend only on the initial a, e, i, ω, and M.

A numerical verification of this claim is provided in Table 3.3. We have selected four satellites with identical initial orbital elements except for the value of the RAAN (see Table 3.2) and we propagated these satellites under the J_2 effect. As shown in Table 3.3 all these slopes coincide up to a relative error of order 10^{-7} (which is the precision of our propagation method).

The dependency of the slopes of the secular components of the osculating elements with respect to the initial Mean anomaly has been tested numerically as follows:

1. We consider an initial set of 100 satellites. The orbital parameters (a, e, i, ω) of each satellite are selected at random in a region of interest. Taking into account that we have already shown that the slopes do not depend on the value of RAAN, we have set this value to zero for all the satellites (i.e. $\Omega = 0.0$).

2. The Mean anomaly $M \in [0, 2\pi]$ is discretized with step of 7.35° for each one of the 100 satellites. Thus, each satellite has 51 different possible values for the Mean anomaly.

3. Finally, each set of initial conditions is propagated using Eqs. (3.8) with a RK of order four during approximately 370 days, with a time step of $20\,sec$.

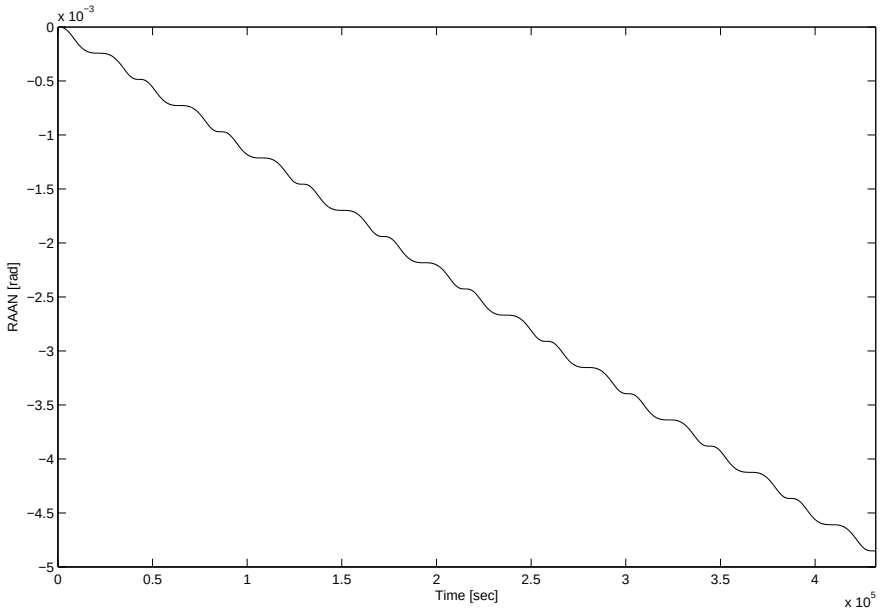

Figure 3.6: Evolution of the RAAN.

	Sat_1	Sat_2	Sat_3	Sat_4
$\dot{a}_{sec}\,(km{\cdot}sec^{-1})$	$-4.402790331{\cdot}10^{-7}$	$-4.402790340{\cdot}10^{-7}$	$-4.402790200{\cdot}10^{-7}$	$-4.402790304{\cdot}10^{-7}$
$\dot{e}_{sec}\,(sec^{-1})$	$-1.906635265{\cdot}10^{-11}$	$-1.906635255{\cdot}10^{-11}$	$-1.906635262{\cdot}10^{-11}$	$-1.906635275{\cdot}10^{-11}$
$\dot{i}_{sec}\,(rad{\cdot}sec^{-1})$	$2.860683558{\cdot}10^{-14}$	$2.860681079{\cdot}10^{-14}$	$2.860682433{\cdot}10^{-14}$	$2.860684176{\cdot}10^{-14}$
$\dot{\omega}_{sec}\,(rad{\cdot}sec^{-1})$	$2.215516231{\cdot}10^{-8}$	$2.215516231{\cdot}10^{-8}$	$2.215516231{\cdot}10^{-8}$	$2.215516231{\cdot}10^{-8}$
$\dot{\Omega}_{sec}\,(rad{\cdot}sec^{-1})$	$-1.223085652{\cdot}10^{-8}$	$-1.223085652{\cdot}10^{-8}$	$-1.223085652{\cdot}10^{-8}$	$-1.223085652{\cdot}10^{-8}$
$\dot{M}_{sec}\,(rad{\cdot}sec^{-1})$	$1.278706109{\cdot}10^{-4}$	$1.278706109{\cdot}10^{-4}$	$1.278706109{\cdot}10^{-4}$	$1.278706109{\cdot}10^{-4}$

Table 3.3: Slopes of the secular components of the osculating elements.

All the satellites present a similar behavior, which is shown next with one particular example. We take, for instance, the satellite whose initial orbital elements are $a = 26,215.017\,km$, $e = 0.090394$, $i = 85.9507°$, $\omega = 208.5061°$, and $\Omega = 0.0°$. The values of the mean anomaly vary between 0° and 360° with a step about 7.35°. Table 3.4 shows how the slopes of the secular components of the osculating elements change depending on the value of the Mean anomaly.

We observe that the slopes of the semi-major axis are the same up to order $10^{-11}\,km/sec$. After 370 days the variation of the semi-major axis will be less than 1 meter ($0.3197\,m$). The slopes of the eccentricity have in all the cases the same value up to order $10^{-14}\,sec^{-1}$. After 370 days, the variation of the eccentricity will be $3.1968{\cdot}10^{-7}$. The slopes of the inclination, $i_{sec}(t)$ are the same up to order $10^{-16}\,rad/sec$. Meaning that after one year (370 days) the variation will be around $10^{-9}\,rad$. We observe that the slopes of $\omega_{sec}(t)$ and $\Omega_{sec}(t)$ have approximately the same value when we change the Mean anomaly. These slopes coincide up to order $10^{-11}\,rad/sec$, meaning that after 370 days, the variation of these elements will be $3.1968{\cdot}10^{-4}\,rad$. All this shows that $a_{sec}(t)$, $e_{sec}(t)$ $i_{sec}(t)$, $\omega_{sec}(t)$, and $\Omega_{sec}(t)$ do not depend significantly on the initial value of M.

However, the slopes of $M_{sec}(t)$ show a difference of order $5.1608{\cdot}10^{-8}\,rad/sec$, which

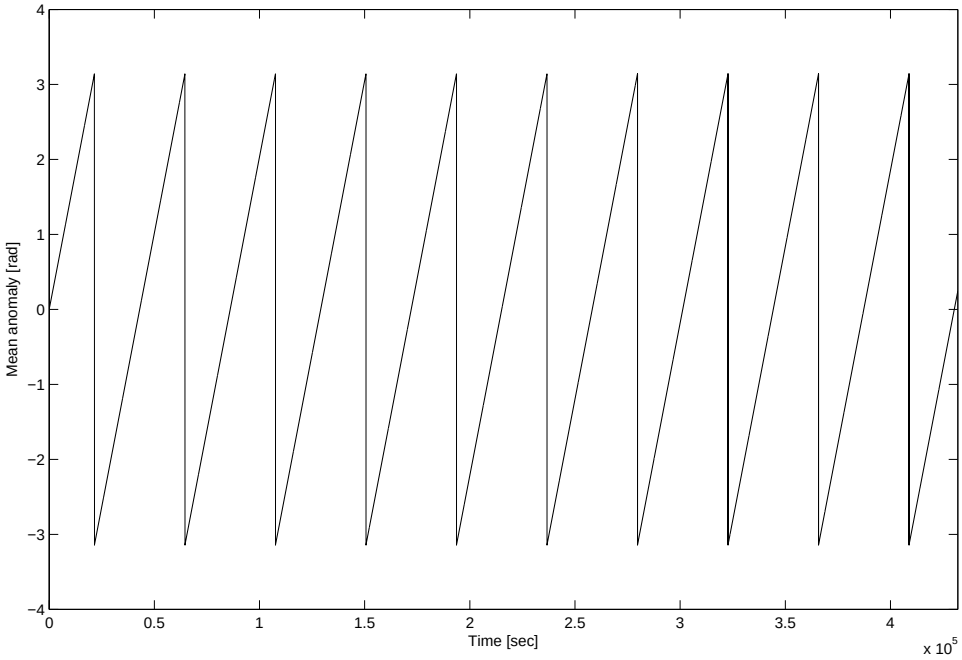

Figure 3.7: Evolution of the Mean anomaly.

represent a difference of about 94° in 370 days of propagation. This extreme difference comes from the fact that the orbital periods of the satellites are not equal. The slope of $M_{sec}(t)$ is equal to n, which is the mean motion of a satellite,

$$\dot{M}_{sec}(t) = n = \frac{2\pi}{T_p},$$

where T_p is the keplerian orbital period of the satellite (related with the semi-major axis). We take from Table 3.4 two different values for the Mean anomaly $M^8 = 0.8975$ and $M^{47} = 5.8985$, which correspond to the 8^{rd} and the 47^{th} set of parameters that we tested. Those values have been selected because, in those cases, the value of $\dot{M}_{sec}$ reaches a minimum $\dot{M}^8_{sec} = 1.487122{\cdot}10^{-4}$ and a maximum $\dot{M}^{47}_{sec} = 1.487638{\cdot}10^{-4}$.

Despite having the same orbital parameters, except for the value of M, the orbital periods of the satellites are, $T^8_p = 42250.6175\,sec$ and $T^{47}_p = 42235.9602\,sec$, respectively. They differ around 14.65 seconds, meaning that after 370 days (or around 740 orbital periods) there will be an offset of around $11,118.9743\,sec$ between both satellites, which corresponds to the 94° of difference that we obtained above.

3.4.2 Non-secular component of the osculating elements.

In this section we have analyzed the non-secular component of the osculating elements. We consider an initial set of orbital elements (a, e, i, ω, Ω, M) and we integrate the system of Eqs. (3.8) applying a Runge Kutta method of order four to determine their

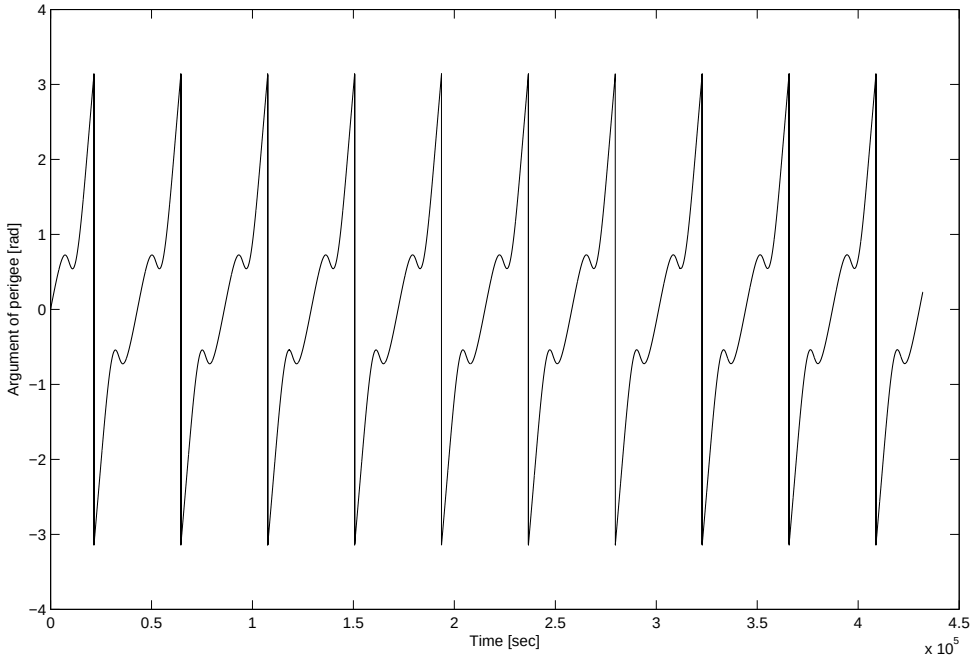

Figure 3.8: Evolution of the argument of perigee in a quasi-circular orbit ($e = 0.0001$).

evolution over time (osculating elements). Furthermore, for each osculating element $q \in \{a, e, i, \omega, \Omega, M\}$, we obtain its secular and non-secular part by linear interpolation as explained before.

In the two body problem it is easy to compute the position and velocity vectors from the orbital elements. Then, we can compute at time t "the real position" ($\mathbf{r}_{J_2}(t)$) and "the approximate or linear position" ($\mathbf{r}_{sec}(t)$), through the real osculating elements $a(t)$, $e(t)$, $i(t)$, $\omega(t)$, $\Omega(t)$, $M(t)$, and the secular part of the osculating elements $a_{sec}(t)$, $e_{sec}(t)$, $i_{sec}(t)$, $\omega_{sec}(t)$, $\Omega_{sec}(t)$, $M_{sec}(t)$, respectively.

The real position of the satellite considers the secular and non-secular terms of the osculating elements, while the approximate position only takes into account the secular terms. Then, the distance:

$$||\mathbf{r}_{J_2}(t) - \mathbf{r}_{sec}(t)||,$$

represents the deviation of the satellite from its real position due to the non-secular perturbations. We compute this deviation at each instant of time and consider the maximum value experienced,

$$\Delta(a, e, i, \omega, \Omega, M) = \max_t ||\mathbf{r}_{J_2}(t) - \mathbf{r}_{sec}(t)||, \tag{3.9}$$

which represents, as a function of the initial conditions, the maximum deviation due to the non-secular components of the osculating elements.

The goal is to determine the best values for the initial orbital elements to reduce the deviation of the satellite. In order to find those regions, we first study numerically the

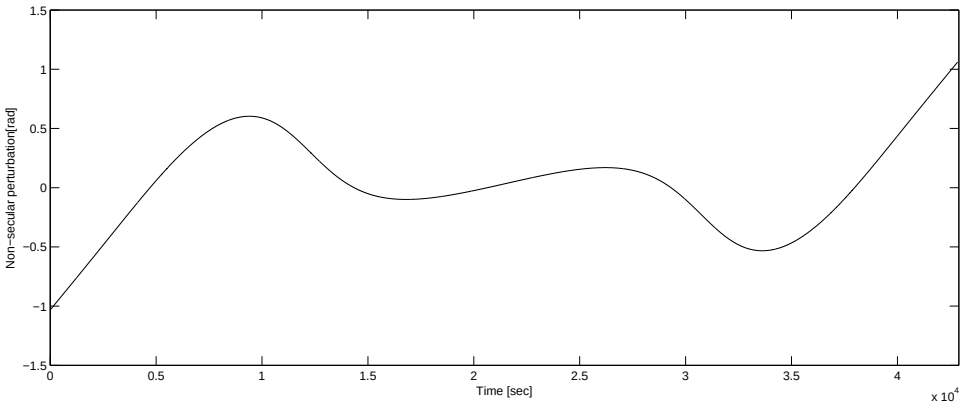

Figure 3.9: Non-secular component of the argument of perigee in a quasi-circular orbit ($e = 0.0001$), in one orbital period.

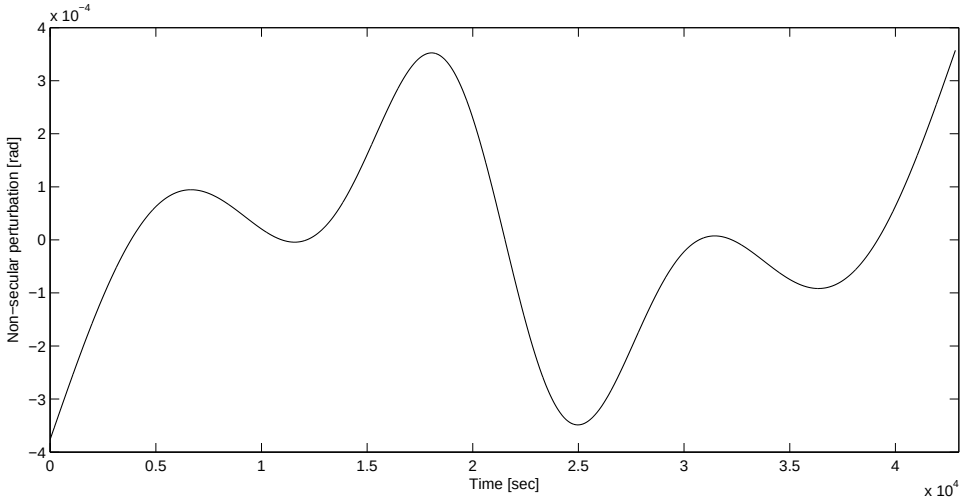

Figure 3.10: Non-secular component of the Mean anomaly in one orbital period.

dependency of the deviation with respect to the initial orbital elements, and then, we search for the best initial conditions.

We use the same methodology to study the dependency of the deviation with respect to each initial orbital element. In the case of the semi-major axis, the procedure is as follows:

- Generate randomly the initial orbital elements of 100 satellites, except the semi-major axis.
- For each satellite, the value of the semi-major axis is discretized in the region $[18000, 29000]$ km with step of 500 m. Then, each satellite has 22 possibilities for the semi-major axis.
- For each of the 100 satellites, it is possible to compute the maximum deviation experienced in terms of the semi-major axis, and to infer the dependency between

them. Each set of initial conditions is propagated using Eqs. (3.8) with a RK of order four during approximately 370 days, with a time step of 20 *sec*.

We observe in Figure 3.11 that the deviation is inversely proportional to the semi-major axis. This is due to the J_2 effect decaying as we move away from the Earth. Figure 3.12 illustrates that the deviation is almost constant until the eccentricity reaches the value $e = 0.15$, and then it grows exponentially as the value of e increases. Regarding the inclination, we have observed that there always exist a value for the inclination which minimizes the deviation, as Figure 3.13 illustrates. Note that, the inclination varies in the range $[0°, 90°]$ because the results in the interval $[90°, 180°]$ will be exactly the same since we are dealing with the same orbit but in a retrograde motion.

The deviation does not depend on the Right Ascension of the Ascending Node. Besides, the deviation varies less than 150 meters as we change the argument of perigee and, in the case of the Mean anomaly it varies less than 10 meters.

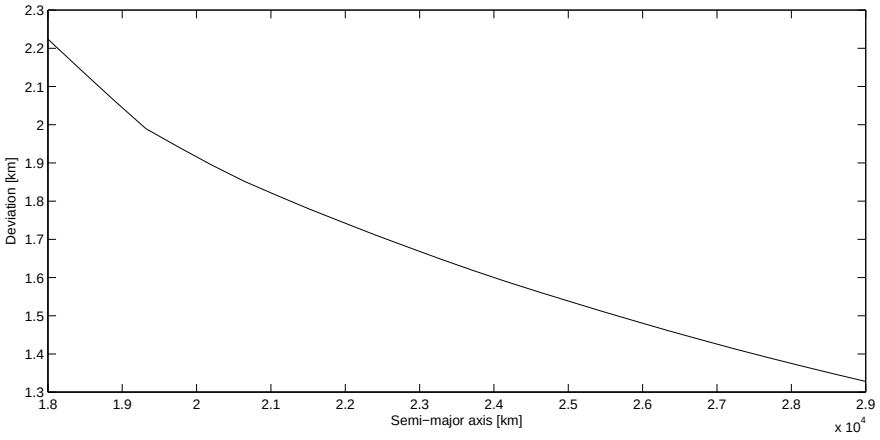

Figure 3.11: Dependency of the deviation with respect to the semi-major axis.

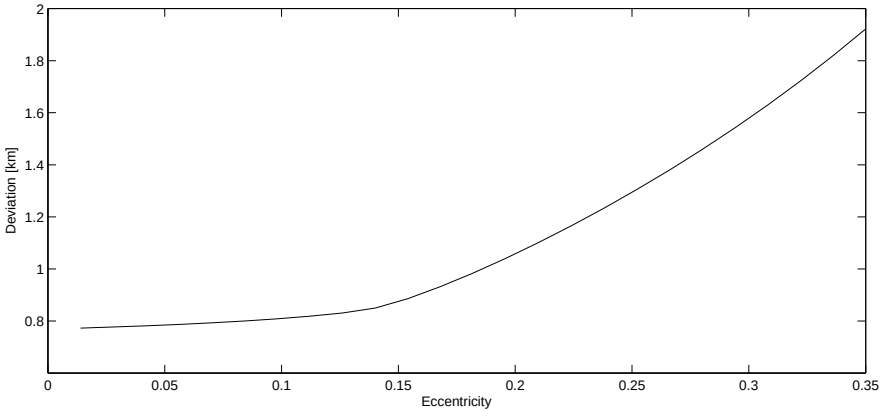

Figure 3.12: Dependency of the deviation with respect to the eccentricity.

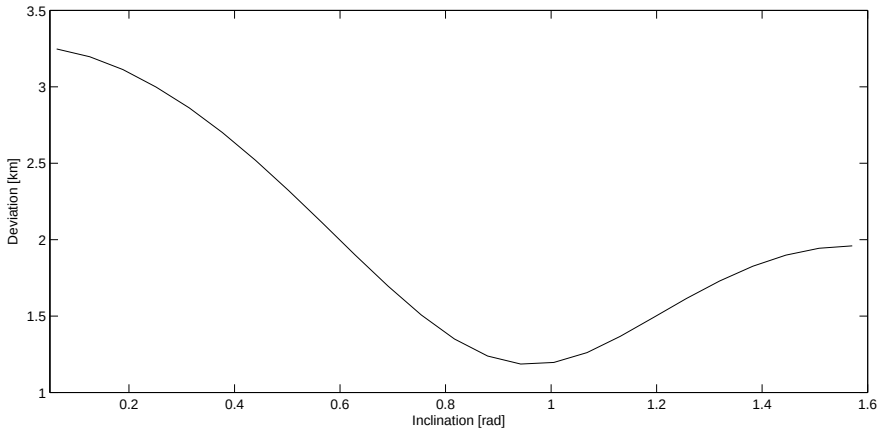

Figure 3.13: Dependency of the deviation with respect to the inclination.

The previous study shows that the main contribution to the deviation come from initial a, e, and i. In order to reduce the deviation it is enough to increase a as much as possible, reduce e to the interval $[0, 0.15]$, and choose the critical value of the inclination corresponding to the chosen a and e.

In mission planning would be useful that given the semi-major axis we were able to compute the range of values for e and i such that they reduce as much as possible the deviation of the satellites. For that purpose, we designed an algorithm that, given the semi-major axis, the argument of perigee, the Right Ascension of the Ascending Node and the Mean anomaly of a satellite, computes and plots the deviation in terms of the eccentricity and the inclination. Figure 3.14 shows the output of the algorithm in one example whose initial data are: $a = 29600.1\,km$, $\omega = 0$, $\Omega = 0$, and $M = 0$.

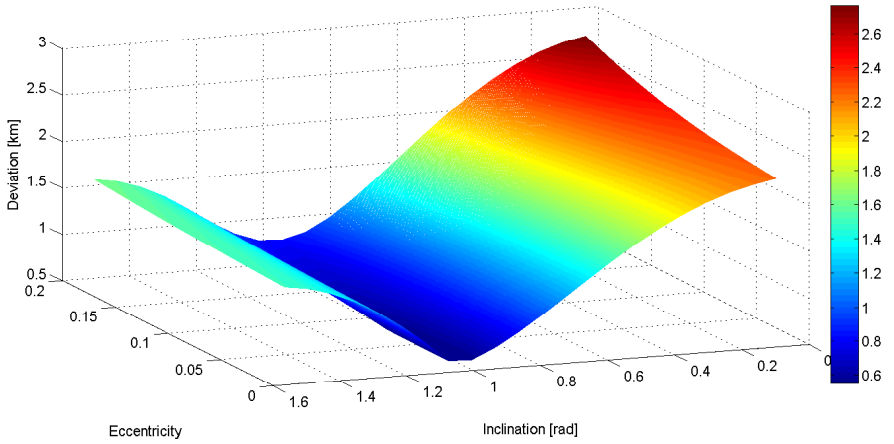

Figure 3.14: Dependency of the deviation with respect to the eccentricity and inclination.

Now, we explore the maximum deviation that a satellite can experience. For that purpose, we consider the worst initial conditions. We select a satellite whose semi-major

axis is $a \geq 18,000.0\,km$ and the eccentricity is $e \leq 0.15$. We know that the argument of perigee, the Right Ascension of the Ascending Node and the Mean anomaly may increase the deviation at most $160\,m$. Then, we vary the inclination in a range $[0, \pi]$, and the maximum deviation experienced will be the worst possible case. We proved numerically that this value is less than $5\,km$.

$$\begin{aligned}
\max_{\substack{a\geq 18000\\ e\leq 0.15\\ i\in[0,2\pi]\\ \omega,\Omega,M\in[0,2\pi]}} \Delta(a,e,i,\omega,\Omega,M) &= \max_{\substack{a\geq 18000\\ e\leq 0.15\\ i\in[0,2\pi]\\ \omega,M\in[0,2\pi]}} \Delta(a,e,i,\omega,0.0,M) \\
&\leq \max_{\substack{a\geq 18000\\ e\leq 0.15\\ i\in[0,2\pi]}} \Delta(a,e,i,0.0,0.0,0.0) + 160\,m \\
&\leq \max_{i\in[0,2\pi]} \Delta(18,000,0.15,i,0.0,0.0,0.0) + 160\,m \\
&\leq 5\,km.
\end{aligned}$$

Consequently, if a tolerance of a few kilometers ($5\,km$) is acceptable for the deviation, then almost all initial conditions are valid.

3.5 Results

A Flower Constellation of N_{sat} satellites has the same semi-major axis, eccentricity, inclination and argument of perigee for each satellite. The Right Ascension of the Ascending Node and the Mean anomaly of each satellite is determined by Eq. (1.42). Our goal is to control the secular and non-secular motion of all the satellites of the constellation.

3.5.1 Secular perturbation in a Flower Constellation

The way to control the secular motion of the satellites in a Flower Constellation is having the same slopes of $a_{sec}(t)$, $e_{sec}(t)$, $i_{sec}(t)$, $\omega_{sec}(t)$, $\Omega_{sec}(t)$, $M_{sec}(t)$ for all the satellites. We show below that this can be attained by just adjusting the semi-major axis of each satellite a few kilometers. This will be possible since $\dot{M}_{sec}$ is related to T_p, which is itself related to the semi-major axis.

In a FC all the satellites have the same semi-major axis, so a new concept of constellation is needed. The satellites of these new constellations have the same values of e, i, and ω, the values of Ω and M will be determined by the lattice theory, but the semi-major axis will be slightly corrected for each satellite. We devote the rest of this section to derive a formula for the correction of the semi-major axis that guarantees the same value of $\dot{M}_{sec}$.

Kepler's Third Law states that *the square of the period of a planet is proportional to the cube of its mean distance to the Sun.* In our problem we have the following relation:

$$a^3 \propto T^2 = \left(\frac{2\pi}{\dot{M}_{sec}}\right)^2.$$

This expression can be rewritten as the following linear expression,

$$\log \dot{M}_{sec} = -\frac{3}{2}\log a + \beta, \tag{3.10}$$

for some constant β. Figure 3.15 illustrates the relation between the semi-major axis and the slope of $M_{sec}(t)$. The larger the semi-major axis is, the smaller the slope of $M_{sec}(t)$ becomes.

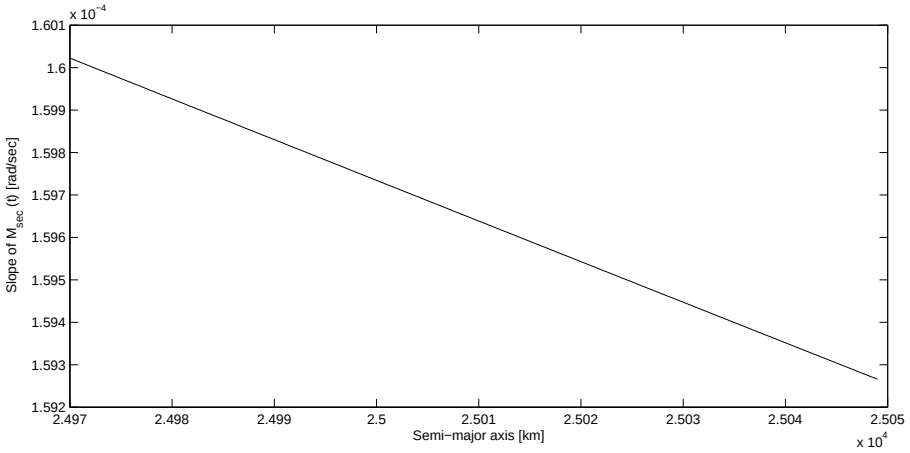

Figure 3.15: Relation between the semi-major axis and the slope of $M_{sec}(t)$.

Using Eq. (3.10), it is possible to obtain a value for β for each value of $\dot{M}^{ij}_{sec}$, where ij represents the index of satellite in the FC as in Eq. (1.42). With the same equation, but changing the value of $\dot{M}^{ij}_{sec}$ by the reference value $\dot{M}^{00}_{sec}$ and β by the value previously computed, we obtain the corrected semi-major axes:

$$\begin{aligned}
\log a_{ij} &= -\frac{2}{3}(\log \dot{M}^{00}_{sec} - \beta) \\
&= -\frac{2}{3}(\log \dot{M}^{00}_{sec} - (\frac{3}{2}\log a + \log \dot{M}^{ij}_{sec})) \\
&= -\frac{2}{3}\log \dot{M}^{00}_{sec} + \log a + \frac{2}{3}\log \dot{M}^{ij}_{sec} \\
&= \log a + \frac{2}{3}(\log \dot{M}^{ij}_{sec} - \log \dot{M}^{00}_{sec}) \\
&= \log a + \frac{2}{3}\log \frac{\dot{M}^{ij}_{sec}}{\dot{M}^{00}_{sec}}.
\end{aligned}$$

Applying the exponential function,

$$\begin{aligned}
a_{ij} &= \exp\left(\log a + \frac{2}{3}\log \frac{\dot{M}^{ij}_{sec}}{\dot{M}^{00}_{sec}}\right) \\
&= a \cdot \exp\left(\log\left(\frac{\dot{M}^{ij}_{sec}}{\dot{M}^{00}_{sec}}\right)^{\frac{2}{3}}\right)
\end{aligned}$$

$$= a\left(\frac{\dot{M}_{sec}^{ij}}{\dot{M}_{sec}^{00}}\right)^{\frac{2}{3}}. \tag{3.11}$$

The following procedure summarizes the method we developed to correct the semi-major axes of all the satellites of a FC:

- Given the data of a Flower Constellation: N_o, N_{so}, N_c, a, e, i, ω, Ω and M, it is possible to compute the values for Ω_{ij} and M_{ij} for each satellite using the lattice theory, where i is the orbit number and j is the number of the satellite in its corresponding orbit. The reference satellite is the one with $i = j = 0$, which has $\Omega_{00} = \Omega$ and $M_{00} = M$.
- Compute the value $\dot{M}_{sec}^{ij}$ which is different for each satellite. $\dot{M}_{sec}^{00}$ is considered as the reference value for the slope of $M(t)$, or in other words, the value that all the satellites should have.
- Compute the new values for a_{ij} using Eq. (3.11).

We conclude that by slightly modifying the semi-major axis of all the satellites we obtain a Flower Constellation whose satellites have the same rate of change of its orbital elements. Meaning that, the secular perturbations affects all the satellites in the same way and consequently the secular motion of the satellites will be identical under the J_2 effect for all the satellites.

3.5.2 Non-secular perturbation in a Flower Constellation

We now turn to reduce the non-secular motion of the satellites of the constellation to an acceptable value. In the case of a Flower Constellation, given the reference satellite whose semi-major axis, argument of perigee, Ω_{00}, and M_{00} are known, we can determine the values for the eccentricity and the inclination that reduce the non-secular motion of the reference satellite as much as possible. However it is not clear whether these values of e and i also work for the remaining satellites of the constellation. In addition to that, we should analyze whether the correction of the semi-major axis affects the selection of e and i considerably or not.

Suppose that we find the inclination and the eccentricity that provides a low deviation of the reference satellite. Since the remaining satellites only differ from the reference one on the RAAN and the Mean anomaly, and we have shown that the deviation changes by at most 10 meters in this case, then the same inclination and eccentricity should be valid for all the satellites. Then, we should conclude that if we find good parameters for the reference satellite, they are good for the remaining satellites of the constellation.

We have studied the dependency of the deviation with respect to the semi-major axis, and we have concluded that if we change a few kilometers the semi-major axis in the correction algorithm, it slightly modifies the non-secular motion of the satellite. Consequently, the values for the eccentricity and inclination selected for the reference satellite are valid for all the satellites of the constellation.

3.5.3 Rigid Constellations

A Flower Constellation of N_{sat} satellites, in which the secular motion is controlled by correcting the semi-major axis of the satellites, and the non-secular motion is reduced, Eq. (3.2) is satisfied and we have a Rigid Constellation. Given the phasing parameters (N_o, N_{so}, N_c) the semi-major axis (a), and the argument of perigee (ω) of a Flower Constellation, it is possible to design a Rigid Constellation as follows:

- Correct the semi-major axis of each satellite to control the secular motion of the satellites.
- Compute the values for the inclination and the eccentricity that reduce the non-secular component of the reference satellite to an acceptable value.

We now illustrate how to design a Rigid Constellation. We start with a Flower Constellation with parameters $N_o = 3$, $N_{so} = 9$, $N_c = 2$, $a = 29600.137\,km$, $e = 0.0$, $i = 56°$ and $\omega = 0.0\,rad$, which correspond with the parameters of Galileo Constellation. We correct the semi-major axis to have all the satellites in the same relative orbits and also the same slopes for $a_{sec}(t)$, $e_{sec}(t)$, $i_{sec}(t)$, $\omega_{sec}(t)$, $\Omega_{sec}(t)$, $M_{sec}(t)$ to control the secular motion. The corrected semi-major axis and the slopes of the secular component of the osculating elements of each satellite are presented in Table 3.5.

Given the semi-major axis, the argument of perigee, the Right Ascension of the Ascending Node and the Mean anomaly of the reference satellite, it is possible to compute the non-secular component in terms of the eccentricity and the inclination as we show in Figure 3.14. Then, to minimize the non-secular component we must select $e = 0.01$ and $i = 56.0009°$, obtaining a deviation of 551.301 meters.

Note that, if we accept a deviation of $5\,km$ then, all Flower Constellations can be corrected into Rigid Constellations.

3.6 Conclusions

In this chapter we provide a new procedure to design a FC that remains a FC under the J_2 effect, named Rigid Constellation. This has been done by controlling the secular and non-secular components of the osculating elements of the satellites through two techniques. The first one consists of changing a few kilometers the semi-major axes in such a way that all the satellites have the same slope of the secular part of their osculating elements. The second consists of searching the values for the eccentricity and the inclination that reduce the deviation as much as possible.

In this way, all the satellites of the constellation will be perturbed the same way. Consequently, the relative position of the satellites (in the osculating elements space) will be maintained over time, and the initial lattice will remain constant within a prescribed tolerance.

Rigid Constellations have two direct applications. First, it validates the theory of the 3D Lattice Flower Constellation [19] (3D-LFC) under the full expression of the potential

function with the J_2 term, assuming that the semi-major axes are corrected and the value of the deviation is small. Second, it shows that in the Global Coverage Problem (with J_2) it will be enough to find a Rigid Constellation that minimizes a slightly modified fitness function (computable using Keplerian propagation). The modified fitness function with respect Eq. (2.4) would be:

$$fitness(FC) = \max_{\omega\in[0,2\pi]} \max_{t\in[0,T_{prop}]} \max_{\mathbf{r}_{gs}\in\text{Earth}} GDOP(FC, \mathbf{r}_{gs}, t) \tag{3.12}$$

$M\,(rad)$	$\dot{a}_{sec}\,(km/s)$	$\dot{e}_{sec}\,(s^{-1})$	$\dot{i}_{sec}\,(rad/s)$	$\dot{\omega}_{sec}\,(rad/s)$	$\dot{\Omega}_{sec}\,(rad/s)$	$\dot{M}_{sec}\,(rad/s)$
0.000	$6.166{\cdot}10^{-12}$	$1.680{\cdot}10^{-14}$	$-9.961{\cdot}10^{-17}$	$-7.087{\cdot}10^{-9}$	$-1.026{\cdot}10^{-9}$	$1.4875{\cdot}10^{-4}$
0.128	$1.885{\cdot}10^{-11}$	$1.699{\cdot}10^{-14}$	$-8.377{\cdot}10^{-17}$	$-7.086{\cdot}10^{-9}$	$-1.026{\cdot}10^{-9}$	$1.4874{\cdot}10^{-4}$
0.256	$3.048{\cdot}10^{-11}$	$1.698{\cdot}10^{-14}$	$-6.800{\cdot}10^{-17}$	$-7.085{\cdot}10^{-9}$	$-1.026{\cdot}10^{-9}$	$1.4873{\cdot}10^{-4}$
0.384	$3.774{\cdot}10^{-11}$	$1.668{\cdot}10^{-14}$	$-5.632{\cdot}10^{-17}$	$-7.085{\cdot}10^{-9}$	$-1.026{\cdot}10^{-9}$	$1.4872{\cdot}10^{-4}$
0.512	$3.728{\cdot}10^{-11}$	$1.617{\cdot}10^{-14}$	$-5.370{\cdot}10^{-17}$	$-7.084{\cdot}10^{-9}$	$-1.026{\cdot}10^{-9}$	$1.4872{\cdot}10^{-4}$
0.641	$2.760{\cdot}10^{-11}$	$1.561{\cdot}10^{-14}$	$-6.314{\cdot}10^{-17}$	$-7.083{\cdot}10^{-9}$	$-1.025{\cdot}10^{-9}$	$1.4871{\cdot}10^{-4}$
0.769	$8.934{\cdot}10^{-12}$	$1.510{\cdot}10^{-14}$	$-8.505{\cdot}10^{-17}$	$-7.083{\cdot}10^{-9}$	$-1.025{\cdot}10^{-9}$	$1.4871{\cdot}10^{-4}$
0.897	$-1.732{\cdot}10^{-11}$	$1.464{\cdot}10^{-14}$	$-1.174{\cdot}10^{-16}$	$-7.083{\cdot}10^{-9}$	$-1.025{\cdot}10^{-9}$	$\mathbf{1.4871{\cdot}10^{-4}}$
1.025	$-4.758{\cdot}10^{-11}$	$1.409{\cdot}10^{-14}$	$-1.547{\cdot}10^{-16}$	$-7.083{\cdot}10^{-9}$	$-1.025{\cdot}10^{-9}$	$1.4871{\cdot}10^{-4}$
1.154	$-7.404{\cdot}10^{-11}$	$1.340{\cdot}10^{-14}$	$-1.859{\cdot}10^{-16}$	$-7.083{\cdot}10^{-9}$	$-1.025{\cdot}10^{-9}$	$1.4871{\cdot}10^{-4}$
1.282	$-8.506{\cdot}10^{-11}$	$1.278{\cdot}10^{-14}$	$-1.968{\cdot}10^{-16}$	$-7.084{\cdot}10^{-9}$	$-1.026{\cdot}10^{-9}$	$1.4872{\cdot}10^{-4}$
1.410	$-7.244{\cdot}10^{-11}$	$1.272{\cdot}10^{-14}$	$-1.794{\cdot}10^{-16}$	$-7.084{\cdot}10^{-9}$	$-1.026{\cdot}10^{-9}$	$1.4872{\cdot}10^{-4}$
1.538	$-4.229{\cdot}10^{-11}$	$1.329{\cdot}10^{-14}$	$-1.423{\cdot}10^{-16}$	$-7.085{\cdot}10^{-9}$	$-1.026{\cdot}10^{-9}$	$1.4873{\cdot}10^{-4}$
1.666	$-1.430{\cdot}10^{-11}$	$1.379{\cdot}10^{-14}$	$-1.078{\cdot}10^{-16}$	$-7.086{\cdot}10^{-9}$	$-1.026{\cdot}10^{-9}$	$1.4873{\cdot}10^{-4}$
1.795	$-4.697{\cdot}10^{-12}$	$1.360{\cdot}10^{-14}$	$-9.359{\cdot}10^{-17}$	$-7.086{\cdot}10^{-9}$	$-1.026{\cdot}10^{-9}$	$1.4874{\cdot}10^{-4}$
1.923	$-1.377{\cdot}10^{-11}$	$1.286{\cdot}10^{-14}$	$-1.011{\cdot}10^{-16}$	$-7.087{\cdot}10^{-9}$	$-1.026{\cdot}10^{-9}$	$1.4874{\cdot}10^{-4}$
2.051	$-3.121{\cdot}10^{-11}$	$1.214{\cdot}10^{-14}$	$-1.200{\cdot}10^{-16}$	$-7.087{\cdot}10^{-9}$	$-1.026{\cdot}10^{-9}$	$1.4875{\cdot}10^{-4}$
2.179	$-4.700{\cdot}10^{-11}$	$1.173{\cdot}10^{-14}$	$-1.387{\cdot}10^{-16}$	$-7.087{\cdot}10^{-9}$	$-1.026{\cdot}10^{-9}$	$1.4875{\cdot}10^{-4}$
2.308	$-5.622{\cdot}10^{-11}$	$1.162{\cdot}10^{-14}$	$-1.505{\cdot}10^{-16}$	$-7.088{\cdot}10^{-9}$	$-1.026{\cdot}10^{-9}$	$1.4875{\cdot}10^{-4}$
2.436	$-5.827{\cdot}10^{-11}$	$1.169{\cdot}10^{-14}$	$-1.536{\cdot}10^{-16}$	$-7.088{\cdot}10^{-9}$	$-1.026{\cdot}10^{-9}$	$1.4875{\cdot}10^{-4}$
2.564	$-5.466{\cdot}10^{-11}$	$1.179{\cdot}10^{-14}$	$-1.495{\cdot}10^{-16}$	$-7.088{\cdot}10^{-9}$	$-1.026{\cdot}10^{-9}$	$1.4875{\cdot}10^{-4}$
2.692	$-4.749{\cdot}10^{-11}$	$1.188{\cdot}10^{-14}$	$-1.403{\cdot}10^{-16}$	$-7.088{\cdot}10^{-9}$	$-1.026{\cdot}10^{-9}$	$1.4875{\cdot}10^{-4}$
2.821	$-3.863{\cdot}10^{-11}$	$1.194{\cdot}10^{-14}$	$-1.287{\cdot}10^{-16}$	$-7.088{\cdot}10^{-9}$	$-1.026{\cdot}10^{-9}$	$1.4875{\cdot}10^{-4}$
2.949	$-2.954{\cdot}10^{-11}$	$1.198{\cdot}10^{-14}$	$-1.167{\cdot}10^{-16}$	$-7.087{\cdot}10^{-9}$	$-1.026{\cdot}10^{-9}$	$1.4875{\cdot}10^{-4}$
3.077	$-2.126{\cdot}10^{-11}$	$1.203{\cdot}10^{-14}$	$-1.058{\cdot}10^{-16}$	$-7.087{\cdot}10^{-9}$	$-1.026{\cdot}10^{-9}$	$1.4875{\cdot}10^{-4}$
3.205	$-1.448{\cdot}10^{-11}$	$1.212{\cdot}10^{-14}$	$-9.730{\cdot}10^{-17}$	$-7.087{\cdot}10^{-9}$	$-1.026{\cdot}10^{-9}$	$1.4874{\cdot}10^{-4}$
3.333	$-9.603{\cdot}10^{-12}$	$1.226{\cdot}10^{-14}$	$-9.160{\cdot}10^{-17}$	$-7.086{\cdot}10^{-9}$	$-1.026{\cdot}10^{-9}$	$1.4874{\cdot}10^{-4}$
3.462	$-6.865{\cdot}10^{-12}$	$1.247{\cdot}10^{-14}$	$-8.922{\cdot}10^{-17}$	$-7.086{\cdot}10^{-9}$	$-1.026{\cdot}10^{-9}$	$1.4874{\cdot}10^{-4}$
3.590	$-6.346{\cdot}10^{-12}$	$1.275{\cdot}10^{-14}$	$-9.031{\cdot}10^{-17}$	$-7.085{\cdot}10^{-9}$	$-1.026{\cdot}10^{-9}$	$1.4873{\cdot}10^{-4}$
3.718	$-8.006{\cdot}10^{-12}$	$1.310{\cdot}10^{-14}$	$-9.479{\cdot}10^{-17}$	$-7.085{\cdot}10^{-9}$	$-1.026{\cdot}10^{-9}$	$1.4873{\cdot}10^{-4}$
3.846	$-1.168{\cdot}10^{-11}$	$1.350{\cdot}10^{-14}$	$-1.023{\cdot}10^{-16}$	$-7.085{\cdot}10^{-9}$	$-1.026{\cdot}10^{-9}$	$1.4872{\cdot}10^{-4}$
3.975	$-1.708{\cdot}10^{-11}$	$1.394{\cdot}10^{-14}$	$-1.125{\cdot}10^{-16}$	$-7.084{\cdot}10^{-9}$	$-1.026{\cdot}10^{-9}$	$1.4872{\cdot}10^{-4}$
4.103	$-2.369{\cdot}10^{-11}$	$1.440{\cdot}10^{-14}$	$-1.243{\cdot}10^{-16}$	$-7.084{\cdot}10^{-9}$	$-1.026{\cdot}10^{-9}$	$1.4872{\cdot}10^{-4}$
4.231	$-3.072{\cdot}10^{-11}$	$1.485{\cdot}10^{-14}$	$-1.367{\cdot}10^{-16}$	$-7.084{\cdot}10^{-9}$	$-1.026{\cdot}10^{-9}$	$1.4872{\cdot}10^{-4}$
4.359	$-3.700{\cdot}10^{-11}$	$1.524{\cdot}10^{-14}$	$-1.477{\cdot}10^{-16}$	$-7.084{\cdot}10^{-9}$	$-1.025{\cdot}10^{-9}$	$1.4872{\cdot}10^{-4}$
4.487	$-4.096{\cdot}10^{-11}$	$1.552{\cdot}10^{-14}$	$-1.549{\cdot}10^{-16}$	$-7.084{\cdot}10^{-9}$	$-1.025{\cdot}10^{-9}$	$1.4871{\cdot}10^{-4}$
4.616	$-4.088{\cdot}10^{-11}$	$1.563{\cdot}10^{-14}$	$-1.555{\cdot}10^{-16}$	$-7.084{\cdot}10^{-9}$	$-1.026{\cdot}10^{-9}$	$1.4872{\cdot}10^{-4}$
4.744	$-3.536{\cdot}10^{-11}$	$1.553{\cdot}10^{-14}$	$-1.474{\cdot}10^{-16}$	$-7.084{\cdot}10^{-9}$	$-1.026{\cdot}10^{-9}$	$1.4872{\cdot}10^{-4}$
4.872	$-2.437{\cdot}10^{-11}$	$1.522{\cdot}10^{-14}$	$-1.307{\cdot}10^{-16}$	$-7.084{\cdot}10^{-9}$	$-1.026{\cdot}10^{-9}$	$1.4872{\cdot}10^{-4}$
5.000	$-1.019{\cdot}10^{-11}$	$1.487{\cdot}10^{-14}$	$-1.093{\cdot}10^{-16}$	$-7.085{\cdot}10^{-9}$	$-1.026{\cdot}10^{-9}$	$1.4873{\cdot}10^{-4}$
5.129	$2.185{\cdot}10^{-12}$	$1.477{\cdot}10^{-14}$	$-9.191{\cdot}10^{-17}$	$-7.086{\cdot}10^{-9}$	$-1.026{\cdot}10^{-9}$	$1.4873{\cdot}10^{-4}$
5.257	$6.575{\cdot}10^{-12}$	$1.514{\cdot}10^{-14}$	$-8.838{\cdot}10^{-17}$	$-7.086{\cdot}10^{-9}$	$-1.026{\cdot}10^{-9}$	$1.4874{\cdot}10^{-4}$
5.385	$-7.675{\cdot}10^{-13}$	$1.588{\cdot}10^{-14}$	$-1.031{\cdot}10^{-16}$	$-7.087{\cdot}10^{-9}$	$-1.026{\cdot}10^{-9}$	$1.4874{\cdot}10^{-4}$
5.513	$-1.696{\cdot}10^{-11}$	$1.653{\cdot}10^{-14}$	$-1.291{\cdot}10^{-16}$	$-7.087{\cdot}10^{-9}$	$-1.026{\cdot}10^{-9}$	$1.4875{\cdot}10^{-4}$
5.642	$-3.247{\cdot}10^{-11}$	$1.671{\cdot}10^{-14}$	$-1.511{\cdot}10^{-16}$	$-7.088{\cdot}10^{-9}$	$-1.026{\cdot}10^{-9}$	$1.4875{\cdot}10^{-4}$
5.770	$-3.806{\cdot}10^{-11}$	$1.653{\cdot}10^{-14}$	$-1.575{\cdot}10^{-16}$	$-7.088{\cdot}10^{-9}$	$-1.026{\cdot}10^{-9}$	$1.4876{\cdot}10^{-4}$
5.898	$-3.216{\cdot}10^{-11}$	$1.636{\cdot}10^{-14}$	$-1.484{\cdot}10^{-16}$	$-7.088{\cdot}10^{-9}$	$-1.026{\cdot}10^{-9}$	$\mathbf{1.4876{\cdot}10^{-4}}$
6.026	$-1.993{\cdot}10^{-11}$	$1.637{\cdot}10^{-14}$	$-1.321{\cdot}10^{-16}$	$-7.088{\cdot}10^{-9}$	$-1.026{\cdot}10^{-9}$	$1.4876{\cdot}10^{-4}$
6.154	$-6.619{\cdot}10^{-12}$	$1.655{\cdot}10^{-14}$	$-1.152{\cdot}10^{-16}$	$-7.088{\cdot}10^{-9}$	$-1.026{\cdot}10^{-9}$	$1.4875{\cdot}10^{-4}$
6.283	$6.167{\cdot}10^{-12}$	$1.680{\cdot}10^{-14}$	$-9.961{\cdot}10^{-17}$	$-7.087{\cdot}10^{-9}$	$-1.026{\cdot}10^{-9}$	$1.4875{\cdot}10^{-4}$

Table 3.4: Slopes of the secular components of the osculating elements in function of the initial Mean anomaly.

Sat. $[i,j]$	$a\,(km)$ corrected	$\dot{a}_{sec}\,(km/s)$	$\dot{e}_{sec}\,(s^{-1})$	$\dot{i}_{sec}\,(rad/s)$	$\dot{\omega}_{sec}\,(rad/s)$	$\dot{\Omega}_{sec}\,(rad/s)$	$\dot{M}_{sec}\,(rad/s)$
$[0,0]$	29600.137	$-2.833\cdot10^{-11}$	$-8.944\cdot10^{-17}$	$-3.227\cdot10^{-16}$	$2.661\cdot10^{-9}$	$-5.228\cdot10^{-9}$	$1.2398266\cdot10^{-4}$
$[0,1]$	29598.872	$8.298\cdot10^{-12}$	$-1.198\cdot10^{-17}$	$9.466\cdot10^{-17}$	$2.638\cdot10^{-9}$	$-5.228\cdot10^{-9}$	$1.2398266\cdot10^{-4}$
$[0,2]$	29597.165	$3.114\cdot10^{-11}$	$3.891\cdot10^{-16}$	$3.549\cdot10^{-16}$	$2.629\cdot10^{-9}$	$-5.228\cdot10^{-9}$	$1.2398266\cdot10^{-4}$
$[0,3]$	29597.843	$2.525\cdot10^{-12}$	$9.406\cdot10^{-16}$	$2.883\cdot10^{-17}$	$2.620\cdot10^{-9}$	$-5.228\cdot10^{-9}$	$1.2398265\cdot10^{-4}$
$[0,4]$	29599.783	$-3.029\cdot10^{-11}$	$8.598\cdot10^{-16}$	$-3.450\cdot10^{-16}$	$2.622\cdot10^{-9}$	$-5.228\cdot10^{-9}$	$1.2398266\cdot10^{-4}$
$[0,5]$	29599.784	$-1.305\cdot10^{-11}$	$-3.276\cdot10^{-16}$	$-1.486\cdot10^{-16}$	$2.617\cdot10^{-9}$	$-5.228\cdot10^{-9}$	$1.2398266\cdot10^{-4}$
$[0,6]$	29597.845	$2.569\cdot10^{-11}$	$-1.847\cdot10^{-16}$	$2.928\cdot10^{-16}$	$2.612\cdot10^{-9}$	$-5.228\cdot10^{-9}$	$1.2398265\cdot10^{-4}$
$[0,7]$	29597.166	$2.198\cdot10^{-11}$	$-4.364\cdot10^{-16}$	$2.506\cdot10^{-16}$	$2.620\cdot10^{-9}$	$-5.228\cdot10^{-9}$	$1.2398266\cdot10^{-4}$
$[0,8]$	29598.874	$-1.811\cdot10^{-11}$	$-1.044\cdot10^{-15}$	$-2.062\cdot10^{-16}$	$2.629\cdot10^{-9}$	$-5.228\cdot10^{-9}$	$1.2398266\cdot10^{-4}$
$[1,0]$	29599.524	$-2.764\cdot10^{-11}$	$-7.800\cdot10^{-16}$	$-3.148\cdot10^{-16}$	$2.628\cdot10^{-9}$	$-5.228\cdot10^{-9}$	$1.2398266\cdot10^{-4}$
$[1,1]$	29599.976	$-1.926\cdot10^{-11}$	$-3.502\cdot10^{-16}$	$-2.194\cdot10^{-16}$	$2.643\cdot10^{-9}$	$-5.228\cdot10^{-9}$	$1.2398266\cdot10^{-4}$
$[1,2]$	29598.165	$2.096\cdot10^{-11}$	$1.680\cdot10^{-16}$	$2.389\cdot10^{-16}$	$2.636\cdot10^{-9}$	$-5.228\cdot10^{-9}$	$1.2398266\cdot10^{-4}$
$[1,3]$	29597.085	$2.650\cdot10^{-11}$	$4.320\cdot10^{-16}$	$3.020\cdot10^{-16}$	$2.623\cdot10^{-9}$	$-5.228\cdot10^{-9}$	$1.2398266\cdot10^{-4}$
$[1,4]$	29598.519	$-1.175\cdot10^{-11}$	$9.635\cdot10^{-16}$	$-1.338\cdot10^{-16}$	$2.623\cdot10^{-9}$	$-5.228\cdot10^{-9}$	$1.2398266\cdot10^{-4}$
$[1,5]$	29600.101	$-3.061\cdot10^{-11}$	$5.169\cdot10^{-16}$	$-3.488\cdot10^{-16}$	$2.622\cdot10^{-9}$	$-5.228\cdot10^{-9}$	$1.2398266\cdot10^{-4}$
$[1,6]$	29599.218	$1.081\cdot10^{-12}$	$-5.280\cdot10^{-16}$	$1.245\cdot10^{-17}$	$2.612\cdot10^{-9}$	$-5.228\cdot10^{-9}$	$1.2398266\cdot10^{-4}$
$[1,7]$	29597.329	$3.094\cdot10^{-11}$	$1.278\cdot10^{-17}$	$3.526\cdot10^{-16}$	$2.607\cdot10^{-9}$	$-5.228\cdot10^{-9}$	$1.2398266\cdot10^{-4}$
$[1,8]$	29597.554	$9.650\cdot10^{-12}$	$-8.179\cdot10^{-16}$	$1.101\cdot10^{-16}$	$2.624\cdot10^{-9}$	$-5.228\cdot10^{-9}$	$1.2398266\cdot10^{-4}$
$[2,0]$	29598.167	$-4.737\cdot10^{-12}$	$-1.048\cdot10^{-15}$	$-5.379\cdot10^{-17}$	$2.627\cdot10^{-9}$	$-5.228\cdot10^{-9}$	$1.2398266\cdot10^{-4}$
$[2,1]$	29599.978	$-3.129\cdot10^{-11}$	$-2.438\cdot10^{-16}$	$-3.565\cdot10^{-16}$	$2.630\cdot10^{-9}$	$-5.228\cdot10^{-9}$	$1.2398266\cdot10^{-4}$
$[2,2]$	29599.522	$-6.135\cdot10^{-12}$	$-1.903\cdot10^{-16}$	$-6.979\cdot10^{-17}$	$2.637\cdot10^{-9}$	$-5.228\cdot10^{-9}$	$1.2398266\cdot10^{-4}$
$[2,3]$	29597.553	$2.915\cdot10^{-11}$	$3.121\cdot10^{-16}$	$3.322\cdot10^{-16}$	$2.634\cdot10^{-9}$	$-5.228\cdot10^{-9}$	$1.2398266\cdot10^{-4}$
$[2,4]$	29597.329	$1.624\cdot10^{-11}$	$6.098\cdot10^{-16}$	$1.851\cdot10^{-16}$	$2.614\cdot10^{-9}$	$-5.228\cdot10^{-9}$	$1.2398266\cdot10^{-4}$
$[2,5]$	29599.216	$-2.352\cdot10^{-11}$	$1.012\cdot10^{-15}$	$-2.680\cdot10^{-16}$	$2.622\cdot10^{-9}$	$-5.228\cdot10^{-9}$	$1.2398266\cdot10^{-4}$
$[2,6]$	29600.101	$-2.443\cdot10^{-11}$	$7.844\cdot10^{-17}$	$-2.783\cdot10^{-16}$	$2.620\cdot10^{-9}$	$-5.228\cdot10^{-9}$	$1.2398266\cdot10^{-4}$
$[2,7]$	29598.522	$1.497\cdot10^{-11}$	$-3.629\cdot10^{-16}$	$1.707\cdot10^{-16}$	$2.609\cdot10^{-9}$	$-5.228\cdot10^{-9}$	$1.2398265\cdot10^{-4}$
$[2,8]$	29597.085	$2.962\cdot10^{-11}$	$-6.970\cdot10^{-17}$	$3.376\cdot10^{-16}$	$2.614\cdot10^{-9}$	$-5.228\cdot10^{-9}$	$1.2398266\cdot10^{-4}$

Table 3.5: Corrected Galileo Flower Constellation.

Chapter 4

Necklace Theory on Flower Constellations

4.1 Introduction

From a mathematical point of view, the theory of Flower Constellations appears to have reached the final level of maturity, but from a practical point of view, the following question arises. Since to obtain full symmetry most of 2D-LFCs involve an unpractically high number of satellites, is it possible to select a subset of them and still obtaining a symmetric phasing distribution? This chapter provides a positive answer to this question and provides a methodology to compute *all* these subsets, subsets that are keeping full symmetry in the (Ω, M)-space. In the (Ω, M)-space the initial orbit plane is made with N_{so} admissible locations (available for the 2D-LFC satellites) and these locations can be seen as a necklace of N_{so} empty pearls. An actual number of satellites (N_{rso}) (actual pearls), less than the number of empty pearls, can be distributed in the empty pearls necklace. The purpose is to find the proper necklaces and associated suitable shifting parameters (to duplicate and shift the initial necklace in the following orbit planes) to obtain the same initial necklace when we reach the last orbit plane.

By solving the problem above we are able to design optimal satellite constellations made of few satellites while keeping the design parameters space as big as the computer can tolerate! To solve this problem, basic number theory knowledge is used. However, to best explain the proposed methodology a final flowchart is provided to clarify the design process.

In a 2D-LFC, where $N_{so} = N_{rso}$, each point in the (Ω, M)-space identifies one satellite of the constellation. Usually, the mission budget limits the number of constellation satellites to an upper assigned value, say $N_{s\,\max}$. The number of satellites in the constellation, which can be computed as the determinant of the 2×2 matrix of Eq. (1.42), satisfies $N_s = N_o N_{so} \leq N_{s\,\max}$. On the other hand, N_o defines the number of orbital planes, a number that is proportional to the number of distinct launches needed to deploy the entire constellation, which is also strongly constrained by the mission budget. The remaining parameter, the configuration number N_c, remains the only (integer) variable to play with. Due to the limited possible values for N_c (they are actually N_o

values, only), the different potential configurations are not so many. This is a strong limitation in the design process. To overcome this limitation, the following idea is proposed and analyzed.

Instead of directly searching for a 2D-LFC made with a given number of satellites, we introduce a fictitious satellite constellation with a much larger number of satellites, and then we extract our constellation as a subset of the larger one. Since we would like to preserve all the nice properties of LFCs, we are automatically led to the following problem: *find all the subsets of N_{rs} real satellites, selected from the fictitious constellation made of $N_s \gg N_{rs}$ total satellites, such that the satellite distribution in the (Ω, M)-space is symmetric in both, M and Ω axes.* Here symmetry should be understood in the following sense: the satellites in each orbit have the same exact pattern of mean anomalies, and orbit planes are uniformly distributed in space.

Finding all these subsets will be high payoff effort as the benefits of the necklace theory applied to 2D-LFC will be outstanding: *new optimal solutions will be found with an assigned minimum number of satellites in a solution space whose dimension is only limited by the available computational capability.*

4.2 Combinatorics of necklaces

4.2.1 The Necklace Problem

Consider a set of N_{rso} satellites that can be arranged in N_{so} available locations (with $N_{so} \geq N_{rso}$) in a given orbit. This set of satellites forms a "necklace" that is rotating along the orbit and comes back to the original setup in an orbital period. If the satellite locations are defined in terms of mean anomaly, then the satellite necklace structure moves rigidly in the mean anomaly space. The question we answer here is: *how many and which are all these necklaces*?

4.2.2 The Necklace Theory

We define some basic concepts and functions of number theory [3] which play an important role from now on.

Definition 25. A real or complex valued function defined on the positive integers is called an *arithmetic function* or a number-theoretic function.

Definition 26. An arithmetic function $f : \mathbb{N} \to \mathbb{C}$ is called *multiplicative* if it is not identically zero and

$$f(mn) = f(m)f(n) \qquad \text{whenever } \gcd(m, n) = 1.$$

Definition 27. The *Euler totient function*, $\varphi : \mathbb{N} \to \mathbb{N}$ is a multiplicative function, defined as follows;

$$\varphi(m) = \#\left\{n \in \mathbb{N} : n \leq m \wedge \gcd(m, n) = 1\right\}. \tag{4.1}$$

It is an arithmetic function that counts the number of positive integers less than or equal to d that are coprime to d; for example a simple computation shows that $\varphi(1) = \varphi(2) = 1$, $\varphi(3) = \varphi(4) = 2$, $\varphi(5) = 4$, $\varphi(6) = 2$, $\varphi(7) = 6$, etc.

Definition 28. The *Möbius function* $\mu : \mathbb{N} \to \{-1, 0, 1\}$ is a multiplicative function that is defined as follows:

$$\mu(n) = \begin{cases} 0 & \text{if } n \text{ has one or more repeated prime factors} \\ 1 & \text{if } n = 1 \\ (-1)^k & \text{if } n \text{ is a product of } k \text{ distinct primes,} \end{cases} \tag{4.2}$$

so $\mu(n) \neq 0$ indicates that n is squarefree, or in other words, if $\mu(n) = 0$ indicates that n has a square factor > 1.

In general, the *necklace problem* is a combinatorial problem which answer the following question: how many different arrangements of n pearls in a circular loop are there, assuming that each pearl come in one of k different colors? Two arrangements that differ only by a rotation of the loop, are consider to be identical. The mathematical solution to this problem is a simple application of Burnside's counting theorem [15], and it is summarized by the following formula:

$$N_k(n) = \frac{1}{n} \sum_{d|n} \varphi(d) k^{n/d},$$

where the sum is taken over all the divisors d of n. In our physical example $k = 2$, and these two "colors" represent the *presence* and the *absence* of a satellite in the admissible locations. Therefore, the total number of satellite necklaces is

$$N_2(n) = \frac{1}{n} \sum_{d|n} \varphi(d)\, 2^{n/d}. \tag{4.3}$$

Mathematically, a necklace will be represented as a subset $\mathcal{G} \subseteq \{1, \cdots, n\}$. Since we only consider unlabeled necklaces, two subsets $\mathcal{G}$ and $\mathcal{G}'$ that differ by an additive constant are considered identical:

$$\mathcal{G} = \mathcal{G}' \iff \exists\, s :\ \mathcal{G} \equiv \mathcal{G}' + s \mod (n).$$

The set of all possible unlabeled necklaces with n pearls and two colors will be identified by $K(n)$. Figure 4.1 shows all possible unlabeled necklaces using three pearls of two colors, i.e. the elements of $K(3)$. Notice that in Figure 4.1, the configurations $\{1, 2\}$, $\{2, 3\}$, and $\{1, 3\}$ are all represented with the set $\{1, 2\}$ because it is possible to obtain $\{1, 3\}$ and $\{2, 3\}$ from $\{1, 2\}$ by performing a suitable rotation. Similarly, the configurations $\{1\}$, $\{2\}$, and $\{3\}$ are all equivalent to $\{1\}$. Therefore $K(3)$ contains only 4 elements: $\emptyset$, $\{1\}$, $\{1, 2\}$, and $\{1, 2, 3\}$. An algorithm [15] has been written to compute all possible necklaces involving a total of N_{so} pearls, of which N_{rso} are black and $N_{so} - N_{rso}$ are white. In order to obtain all possible necklaces with N_{so} pearls, it is necessary to call the algorithm with $N_{rso} = 0, 1, \cdots, N_{so}$.

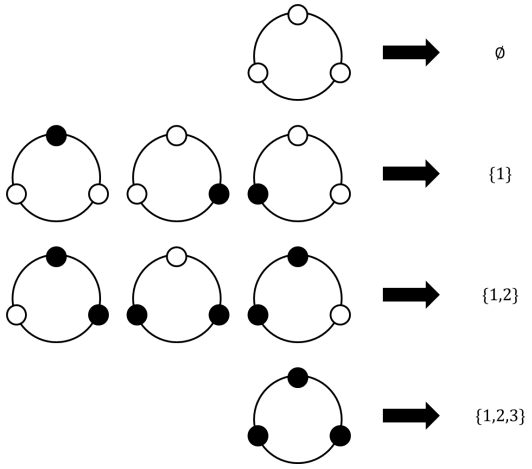

Figure 4.1: Unlabeled necklaces with three pearls and two colors.

4.2.3 Symmetries of the necklaces

Let $\mathcal{G}$ be a necklace such as $\mathcal{G} \in K(n)$. We say that $\mathcal{G}$ has a symmetry of length r if $\mathcal{G}$ and $\mathcal{G} + r$ coincide modulo n.
As an example, consider the necklace $\mathcal{G} = \{1, 3, 5, 7\} \in K(8)$. What symmetries does it have?

- $r = 2$ is a symmetry, since $\mathcal{G} + 2 = \{3, 5, 7, 9\}$ is equivalent to $\mathcal{G}$ modulo 8.
- $r = 4$ and $r = 6$ are also symmetries, since $\{5, 7, 9, 11\}$ and $\{7, 9, 11, 13\}$ reduce to $\{1, 3, 5, 7\}$ modulo 8.
- $r = 1$ is not a symmetry, since $\{2, 4, 6, 8\}$ and $\{1, 3, 5, 7\}$ do not coincide modulo 8.

From the example it is easy to see that if r is a symmetry of a necklace, then any multiple of r is also a symmetry. This remark motivates our following definition: for each necklace $\mathcal{G} \in K(n)$, the *symmetry number* of $\mathcal{G}$, denoted $\mathrm{Sym}(\mathcal{G})$, is the shortest of the symmetries of $\mathcal{G}$. Note that $\mathrm{Sym}(\mathcal{G})$ always divides n.

$$\mathrm{Sym}(\mathcal{G}) = \min\{1 \leq r \leq n : \mathcal{G} + r \equiv \mathcal{G} \mod (n)\}. \tag{4.4}$$

4.2.4 Necklaces and 2D Lattice Flower Constellations

To generate the necklaces the following idea is adopted: consider a standard 2D-LFC (with parameters N_{so}, N_o, and N_c), and, instead of placing all satellites in the admissible locations, as provided by Eq. (1.42), a subset (necklace) of admissible locations $\mathcal{G} \subseteq \{1, 2, \cdots, N_{so}\}$ is selected for actual satellites in the first orbital plane, and then this configuration is duplicated for each subsequent orbital plane using a constant shifting parameter (an integer $k \in \{0, 1, \cdots, N_{so} - 1\}$). The subset $\mathcal{G}$ can be any necklace. Once $\mathcal{G}$ and the shifting parameters are given, the constellation is automatically determined. Figure 4.2 shows the various positions of a satellite in the second orbital

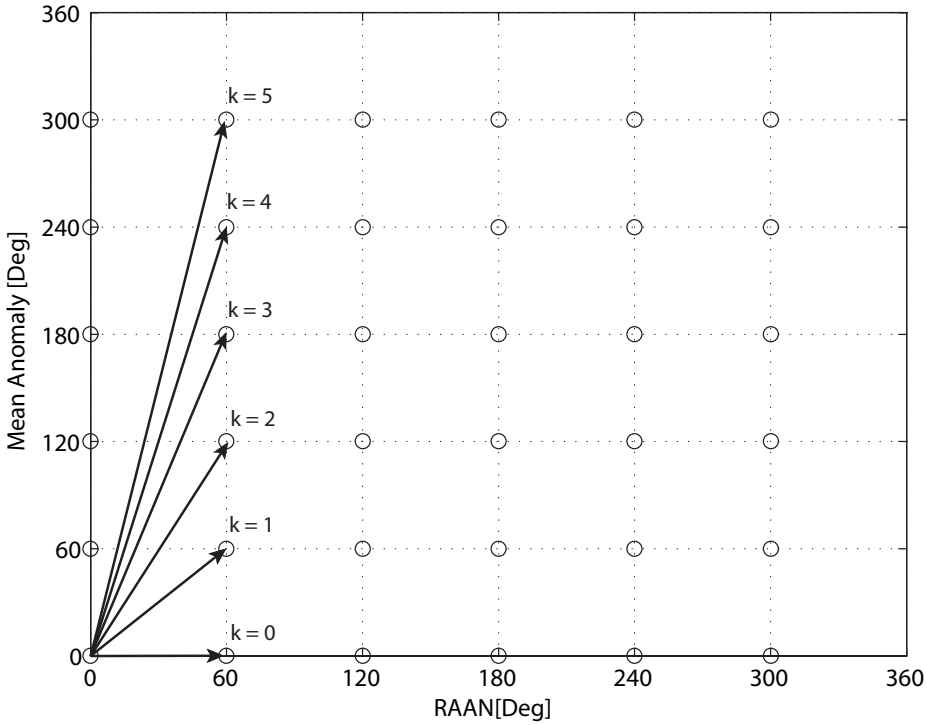

Figure 4.2: The shifting determines the location of the satellites in the constellation.

plane with respect the first one in the first orbital plane as a function of the shifting parameter k.
To perform a correct and unique shifting between subsequent orbital planes two problems must be taken into consideration:

- **Consistency problem**. Due to the modular nature of the Ω parameter, the shifting has to be chosen in such a way that the group of satellites (necklace) in the orbit with $\Omega = 0$ coincides with the group of satellites (necklace) in the orbit with $\Omega = 2\pi$. This problem is discussed in detail in the next subsection.

- **Minimality problem**. Sometimes, for the same $\mathcal{G}$, there are two values of the shifting parameter generate the same distribution of satellites in the (Ω, M)-space. This is discussed later, but it is solved by simply taking $0 \leq k \leq \mathrm{Sym}(\mathcal{G}) - 1$.

Satellite constellations obtained from the above procedure are called *Necklace Flower Constellations* (NFC).

4.2.5 ΔM-shifting between subsequent orbit planes

The first satellite ($j = 0$) in the first or initial orbit ($i = 0$) is chosen (without loss of generality) as $M_{00} = 0$ and $\Omega_{00} = 0$. Taking into account Eq. (1.42) the mean anomaly

of our satellite in the next orbit will be:

$$M_{10} = -\frac{2\pi N_c}{N_o N_{so}}. \tag{4.5}$$

Then, the amount ΔM, called ΔM-Shifting between subsequent orbits, will be:

$$\Delta M = -\frac{2\pi N_c}{N_o N_{so}} + k\frac{2\pi}{N_{so}}, \tag{4.6}$$

where k is the shifting parameter. This means that the mean anomalies of the satellites in the second orbit can be obtained by adding ΔM to the mean anomalies of the satellites of the first orbit. Similarly, the mean anomalies on the third orbit are the mean anomalies on the second plus ΔM, and so on.
After a rotation of 360° of the initial orbit, the mean anomaly of the satellite will increase by:

$$\begin{aligned} N_o \Delta M &= N_o \left(-\frac{2\pi N_c}{N_o N_{so}} + k\frac{2\pi}{N_{so}} \right) \\ &= \frac{2\pi}{N_{so}}(kN_o - N_c). \end{aligned} \tag{4.7}$$

Figure 4.3 shows the meaning of the value ΔM in a (Ω, M)-space of a NFC $\mathcal{G} = \{1, 3, 5, 7\}$ with $N_{so} = 8$, $N_o = 6$ and $N_c = 2$.

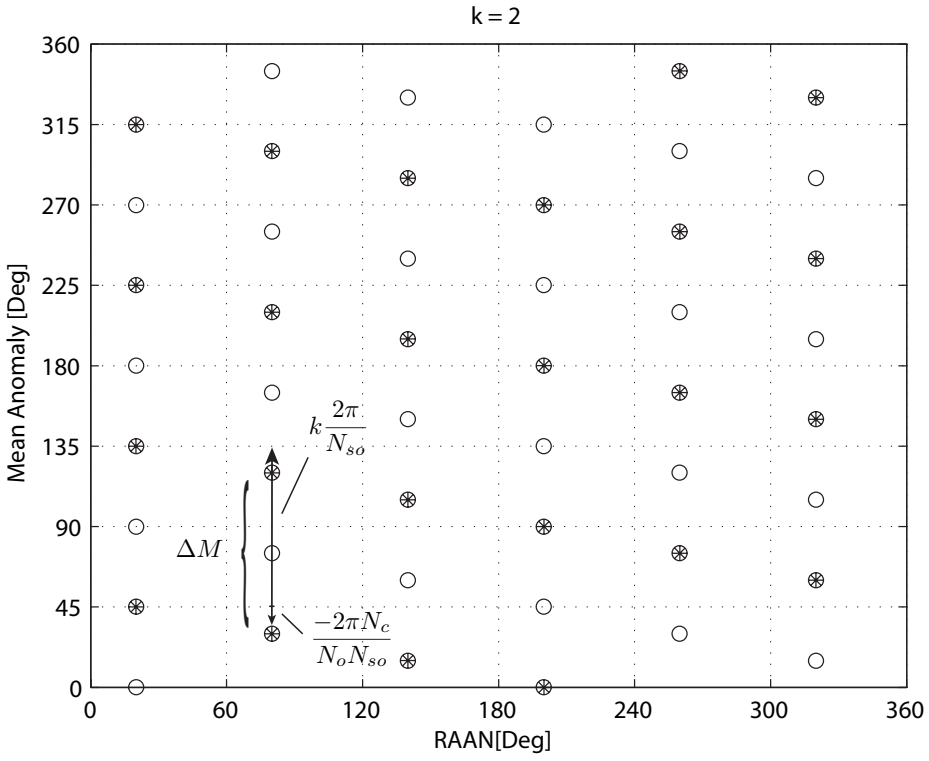

Figure 4.3: The amount ΔM in the (Ω, M)-space.

4.2.6 Admissible pair $(\mathcal{G}, k)$

Let $\mathcal{G}$ be a necklace such as $\mathcal{G} \in K(N_{so})$ and a shifting parameter $k \in \{0, 1, \cdots, N_{so}-1\}$, the pair $(\mathcal{G}, k)$ is called admissible if the distribution of satellites in the initial orbit is invariant by adding $N_o \Delta M$ to the mean anomaly of each satellite.

$$\frac{2\pi}{N_{so}}\mathcal{G} + \frac{2\pi}{N_{so}}(kN_o - N_c) \equiv \frac{2\pi}{N_{so}}\mathcal{G} \mod (2\pi). \tag{4.8}$$

The logic behind this equation is the following: the term $\frac{2\pi}{N_{so}}\mathcal{G}$ represents the mean anomalies of the satellites in the first orbit plane, the second term represents the shifting in mean anomaly that all satellites will suffer due to the shifting between the first and the last orbit and, finally, the right hand side represents the mean anomalies of the satellites in the last plus one orbit, that must coincide with the initial mean anomalies up to some integer multiple of 2π. Multiplying Eq. (4.8) by $\frac{N_{so}}{2\pi}$ and using the definition of symmetry number, the condition above translates into

$$\mathrm{Sym}(\mathcal{G}) | kN_o - N_c. \tag{4.9}$$

Equation (4.9) represents the solution to the *consistency problem*, that is, it provides the values of the shifting parameters (k) that are all *admissible* to create a NFC. Again, these values of k are such that the initial necklace in orbital plane $\Omega = 0$ is the same when shifted N_o times by the mean anomaly variation given in Eq. (4.6).

Figures 4.4 and 4.5 show two examples of 2D-LFCs generated by an admissible pair $(\mathcal{G}, k)$. In both cases, the design parameters were $N_{so} = 9$, $N_o = 6$, and $N_c = 3$. The necklace in Figure 4.4 is $\mathcal{G} = \{1, 4, 6\}$ that has symmetry number $\mathrm{Sym}(\mathcal{G}) = 9$, and shifting parameter $k = 2$. The consistency condition is satisfied since $9 | 2 \cdot 6 - 3$, so the pair $(\{1, 4, 6\}, 2)$ is admissible. This can be seen in the figure as follows: shifting the three satellites of the last orbit (the one with $\Omega = 320°$) with $\Delta M = 60°$ as given by Eq. (4.6) for $k = 2$, reproduces exactly the configuration in the first orbit (the one with $\Omega = 20°$). In Figure 4.5, the necklace is $\mathcal{G} = \{1, 4, 7\}$ which has symmetry number $\mathrm{Sym}(\mathcal{G}) = 3$, and shifting parameter $k = 2$. Again, the consistency condition is satisfied: $3 | 2 \cdot 6 - 3$.

As we mentioned before, the minimality problem is solved by restricting the range of values of k to the interval $[0, \mathrm{Sym}(\mathcal{G}) - 1]$. It is clear that $(\mathcal{G}, k)$ and $(\mathcal{G}, k')$ will generate the same constellation if and only if $k - k'$ is an integer multiple of $\mathrm{Sym}(\mathcal{G})$. This is impossible for two values in the proposed interval. Figure 4.5 shows an example of this situation: in this 2D-LFC ($N_{so} = 9$, $N_o = 6$, and $N_c = 3$) the necklace $\mathcal{G} = \{1, 4, 7\}$, which has $\mathrm{Sym}(\mathcal{G}) = 3$, generates the same configuration for $k = 2$, $k = 5$, and $k = 8$. This discussion proves our main result:

Theorem 29. Each NFC corresponds with one (and only one) pair $(\mathcal{G}, k)$ with $\mathcal{G} \in K(N_{so})$, $0 \leq k \leq \mathrm{Sym}(\mathcal{G}) - 1$, and $\mathrm{Sym}(\mathcal{G}) | kN_o - N_c$.

Figure 4.6, 4.7, and 4.8 show the only three possible NFCs (according to our main result) induced by the necklace $\mathcal{G} = \{1, 4, 7, 10\} \in K(12)$, which has symmetry number $\mathrm{Sym}(\mathcal{G}) = 3$. The underlying 2D-LFC has parameters $N_{so} = 12$, $N_o = 9$, and $N_c = 3$, so the three possible values of $k \in \{0, 1, 2\}$ are admissible.

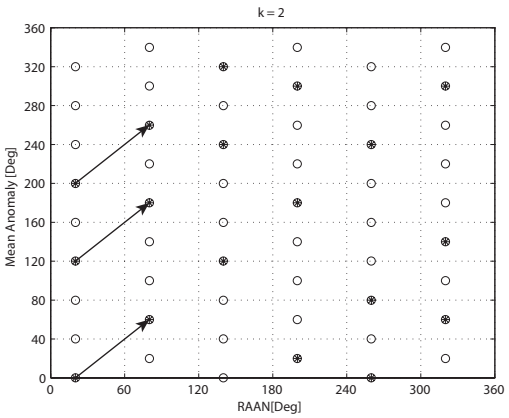

Figure 4.4: NFC generated by an admissible pair.

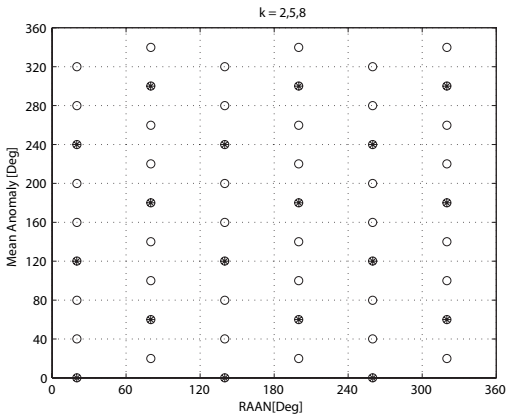

Figure 4.5: Different values of k can generate the same configuration.

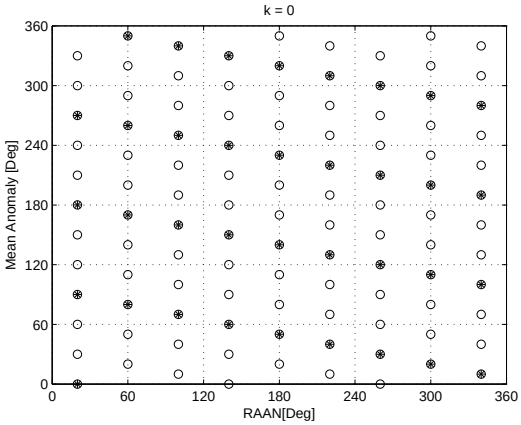

Figure 4.6: NFC with $\mathcal{G} = \{1, 4, 7, 10\}$ and $k = 0$

4.2.7 The Diophantine Equation for the Shifting parameter

The admissibility condition for a pair $(\mathcal{G}, k)$ given in Eq. (4.9), motivates us to study the Diophantine equation $d|ak - b$, where a, b, d are given (positive) integers and the unknown k takes integer values in the range $[0, d-1]$. All the solutions can be obtained trivially by trial and error (since there are finitely many possibilities for k), but we would need a closed formula for its number of solutions:

Lemma 30. The number of solutions of this diophantine equation, denoted by $Y(d, a, b)$, is exactly:

$$Y(d, a, b) = \begin{cases} 0 & \text{if } \gcd(d, a) \nmid b \\ \gcd(d, a) & \text{otherwise.} \end{cases} \tag{4.10}$$

Proof. Independently of the value of k, the product ak is always divisible by $\gcd(d, a)$, so when $\gcd(d, a) \nmid b$, it is impossible to have $\gcd(d, a)|ak-b$, and therefore we will never

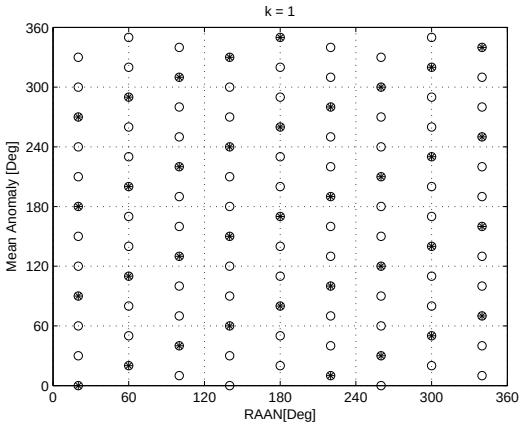

Figure 4.7: NFC with $\mathcal{G} = \{1, 4, 7, 10\}$ and $k = 1$

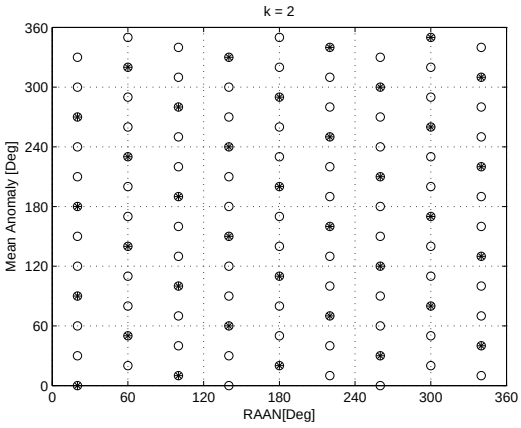

Figure 4.8: NFC with $\mathcal{G} = \{1, 4, 7, 10\}$ and $k = 2$

have $d|ak-b$. In the case where $\gcd(d,a)|b$, we can divide a, b, and d by $\gcd(d,a)$, and reduce the problem to the equation $d'|a'k-b'$ where $a' = a/\gcd(d,a)$, $b' = b/\gcd(d,a)$, and $d' = d/\gcd(d,a)$. This problem has only one solution in the interval $[0, d'-1]$, since a' and d' have no common factor, and therefore has $d/d' = \gcd(d,a)$ solutions in the $[0, d-1]$. □

4.3 Counting Necklace Flower Constellations

In order to successfully implement the necklace theory into an optimization process, it is important to have an algorithm providing all the necklaces that can be obtained from a 2D-LFC with parameters N_{so}, N_o, and N_c. However, before listing all these necklaces it is important to know how many they are. The total number of necklaces, here denoted by $W(N_{so}, N_o, N_c)$, is exactly the number of admissible pairs;

$$\#\{(\mathcal{G}, k) : \mathcal{G} \in K(N_{so}),\ 0 \leq k \leq \mathrm{Sym}(\mathcal{G}) - 1,\ kN_o \equiv N_c \mod (\mathrm{Sym}(\mathcal{G}))\}. \quad (4.11)$$

Let $X(d)$ be the number of necklaces with symmetry number equal to d, then Eq. (4.11) can be rewritten as,

$$W(N_{so}, N_o, N_c) = \sum_{d|N_{so}} X(d) Y(d, N_o, N_c). \quad (4.12)$$

It should be natural to adopt the notation $X(d, N_{so})$ rather than $X(d)$ since we are considering necklaces in $K(N_{so})$. However, the number of necklaces with symmetry number d in $K(N_{so})$ is on a one-to-one correspondence with the number of necklaces in $K(d)$ with symmetry number d. This shows that $X(d, N_{so})$ does not depend on N_{so}, as long as $d|N_{so}$. For practical purposes we can define $X(d) = X(d, d)$, i.e. the number of necklaces in $K(d)$ with symmetry number equal to d. A simple corollary of this discussion is the formula

$$\sum_{d|n} X(d) = N_2(n), \quad (4.13)$$

where $N_2(n)$ is given in Eq. (4.3). Equation (4.13) follows from the fact that $X(d) = X(d, n)$ for any $d|n$, and that any necklace in $K(n)$ has a symmetry number that divides n.

Consider two positive integers n and m. Denote $(n : m^\infty)$ the integer obtained by removing from n all the prime factors corresponding to the primes that appear in m. For instance, $(120 : 70^\infty) = 3$, since $120 = 2^3 \cdot 3 \cdot 5$ and the primes 2 and 5 appear in $70 = 2 \cdot 5 \cdot 7$.

Now we have all the tools needed to state our main counting result:

Theorem 31. Assume $\gcd(N_{so}, N_o, N_c) = 1$. Then,

$$W(N_{so}, N_o, N_c) = N_2(N_{so} : N_o^\infty),$$

regardless of the value of N_c.

Proof. We will use Eq. (4.12) to compute the value of $W(N_{so}, N_o, N_c)$. In this equation, we have a sum ranging over all divisors d of N_{so}. However, if the divisor d has a common factor with N_o, then it can not have any common factor with N_c by our assumption $\gcd(N_{so}, N_o, N_c) = 1$, and therefore $Y(d, N_o, N_c) = 0$ according to Eq. (4.10). This means that it is enough to consider divisors of $(N_{so} : N_o^\infty)$. For any of these divisors, we have $Y(d, N_o, N_c) = 1$, since $\gcd(d, N_o) = 1$. All together this means that

$$W(N_{so}, N_o, N_c) = \sum_{d|(N_{so}:N_o^\infty)} X(d),$$

which is equal to $N_2(N_{so} : N_o^\infty)$ by Eq. (4.13). □

We derive from Theorem 31, two particular cases of independent interest:

Corollary 32. If $\gcd(N_{so}, N_o) = 1$, then $W(N_{so}, N_o, N_c) = N_2(N_{so})$.

Proof. When N_{so} and N_o have no common factors, then $(N_{so} : N_o^\infty) = N_{so}$, since there are no primes to remove from N_{so}. Knowing this, the result follows immediately from Theorem 31. □

Corollary 33. If $N_{so}|N_o$ and $\gcd(N_c, N_{so}) = 1$, then $W(N_{so}, N_o, N_c) = 2$.

Proof. The assumption $N_{so}|N_o$, implies that all the primes in N_{so} appear in N_o, and therefore $(N_{so} : N_o^\infty) = 1$. By Theorem 31, we conclude $W(N_{so}, N_o, N_c) = N_2(1) = 2$. □

Theorem (31) is particularly useful with Harmonic Flower Constellations that are 2D-LFCs with the additional constraint $\gcd(N_{so}, N_o, N_c) = 1$ (see Ref. [7]).

It would be nice to have a simple closed formula for $W(N_{so}, N_o, N_c)$ that works in general. The following results constitute positive steps toward the general solution. First of all, we search a formula for $X(d)$.

Theorem 34. (**Moebius' Inversion Formula**) Let $f : \mathbb{N} \to \mathbb{C}$ and $F : \mathbb{N} \to \mathbb{C}$ be any functions such that:

$$F(m) = \sum_{d|m} f(d).$$

Then,

$$f(m) = \sum_{d|m} \mu\left(\frac{m}{d}\right) F(d) \quad \forall m \in \mathbb{N}.$$

Proof.

$$\begin{aligned} \sum_{d|m} \mu\left(\frac{m}{d}\right) F(d) &= \sum_{d|m} \mu\left(\frac{m}{d}\right) \sum_{e|d} f(e) \\ &= \sum_{d|m} \sum_{e|d} \mu\left(\frac{m}{d}\right) f(e). \end{aligned}$$

Now, by setting $d = ed'$,

$$\begin{aligned} \sum_{d|m} \sum_{e|d} \mu\left(\frac{m}{d}\right) f(e) &= \sum_{e|m} \sum_{d'|\frac{m}{e}} \mu\left(\frac{m}{ed'}\right) f(e) \\ &= \sum_{e|m} \sum_{d'|\frac{m}{e}} \mu\left(\frac{m/e}{d'}\right) f(e) \\ &= \sum_{e|m} \left[f(e) \sum_{d'|\frac{m}{e}} \mu\left(\frac{m/e}{d'}\right) \right]. \end{aligned}$$

By setting $d'' = \frac{m/e}{d'}$,

$$\begin{aligned} \sum_{e|m} \left[f(e) \sum_{d'|\frac{m}{e}} \mu\left(\frac{m/e}{d'}\right) \right] &= \sum_{e|m} f(e) \sum_{d''|\frac{m/e}{d'}} \mu(d'') \\ &= \sum_{e|m} f(e) \begin{cases} 1 & \text{if } \frac{m}{e} = 1, \\ 0 & \text{otherwise.} \end{cases} \\ &= f(m). \end{aligned}$$

□

Theorem 35. Let $f : \mathbb{N} \to \mathbb{C}$ be a multiplicative function. Then,

$$F(m) = \sum_{d|m} f(d)$$

is multiplicative.

Proof.

$$F(mn) = \sum_{d|mn} f(d).$$

Every divisor c of mn can be expressed in the form $c = ab$ where $a|m$ and $b|n$. Moreover, $\gcd(a, b) = 1$, $\gcd(m/a, n/b) = 1$ and there is a one-to-one correspondence between the set of products ab and the divisors c of mn. Hence,

$$\begin{aligned} F(mn) &= \sum_{\substack{a|m \\ b|n}} f(ab) \\ &= \sum_{\substack{a|m \\ b|n}} f(a)f(b) \\ &= \sum_{a|m} f(a) \sum_{b|n} f(b) = F(m)F(n). \end{aligned}$$

□

Theorem 36. Let $F : \mathbb{N} \to \mathbb{C}$ be a multiplicative function. Then,

$$f(m) = \sum_{d|m} \mu\left(\frac{m}{d}\right) F(d)$$

is multiplicative.

Proof. Every divisor c of mn can be expressed in the form $c = ab$ where $a|m$ and $b|n$. Moreover, $\gcd(a, b) = 1$, $\gcd(m/a, n/b) = 1$ and there is a one-to-one correspondence between the set of products ab and the divisors c of mn. Hence,

$$\begin{aligned} f(mn) &= \sum_{d|mn} \mu\left(\frac{mn}{d}\right) F(d) \\ &= \sum_{\substack{a|m \\ b|n}} \mu\left(\frac{ab}{d}\right) F(ab) \\ &= \sum_{a|m} \mu\left(\frac{a}{d}\right) F(a) \sum_{b|n} \mu\left(\frac{b}{d}\right) F(b) \\ &= f(m)f(n). \end{aligned}$$

□

Theorem 37. Let

$$F(m) = \frac{\varphi(n)}{n}$$

be a multiplicative function. Then,

$$f(m) = \sum_{d|m} \mu\left(\frac{m}{d}\right) \frac{\varphi(d)}{d}$$

is also multiplicative function. Moreover,

$$f(n) = \frac{\mu(n)}{n} \qquad \forall n \in \mathbb{N}.$$

Proof. Using theorem 36 is trivial that $f(m)$ is a multiplicative function. Let $p \in \mathbb{N}$ a prime.

$$\begin{aligned} f(p) &= \sum_{d|p} \mu\left(\frac{p}{d}\right) \frac{\varphi(d)}{d} \\ &= \mu\left(\frac{p}{1}\right) \frac{\varphi(1)}{1} + \mu\left(\frac{p}{p}\right) \frac{\varphi(p)}{p} \\ &= -1 + 1 \cdot \frac{p-1}{p} \\ &= -\frac{1}{p}. \end{aligned}$$

Let $p^k \in \mathbb{N}$ a power of a prime.

$$\begin{aligned} f(p^k) &= \sum_{d|p^k} \mu\left(\frac{p^k}{d}\right) \frac{\varphi(d)}{d} \\ &= \sum_{i=0}^{k} \mu\left(p^{k-i}\right) \frac{\varphi(p^i)}{p^i} \\ &= 1 \cdot \frac{\varphi(p^k)}{p^k} - \frac{\varphi(p^{k-1})}{p^{k-1}} \\ &= 0. \end{aligned}$$

Let $n \in \mathbb{N}$. If n has a power of a prime, then $f(n) = 0$. Otherwise:

$$\begin{aligned} f(n) &= f(p_1 p_2 \dots p_m) \\ &= f(p_1) f(p_2) \dots f(p_m) \\ &= \frac{-1}{p_1} \frac{-1}{p_2} \dots \frac{-1}{p_m} \\ &= \frac{\mu(n)}{n} \qquad \forall n. \end{aligned}$$

□

Theorem 38. For any positive integer d, we have

$$X(d) = \frac{1}{d} \sum_{e|d} \mu(e) 2^{d/e}.$$

Proof. The idea is to invert Eq. (4.13) using Moebius' inversion formula given in Theorem 34:

$$X(d) = \sum_{e|d} \mu(d/e) N_2(e)$$

$$= \sum_{e|d} \sum_{f|e} \mu(d/e) \frac{\varphi(f)}{e} 2^{e/f}.$$

Writing $r = e/f$, and changing the order of summation, we get:

$$X(d) = \sum_{r|d} \frac{2^r}{r} \sum_{f|\frac{d}{r}} \mu\left(\frac{d}{rf}\right) \frac{\varphi(f)}{f}.$$

Finally, the theorem of multiplicative arithmetic functions show that the second sum reduces to $\mu(d/r)/(d/r)$, and therefore

$$\begin{aligned} X(d) &= \sum_{r|d} \frac{2^r}{r} \frac{\mu(d/r)}{d/r} \\ &= \frac{1}{d} \sum_{r|d} \mu(d/r) 2^r, \\ &= \frac{1}{d} \sum_{e|d} \mu(e) 2^{d/e}. \end{aligned}$$

The last equality is true by writing $r = d/e$ and we have what the theorem states. □

For the cases not included in theorem 31 (or in any of its corollaries) the following formula for $W(N_{so}, N_o, N_c)$ is provided.

Theorem 39. If $N_{so}|N_o$ and $N_c = 0$ then, $W(N_{so}, N_o, N_c) = 2^{N_{so}}$.

Proof. The following observation should be noted: for any divisor d of N_{so}, we have $Y(d, N_o, 0) = d$, since d also divides N_o. Therefore, using Eq. (4.12) and theorem 38, we can write

$$\begin{aligned} W(N_{so}, N_o, N_c) &= \sum_{d|N_{so}} X(d) d \\ &= \sum_{d|N_{so}} \sum_{e|d} \mu(e) 2^{d/e}. \end{aligned}$$

Now, by setting $d = ek$, and changing the order of summation, the previous equation reduces to:

$$W(N_{so}, N_o, N_c) = \sum_{k|N_{so}} \sum_{e|\frac{N_{so}}{k}} \mu(e) 2^k.$$

The sum $\sum_{e|r} \mu(e)$ is equal to 1 when $r = 1$ and 0 otherwise. In particular, the sum above (the one depending on e) will vanish unless $k = N_{so}$. But this shows $W(N_{so}, N_o, N_c) = 2^{N_{so}}$, as claimed. □

A formula to compute all possible configurations given N_{so}, N_o and N_c has been studied, but it will be useful a formula providing all the possible configurations that can be obtained from a 2D-LFC with parameters N_{so}, N_o, N_c and the number of real satellites

per orbit $N_{rso} \leq N_{so}$. The number of constellations satisfying the previous condition, denoted by $\tilde{W}(N_{so}, N_o, N_c, N_{rso})$, corresponds with the number of admissible pairs;

$$\{(\mathcal{G}, k) : \mathcal{G} \in K(N_{so}),\ 0 \leq k \leq \mathrm{Sym}(\mathcal{G}) - 1,\ |\mathcal{G}| = N_{rso},\ kN_o \equiv N_c \mod (\mathrm{Sym}(\mathcal{G}))\}. \tag{4.14}$$

We examine a simple case. If $N_{so} = 24$ and $N_{rso} = 6$ by exploring all the possibilities for the symmetry number of a given necklace $\mathcal{G}$ since $\mathrm{Sym}(\mathcal{G})|N_{so}$ we have the following cases:

- $Sym(\mathcal{G}) = 1, 2, 3, 6$. These cases are not possible, since we have to distribute 6 satellites in $N_{so}/Sym(\mathcal{G}) = 24, 12, 8, 4$ subsets (each one with the same number of satellites), respectively.
- $Sym(\mathcal{G}) = 4, 8, 12, 24$. These cases can be attained by putting 1,2,3,6 satellites in each of the $N_{so}/Sym(\mathcal{G}) = 6, 3, 2, 1$ subsets, respectively.

It is easy to infer that the number of subsets $(N_{so}/Sym(\mathcal{G}))$ must divide the real number of satellite per orbit (N_{rso}), which translates into the following condition,

$$\frac{N_{so}}{Sym(\mathcal{G})} | N_{rso}.$$

In other words, N_{so} must divide $Sym(\mathcal{G}) \cdot N_{rso}$. Then, by exploring all the possible symmetry numbers, which correspond with the divisors of N_{so}, the Eq. (4.14) can be reformulated as:

$$\tilde{W}(N_{so}, N_o, N_c, N_{rso}) = \sum_{\substack{\lambda | N_{so} \\ N_{so} | \lambda N_{rso}}} \#\{\mathcal{G} \in K(N_{so}) : |\mathcal{G}| = N_{rso}, Sym(\mathcal{G}) = \lambda\}\, Y(\lambda, N_o, N_c). \tag{4.15}$$

where $Y(\lambda, N_o, N_c)$ has been already define in Eq. (4.10).

Despite of the difficulty to analyze the previous formula we have a counting result,

Theorem 40. If $\gcd(N_{so}, N_{rso}) = 1$ then,

$$\tilde{W}(N_{so}, N_o, N_c, N_{rso}) = N_2(N_{so}, N_{rso})\, Y(N_{so}, N_o, N_c),$$

where $N_2(m, n)$ represents the number of necklaces in two colors with n pearls, of which m are in black color and $n - m$ are in white.

Proof. If $\gcd(N_{so}, N_{rso}) = 1$ the only symmetry number λ that satisfies the conditions $\lambda | N_{so}$ and $N_{so} | \lambda N_{rso}$ is $\lambda = N_{so}$. Then,

$$\tilde{W}(N_{so}, N_o, N_c, N_{rso}) = \#\{\mathcal{G} \in K(N_{so}) : |\mathcal{G}| = N_{rso}, Sym(\mathcal{G}) = N_{so}\}\, Y(N_{so}, N_o, N_c).$$

The number of necklaces $\mathcal{G}$ satisfying $|\mathcal{G}| = N_{rso}$ and $Sym(\mathcal{G}) = N_{so}$ corresponds to $N_2(N_{so}, N_{rso})$. All together means that

$$\tilde{W}(N_{so}, N_o, N_c, N_{rso}) = N_2(N_{so}, N_{rso})\, Y(N_{so}, N_o, N_c).$$

□

It would be nice to have a closed formula for $\tilde{W}(N_{so}, N_o, N_c, N_{rso})$. The following result constitute a positive step to reach that goal.

$$\tilde{W}(N_{so}, N_o, N_c, N_{rso}) = \sum_{d|N_{so}} \tilde{X}(d, N_{rso}, N_{so}) Y(d, N_o, N_c) \tag{4.16}$$

where the function $\tilde{X}(d, N_{rso}, N_{so})$ represents the number of necklaces with N_{so} admissible locations, of which N_{rso} are occupied by a satellite and the symmetry of the necklace is d.

Number theory will be a fundamental tool to reach a closed formula for $\tilde{X}(d, N_{rso}, N_{so})$ which is still missing.

4.4 Design of Necklace Flower Constellations

To sum up, the design of a Necklace Flower Constellation is as follows: given the number of admissible locations per orbit N_{so}, and the real number of satellites per orbit N_{rso}, it is possible to determine all the different configurations to distribute the satellites in the first orbit of our constellation. After that, an initial necklace is selected and it is possible to compute its symmetry number. Finally, the values of the shifting that give different Necklace Flower Constellations are computed.

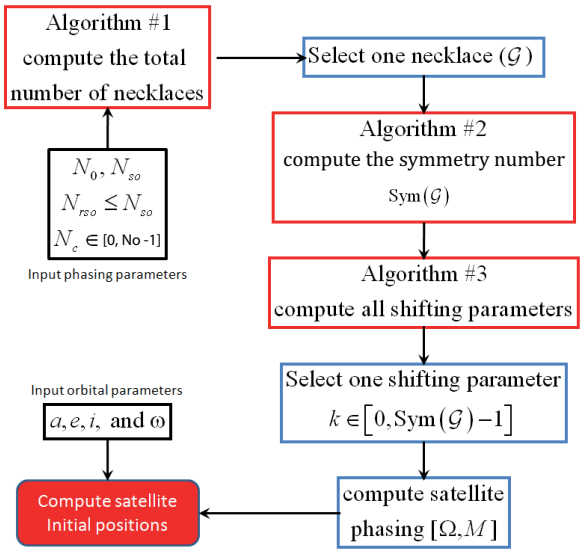

Figure 4.9: Program Flowchart.

The flowchart given in Figure 4.9 summarizes the design procedure described above and it can be read as follows. As input we have the mission parameters, N_o and N_{rso}, indicating the number of orbit planes and the number of satellites per orbit plane, and an arbitrary number of potential locations (per orbit plane) where to locate our satellites, $N_{so} \geq N_{rso}$. Now, by choosing a value for the configuration number N_c in the interval $[0, N_o - 1]$ we can compute all possible necklaces of the N_{rso} satellites in the N_{so}

potential locations. Now, by selecting one of these necklaces, say $\mathcal{G}$, we can compute $\mathrm{Sym}(\mathcal{G})$ and all the possible values of the shifting parameter $k \in [0, \mathrm{Sym}(\mathcal{G}) - 1]$ that give different configurations for our constellation. At this point using the selected necklace and a shifting parameter we compute the phasing of all the $N_{rs} = N_{rso}\, N_o$ satellites in the (Ω, M)-space as shown in Figure 4.2. The location of the satellites in the first orbit is given by the necklace $\mathcal{G}$ and the location of the satellites in subsequent orbits is controlled by the shifting parameter k. Finally, optimize the common orbital parameters (a, e, i and ω) to minimize the mission cost function.

Note that, the formulas that we obtained for the total number of Necklace Flower Constellation can be used in practice to select values of N_c (given N_{so} and N_o) that produces the largest number of different patterns. This is useful since the more configurations there are, the more design possibilities we have.

A 27 satellite constellation is designed to illustrate a practical example of usage. The number of orbital planes is three, $N_o = 3$. By using the 2D-LFC theory the remaining parameters must be $N_{so} = 9$ and $N_c \in \{0, 1, 2\}$. Consequently, we have three unique design possibilities illustrated in Figures 4.10, 4.11, and 4.12.

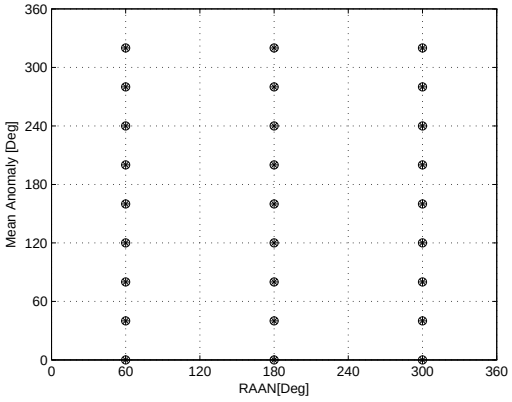

Figure 4.10: 2D-LFC with $N_c = 0$, $\Omega_{00} = 60.0°$, and $M_{00} = 0.0$

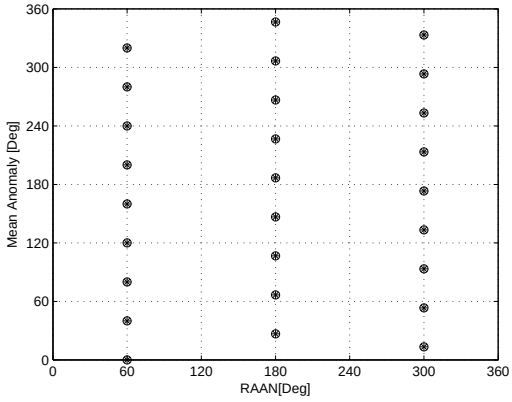

Figure 4.11: 2D-LFC with $N_c = 1$, $\Omega_{00} = 60.0°$, and $M_{00} = 0.0$

However, by using the NFC theory there exist more design possibilities. Consider a NFC with parameters $N_o = 3$, $N_{so} = 12$, $N_{rso} = 9$, and $N_c \in \{0, 1, 2\}$. First of all, as the theory states, the first orbit of the constellation is given by a necklace. In particular, there are 19 different necklaces to associate to the first orbit. These are:

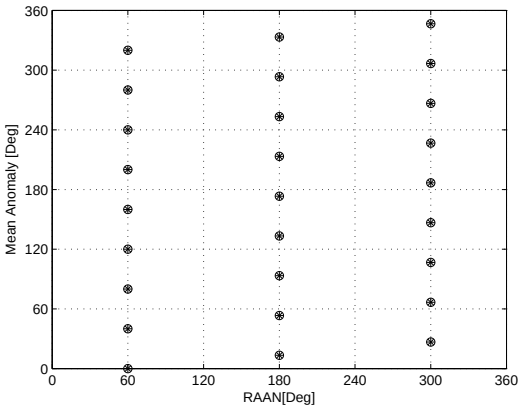

Figure 4.12: 2D-LFC with $N_c = 2$, $\Omega_{00} = 60.0°$, and $M_{00} = 0.0$

$\mathcal{G}_1 = \{1, 2, 3, 4, 5, 6, 7, 8, 9\}$, $\mathcal{G}_2 = \{1, 2, 3, 4, 5, 6, 7, 8, 10\}$,
$\mathcal{G}_3 = \{1, 2, 3, 4, 5, 6, 7, 9, 10\}$, $\mathcal{G}_4 = \{1, 2, 3, 4, 5, 6, 8, 9, 10\}$,
$\mathcal{G}_5 = \{1, 2, 3, 4, 5, 7, 8, 9, 10\}$, $\mathcal{G}_6 = \{1, 2, 3, 4, 6, 7, 8, 9, 10\}$,
$\mathcal{G}_7 = \{1, 2, 3, 5, 6, 7, 8, 9, 10\}$, $\mathcal{G}_8 = \{1, 2, 4, 5, 6, 7, 8, 9, 10\}$,
$\mathcal{G}_9 = \{1, 3, 4, 5, 6, 7, 8, 9, 10\}$, $\mathcal{G}_{10} = \{1, 2, 3, 4, 5, 6, 7, 9, 11\}$,
$\mathcal{G}_{11} = \{1, 2, 3, 4, 5, 6, 8, 9, 11\}$, $\mathcal{G}_{12} = \{1, 2, 3, 4, 5, 7, 8, 9, 11\}$,
$\mathcal{G}_{13} = \{1, 2, 3, 4, 6, 7, 8, 9, 11\}$, $\mathcal{G}_{14} = \{1, 2, 3, 5, 6, 7, 8, 9, 11\}$,
$\mathcal{G}_{15} = \{1, 2, 4, 5, 6, 7, 8, 9, 11\}$, $\mathcal{G}_{16} = \{1, 2, 3, 4, 5, 7, 8, 10, 11\}$,
$\mathcal{G}_{17} = \{1, 2, 3, 4, 6, 7, 8, 10, 11\}$, $\mathcal{G}_{18} = \{1, 2, 3, 5, 6, 7, 8, 10, 11\}$,
$\mathcal{G}_{19} = \{1, 2, 3, 5, 6, 7, 9, 10, 11\}$.

Only two particular cases are analyzed. The necklace $\mathcal{G}_4$ has symmetry number equal to twelve $\mathrm{Sym}(\mathcal{G}_4) = 12$. When $N_c = 0$ the consistency condition (see Eq. (4.9)) implies that the shifting parameter must be $k \in \{0, 4, 8\}$. While for the other values for $N_c \in \{1, 2\}$ there are no values for the shifting parameter that satisfy the consistency condition. By using necklace $\mathcal{G}_4$ we have three new designs for the constellation illustrated in Figures 4.13, 4.14, and 4.15.
The necklace $\mathcal{G}_{19}$ has symmetry number equal to four $\mathrm{Sym}(\mathcal{G}_{19}) = 4$. When $N_c = 0$ the consistency condition (see Eq. (4.9)) implies that the shifting parameter must be $k = 0$. When $N_c = 1$ the shifting parameter must be $k = 3$, and finally when $N_c = 2$ the shifting parameter must be $k = 2$. Then, with the necklace $\mathcal{G}_{19}$ there exist three different possibilities for design the constellation illustrated in Figures 4.16, 4.17, and 4.18.

Only two necklaces have been analyzed. Note that, the more necklaces can be associated to the first orbit, the more design possibilities there are.

4.5 Conclusions

The cost of the missions is one of the most important factors to account when building a Constellations of satellites. The theory of necklaces allows us to reduce the number

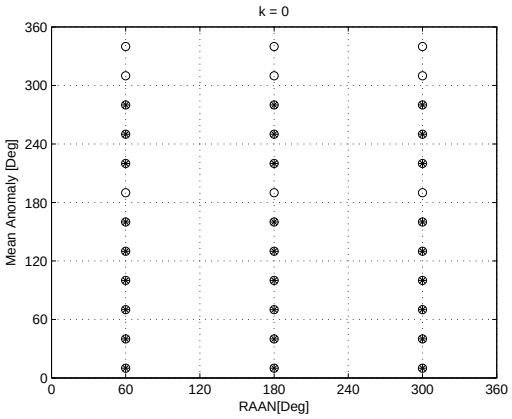

Figure 4.13: NFC with $N_c = 0$, $\Omega_{00} = 60.0$, $k = 0$, and $\mathcal{G}_4$.

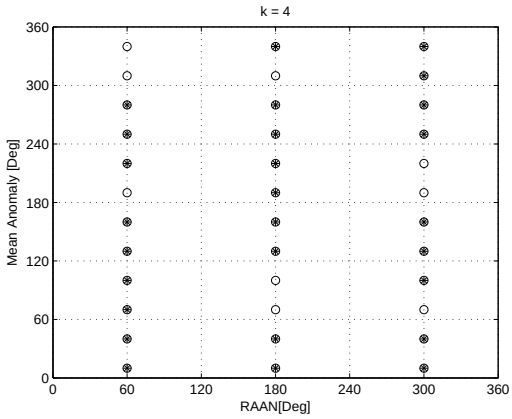

Figure 4.14: NFC with $N_c = 0$, $\Omega_{00} = 60.0$, $k = 4$, and $\mathcal{G}_4$.

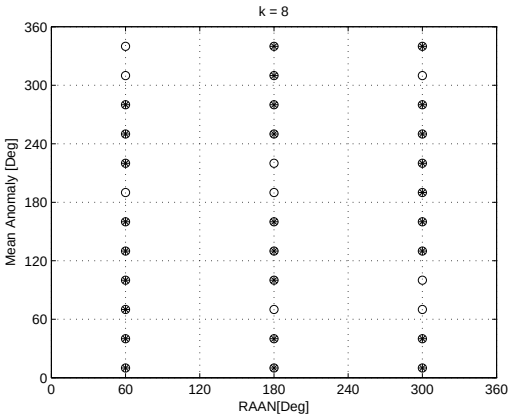

Figure 4.15: NFC with $N_c = 0$, $\Omega_{00} = 60.0$, $k = 8$, and $\mathcal{G}_4$.

of satellites in a Flower Constellation without losing their symmetric character. We have shown what parameters are needed to define one of these objects (basically, a pair $(\mathcal{G}, k)$ consisting of a necklace and a positive integer), and which constrains have to be imposed on these parameters. We have also written algorithms, that enumerate and plot all the possible necklace constellations that can be extracted from a 2D Lattice Flower Constellation.

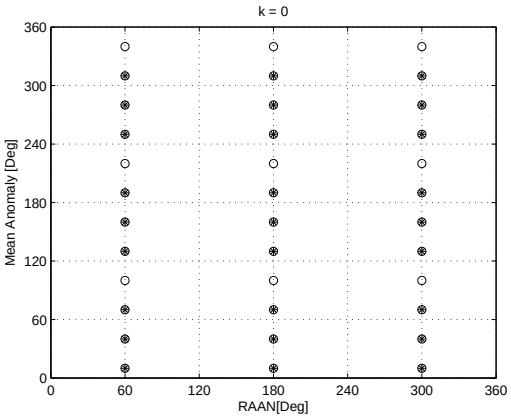

Figure 4.16: NFC with $N_c = 0$, $\Omega_{00} = 60.0$, $k = 0$, and $\mathcal{G}_{19}$.

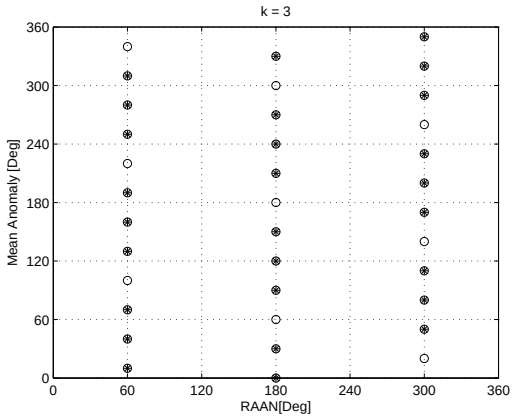

Figure 4.17: NFC with $N_c = 1$, $\Omega_{00} = 60.0$, $k = 3$, and $\mathcal{G}_{19}$.

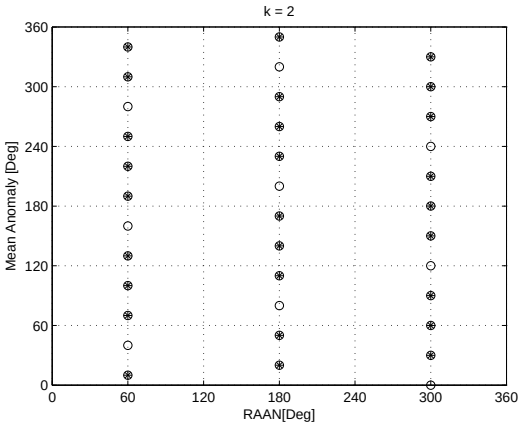

Figure 4.18: NFC with $N_c = 2$, $\Omega_{00} = 60.0$, $k = 2$, and $\mathcal{G}_{19}$.

Conclusions and future work

This work approaches the problem of designing optimal constellations, from a geometric point of view, since we seek those constellations with excellent geometry, and from an economical point of view because we allow fuel savings by seeking stable constellations, and also design savings in the constellation, since we try to reduce the number of satellites required while keeping the characteristics of a 2D-LFC. The main results can be summarized in the following points:

- We found optimal 2D-LFCs for solving global positioning problems by using evolutionary algorithms and a number of satellites varying between 18 and 40.

- Thanks to the 2D-LFCs, eccentric orbits have been included in the search of optimal configurations, finding in some cases orbits with $e \approx 0.3$.

- We found 2D-LFCs such that they improve the existing GLONASS or Galileo constellations with the same number of satellites by using our metric, which is the maximum GDOP value experienced in 30,000 ground stations randomly distributed over the Earth surface during the propagation time.

- We propose a new method for designing stable 2D-LFCs, we call them Rigid Constellations. In these constellations the relative positions of the satellites are almost constant (in the osculating elements space), so the structure of *Flower Constellation* is preserved over time.

- We verified numerically that all *Flower Constellation* can become into a *Rigid Constellation* if we accept a deviation of $5\,km$.

- We obtained Rigid Galileo Constellation by correcting the semi-major axes of the satellites of the Galileo Constellation and seeking the eccentricity and inclination that minimize the deviation of the satellites.

- We propose two direct applications of Rigid Constellations. First, it validates the theory of the 3D Lattice Flower Constellation [19] (3D-LFC) under the full expression of the potential function with the J_2 term, assuming that the semi-major axes are corrected and the value of the deviation is small. Second, it shows that in the Global Coverage Problem (with J_2) it will be enough to find a Rigid Constellation that minimizes a slightly modified fitness function (computable using Keplerian propagation).

- We reduce the number of satellites in a 2D-LFC by using the Necklace Theory, while keeping the symmetries and all the properties of this kind of constellations. We obtain the Necklace Flower Constellation (NFC).
- We applied number theory to solve the consistency and minimality problems that appear in Necklace Flower Constellations.
- We developed different theorems to determine the number of Necklace Flower Constellations that can be obtained as a subset of a 2D-LFC.

Some of the future research that will be performed is:

- We will find optimal configurations with more than 30,000 ground stations distributed according to geographical factors instead of randomly over the Earth surface.
- In the search of optimal configurations, if one has a constellation whose GDOP is greater than 99 at any ground station at any given time, it is automatically disregarded. Future research will consider these cases in detail.
- We will study the low thrust needed to reduce the deviation in Rigid Constellations to zero.
- We will design Rigid Constellations including more terms in the potential function.
- We will determine a close formula for $\tilde{W}(N_{so}, N_o, N_c, N_{rso})$ and $\tilde{X}(d, N_{rso}, N_{so})$.
- We will extend the necklace theory to the 3D-LFC.

Through this work we have raised awareness of the importance of studying different satellite constellations to design a space mission. This thesis is the starting point for future research about satellite constellations.

Conclusiones y trabajo futuro

El presente trabajo aborda el problema del diseño de constelaciones óptimas, desde un punto de vista geométrico, puesto que buscamos aquellas constelaciones con una geometría excelente, y desde un punto de vista económico ya que permitimos un ahorro en combustible al buscar constelaciones estables, y también un ahorro en el diseño de la constelación, ya que tratamos de reducir el número de satélites necesarios, de manera que siga teniendo las propiedades características de una 2D-LFC, pero su número de satélites se vea notablemente reducido. Los principales resultados pueden resumirse en los siguientes puntos:

- Encontramos 2D-LFCs óptimas para resolver problemas de posicionamiento global, utilizando algoritmos evolutivos y con un número de satélites variando entre 18 y 40.

- Gracias a las 2D-LFCs incluimos órbitas excéntricas en la búsqueda de configuraciones óptimas, encontrando en algunos casos órbitas con $e \approx 0.3$.

- Encontramos 2D-LFCs que mejoran a las existentes Galileo o GLONASS con el mismo número de satélites, utilizando la métrica del máximo GDOP experimentado en 30000 estaciones terrestres en el tiempo de propagación.

- Proponemos un nuevo método para diseñar 2D-LFCs estables que denominamos constelaciones rígidas, del inglés *Rigid Constellations*. Las posiciones relativas de los satélites en dicha constelación son prácticamente constantes (en el espacio de los elementos osculadores), de tal manera que la configuración de *Flower constellation* se mantiene con el paso del tiempo.

- Verificamos numéricamente que toda *Flower Constellation* puede convertirse en *Rigid Constellation* si aceptamos una desviación de $5\,km$.

- Hemos corregido los semiejes de los satélites de la constelación Galileo y hemos buscado la excentricidad e inclinación que minimizan la perturbación no secular que afecta a los satélites para obtener una constelación rígida.

- Encontramos dos aplicaciones directas de la teoría de las Rigid Constellations. La primera consiste en validar la teoría de las 3D-LFCs, en el caso en que la función potencial no sea promediada en un periodo orbital, asumiendo que los semiejes son corregidos y el valor de la desviación es aceptable. La segunda aplicación sirve para resolver problemas de cobertura global en los que se incluye el efecto

del zonal J_2 en el potencial. Será suficiente con encontrar una *Rigid Constellation* que minimice una función fitness ligeramente modificada y podremos propagar los satélites en un modelo kepleriano.

- Reducimos el número de satélites que componen una 2D-LFC, manteniendo las simetrías y propiedades peculiares de este tipo de constelaciones mediante la teoría de collares, del inglés *necklace theory*. Obteniendo las denominadas *Necklace Flower Constellations*.
- Utilizando teoría de numeros resolvemos los problemas de consistencia y minimalidad inmersos en el diseño de *Necklace Flower Constellations*.
- Desarrollamos diferentes teoremas para determinar la cantidad de *Necklace Flower Constellations* que podemos obtener como subconjunto de una 2D-LFC.

Algunas de las investigaciones futuras que serán realizadas a posteriori son:

- Buscar configuraciones óptimas con más de 30000 estaciones terrestres y distribuirlas por razones geográficas en lugar de aleatoriamente en la superficie terrestre.
- En la búsqueda de configuraciones óptimas, si una constelación presentaba un GDOP mayor que 99 en alguna estación terrestre en algún instante determinado, quedaba automáticamente descartada. Una investigación futura será considerar detalladamente estos casos.
- Estudiaremos los impulsos necesarios para conseguir una desviación igual a cero en una *Rigid Constellation*.
- Diseñar *Rigid Constellations* incluyendo más términos perturbadores en la función potencial.
- Determinar una formula cerrada para las funciones $\tilde{W}(N_{so}, N_o, N_c, N_{rso})$ y $\tilde{X}(d, N_{rso}, N_{so})$.
- Extender la teoría de los necklaces a las 3D-LFCs.

Mediante este trabajo nos hemos concienciado de la importancia que tiene el estudio de diferentes constelaciones de satélites para diseñar una misión espacial. Esta tesis constituye el punto de partida de futuras investigaciones en torno a las constelaciones de satélites.

Bibliography

[1] Abad A., "Astrodinámica", Bubok Publishing S.L., 2012.

[2] Abdelkhalik O., and Mortari D., "Orbit Design for Ground Surveillance Using Genetic Algorithms," *Journal of Guidance Dynamics and Control*, Vol. 29, No 3, Sep. 2006.

[3] Apostol T.M., "Introduction to Analytic Number Theory," Undergraduate Texts in Mathematics, Springer. ISBN 0-387-90163-9.

[4] Apostol T.M., "Calculus 1. Cálculo con funciones de una variable, con una introducción al Álgebra Lineal," Editorial Reverté, 2006.

[5] Apostol T.M., "Calculus 2. Cálculo con funciones de varias variables y Álgebra Lineal, con aplicaciones a la ecuaciones diferenciales y las probabilidades," Editorial Reverté, 2006.

[6] Arnold V.I. "Mathematical Methods of Classical Mechanics," Second Edition, Springer, 1989.

[7] Avendaño M., Davis J.J., and Mortari D., "The Lattice Theory of Flower Constellations," *AAS/AIAA Space Flight Mechanics Meeting*, Paper AAS 10-172, San Diego, CA, February 2010.

[8] Avendaño M., and Mortari D., "Rotating Symmetries in Space: The Flower Constellations," *AAS/AIAA Space Flight Mechanics Meeting Conference*, Paper AAS 19-189, Savannah, GA, February 2009.

[9] Avendaño M., and Mortari D., "New Insights on Flower Constellation Theory," Submitted for publication to the *IEEE Transactions on Aerospace and Electronic Systems*, in print.

[10] Battin R.H., "An Introduction to the Mathematics and Methods of Astrodynamics," Revised Edition, AIAA Education Series, 1999.

[11] Blitzer L., " Handbook of orbital perturbations," Astronautics 453, University of Arizona.

[12] Bruccoleri C., "Flower Constellation Optimization and Implementation," Dissertation, December, 2007.

[13] Bruccoleri C., and Mortari D., "The Flower Constellations Visualization and Analysis Tool," *IEEE Aerospace Conference*, Big Sky, Montana, March 2005., pp. 601 - 606.

[14] Casanova D., Avendaño M., and Mortari D., "Necklace Theory on Flower Constellations," *The 21st AAS/AIAA Space Flight Mechanics Meeting*, Paper AAS 11-226, New Orleans, LA, February 2011.

[15] Cattell K., and Ruskey D., "Fast Algorithms to Generate Necklaces, Unlabeled Necklaces, and Irreducible Polynomials over $GF(2)$," *Journal of Algorithms* Vol. 37, pp. 267 - 282. doi:10.1006/jagm.2000.1108

[16] Chobotov V.A., "Orbital Mechanics," AIAA Education Series, 2002.

[17] Danby J.M.A., "Fundamentals of Celestial Mechanics," Second Edition, Willmann-Bell,Inc. 1964.

[18] Davis J.J., " Constellation reconfiguration: tools & analysis," Dissertation, Texas A&M University, May, 2010.

[19] Davis J.J., Avendaño M. E., and Mortari D., "Elliptical Lattice Flower Constellations for Global Coverage," *AAS/AIAA Space Flight Mechanics Meeting Conference*, Paper AAS 10-173, San Diego, CA, February 8Ű12 2010.

[20] Draim J., "Satellite Constellation: The Breakwell Memorial Lecture," *Proceedings of the 55th International Astronautical Congress*, Vancuver, Canada, 2004.

[21] Draim J., "Common Period Four-Satellite Continuous Coverage Constellation," *AIAA/AAS Astrodynamics Specialists Conference*, Williamsburg, VA, August 1986.

[22] Eberhart R.C., and Shi Y., "Comparison between genetic algorithms and particle swarm optimization," *Evolutionary Programming VII*, San Diego, CA, March 1998, pp.611-616.

[23] Fonseca C. M., and Fleming P.J., "An overview of evolutionary algorithms in multiobjective optimization," *Evolutionary Computation*, Vol. 3, Spring 1995, pp.1-16.

[24] Goldstein H., "Mecánica clásica", Aguilar, 1972.

[25] Guochang Xu, "Orbits", Springer, 2008.

[26] Hassan R., Cohanim B., and Venter G., "A Comparison of Particle Swarm Optimization and the Genetic Algorithm," 46^{th} *AIAA/ASME/ASCE/AHS/ASC Structures, Structural Dynamics & Materials Conference*, Paper AIAA 2005-1897, Austin, Texas, 18-21 April, 2005.

[27] Hofmann-Wellenhof B., Lichtenegger H., and Collins J., "Global Positioning System: Theory and Practice," New York: Springer-Verlag, 1997.

[28] Kaplan E.D., and Hegarty, C.J., "Understanding GPS: principles and applications," Artech House Publishers, 1996.

[29] Kellogg O.D., "Foundations of Potential Theory," New York: Dover Publications, Inc., 1929.

[30] Knight K., "Mathematical Statistics," Chapman and Hall, 2000.

[31] Langley R. B., "Dilution Of Precision," *GPS World*, May 1999.

[32] Maini A.K., and Agrawal V., "Satellite Tehcnology: Principles and Applications," Wiley, 2007.

[33] Montenbruck O., "Satellite Orbits: Models, Methods, and Applications", Springer, 2005.

[34] Mortari D., Wilkins M.P., and Bruccoleri C., "The Flower Constellation," *The Journal of the Astronautical Sciences*, Vol. 52, January-June 2004, pp. 107-127.

[35] Mortari D., and Wilkins M.P., "The Flower Constellation Set Theory Part I: Compatibility and Phasing," *IEEE Transactions on Aerospace and Electronic Systems*, Vol. 44, July 2008, pp. 953-963.

[36] Mortari D., Avendaño M., and Davalos P., "Uniform distribution of point on a sphere with application in aerospace engineering," *The 21st AAS/AIAA Space Flight Mechanics Meeting*, Paper AAS 11-261, New Orleans, LA, February 2011.

[37] Newton I., "The Mathematical Principles of Natural Philosophy", Translated into Enslish by Andrew Motte, 1729.

[38] Noureldin A., Karamat T.B., and Georgy J., "Fundamentals of Inertial Navigation, Satellite-based Positioning and their Integration," Springer

[39] Parkinson B., and Spilker Jr., "Global Positioning System: Theory and Applications," American Institute of Aeronautics and Astronautics, Inc. 1996.

[40] Piriz R., Martin-Peiro B., and Romay-Merino M., "The Galileo Constellation Design: A Systematic Approach," *Proceedings of the* 18^{th} *International Tehcnical Meeting of the Satellite Division of the Institute of Navigation*, Long Beach, CA, September 2005.

[41] Pollard H., "Mathematical Introduction to Celestial Mechanics", Prentice-Hall, Inc. 1966.

[42] Richharia M., and Westbrook L.D., "Satellite Systems for Personal Applications. Concepts and Technology," Wiley, 2010.

[43] Schaub H., and Junkins J.L., "Analytical Mechanics of Aerospace Systems," Reston, VA: American Institute of Aeronautics and Astronautics, Inc., Reston, VA, 2003.

[44] Sivanandam S.N., and Deepa S.N., "Introduction to Genetic Algorithms,"ISBN:978-3-540-73189-4, Springer.

[45] Vallado D., "Fundamentals of Astrodynamics and Applications", Second Edition, Space Technology Library, 2001.

[46] Walker J.G., "Continuous Whole-Earth Coverage by Circular Orbit Satellite Patterns," *Royal Aircraft Establishment*, Tech. Rep. 77044 Vol. 44, March 1977.

[47] Walker J.G., "Satellite Constellations," *Journal of the British Interplanetary Society*, Vol. 37, Dec. 1984, pp. 559-572.

[48] Walker J.G., "Satellite Constellations," *International Conference on Maritime and Aeronautical Satellite Communication and Navigation*, London, England, March 1978, pp. 119-122.

[49] Weise T., "Global Optimization Algorithms - Theory and Application-," online version 2009-06-26

[50] Wilkins M. P., and Mortari D., "The Flower Constellation Set Theory Part II: Secondary Paths and Equivalency," *IEEE Transactions on Aerospace and Electronic Systems*, Vol. 44, July 2008, pp. 964-976.

[51] Wilkins M.P. "The Flower Constellations - theory, design process, and applications," PhD dissertation, Dep. of Aerospace Eng., Texas A&M University, College Station, TX, 2004.

[52] Yarlagadda R., Ali I., Al-Dhahir N., and Hershey J., "GPS GDOP metric," *IEE Proc.-Radar, Sonar Navigation*, Vol 147, No 5, Oct. 2000, DOI:10.1049/ip-rsn:20000554

[53] Zheng Z., Huang C., Feng C., and Zhang F., "Selection of GPS Satellites for the Optimum Geometry", Chinese Astronomy and Astrophysics, Vol. 28, Issue 1, JanuaryŰMarch 2004, pp. 80Ű87.

[54] Zhong E., and Huang T., "Geometric Dilution of Precision in Navigation Computation," *Proceedings of the Fifth International Conference on Machine Learning and Cybernetics*, Dalian, 13-16 August, 2006.